学位論文

Numerical simulations of the collapsar jets of Gamma-Ray Bursts

(ガンマ線バーストのコラプサーモデルにおけるジェットの数値シミュレーション)

平成 28 年 2 月博士 (理学) 申請

東京大学大学院理学系研究科
天文学専攻
ハミダニ ハミド

NUMERICAL SIMULATIONS OF THE COLLAPSAR JETS OF GAMMA-RAY BURSTS

By

Hamid Hamidani

Supervised by

Professor Hideyuki Umeda

School of science
Department of Astronomy
University of Tokyo

A Dissertation submitted for the degree of

Doctor of Philosophy

In Astronomy

February 2016

SCHOOL OF SCIENCE
THE UNIVERSITY OF TOKYO

To my parents, my five sisters & brothers.

For their kindness and love

To all my teachers, with gratitude…

"The true conquests, the only ones that cause no regret, are those made over ignorance."

– The man who conquered the world, Napoleon Bonaparte (November 26, 1797)

DECLARATION

This dissertation is the result of my own work and includes nothing, which is the outcome of work done in collaboration except where specifically indicated in the text. It has not been previously submitted, in part or whole, to any university of institution for any degree, diploma, or other qualification.

Signed:_____

Date:_____

Hamid Hamidani

University of Tokyo

ABSTRACT

Using the collapsar scenario for Long Gamma Ray Bursts (GRBs), I present series of numerical simulations to investigate the properties of expanding jets, driven by engines deploying the same total energy differently. I include a wide range of engine durations (T_{inj} from 0.1 to 100 sec), as well as different initial opening angles (θ_0 from 1 to 90°), for the same deployed energy (10^{52} erg). Then, I examine the produced diversity of jets, considering the effect of the opening angle. I employ an AMR 2D special relativistic hydrodynamical code, using an initially 25 solar mass Wolf-Rayet star as the progenitor. I analyze the effect of the initial parameters on the jet's hydrodynamic properties, the three radiative phases, and discuss the implications on GRB prompt emission and SN energy. My results show that the engine's duration dramatically affects the three radiative phases launch and contribution in the jet. As a consequence, the expanding jet's hydrodynamical properties differ. In particular outflow collimation and relativistic acceleration. The implication of this is that *brief* engines (with $T_{inj} < T_{breakout}$, either due to short T_{inj} or large θ_0) represent excellent systems to explain the debated *low-luminosity* GRBs (*ll*GRBs), producing the two peculiar features of *ll*GRBs: i) the estimated *ll*GRBs rate at least about 100 times higher than that of GRBs, and ii) potentially energetic SN emission. I find that these two features only arise from *brief* engines. The conclusion is that *brief* engines should dominate collapsar events, at least at low redshift.

Subject heading: gamma-ray: burst – hydrodynamics – relativistic processes – shock waves – ISM: jet and outflows – supernovae: general

PREFACE

About five decades have passed since the first discovery of a Gamma-Ray Burst by a pure chance (hereafter GRB). Still our struggle to understand GRBs is just in its beginning and our understanding of GRBs is quite primitive.

The allegory of the cave[1], would illustrate our incapacity to travel to GRBs sites, see what is happening out there or take samples. We are like chained people in the bottom of a cave with our heads toward the bottom of the cave, where all that can be seen is shadows on the cave wall; random shadows of objects, themselves copies of the true objects in the outside real world. Although in darkness upon darkness, these people, in their frame, are free in their world. They start naming the shadows, classifying them based on likenesses, and having opinions and conjunctures on what the eye is able to see. It is the first part of Plato's divided line[2], but the lowest in wisdom. The eye starts to make predictions on the shadows, from which some belief is born. With math and imagination, the people move to the world of ideas and knowledge and start to converge to the truth of shadows, making hypotheses and moving to conclusions, conclusions involving some unseen truth. Finally, the smartest of the chained people would get into the highest level of Plato's divided line (DE): that of reason and the understanding of only the intelligible. Even if the eye cannot see and the body is chained, the mind is freed to the world of wisdom, converging toward the first principle, the truth. Some of these chained people live for a challenge, and tough as the situation seems, their first inspiration is always born from a continuous *"I don't know"*[3]. Their effort to understand the truth, imagine the sunny day outside the cave would be admirable and deserves immense admiration.

I think that the human effort to understand the nature of GRBs, made in the last five decades, deserves immense respect and admiration. Considering the spatial and temporal scale of GRBs, we, in our tiny planet in the Milky Way, itself tiny considering the scale of GRBs and the universe, although free in our world, we are at the bottom of an even deeper cave. Cosmic GRBs, occurring billions years back in time, are as ambiguous to our world as the Sun would be to the mind of enchained people in a cave.

The best that could be seen of GRBs phenomenology is partial shadows of GRBs, shadows of distorted GRBs – as during their millions years journey, GRBs photons are

extinct, redshifted, attenuated etc. Light curves, spectrums, afterglows, and so on, are all shadows of a distorted truth on GRBs at the detector's very narrow field of view in a vast universe (Swift, Fermi etc.), as shadows of fake objects in the bottom of a deep cave. We name shadows (GRB 980425, GRB 060218 etc.), classify them, Short GRB, Long GRB, *low luminosity* GRB etc. With the first data, Hundreds of models and opinions have been developed, most of which did not survive (e.g. galactic models), but had the honor of paving the way to understand the truth on GRBs and the universe. The fruit of human genius is theoretical models, describing GRBs' intelligible: fireball model, collapsar model… These models are to us as the Sun would be to the people of the cave; these models are light with which we can see, light that illuminate a GRB astronomy full of darkness; light and our best hope to get to the unseen, to the universe, to the truth. All the glory and respect goes to their pioneers, and to all the researchers that worked their mind devotedly on GRB mystery in the last five decades.

In a context where GRB data is increasing, and with it the diversity of GRBs, after a "Swift revolution", crucial questions on the *"how"* and *"why"* of GRBs, on the origin of diverse GRBs are in the center of attention of scientists. Among the newly discovered GRBs is one class of particularly *low luminosity* GRBs. My thesis explores the model which represents state-of-the-art in our understanding of GRBs – the *"collapsar model"* – numerically, in a domain never explored before. I explore one possible origin of the particular class of *low luminosity* GRBs, an origin that might explain these events particular features, and might contribute to the understanding of GRBs and massive stars death. Just like chained people in the bottom of a deep cave, I had to give up on seeing the true nature of *low luminosity* GRBs with my eyes. Instead, I try to see them with numerical simulations as it follows in this thesis. A humble thesis – carrying a tiny idea – as this one cannot solve the enigma of GRBs, but my best hope is that it would be one original thought, that might echo in a wise man heart one day, a one "imperfect" step toward the truth.

It is said that people are motivated in three ways: reward, punishment and inspiration. I decided to enroll into a Doctor degree and study GRBs motivated by the last and not the first two the three. For someone who loved astronomy since childhood, I had the extraordinary luck of having great teachers, professor Jamal Mimouni and professor Nidhal Guessoum. I was so inspired that I decided to follow their path: live for both research and public outreach. As in Plato allegory, one of the chained persons finds his

way to the outside, sees the Sun and grasps the truth. He later goes back to the cave, where his people are limited to shadows, and speaks of the truth. As my teachers played this role perfectly and saved no effort to teach me, I would like to be an instrument to spread this amazing knowledge, this truth, this light that is called astronomy to the next generation. As my teachers often said, "*it is an ideal that deserves living for*".

Since the antiquity, the heavens, the sky, and the stars that decorated it, have fascinated the human heart. Monastic religions inspired with the stars and used them to vehicle the divine message[4]; as Abraham's (the father of the three monastic religions) first inspiration for a single God was the night sky and its stars. Stars have inspired and had the same impact on people and civilizations throughout the globe and the times: ancient Egyptians, Greeks, Roman, and Arabic etc. The human heart imagination was, is, and will always be fascinated by stars: philosophy, romance, poetry, music, etc. GRBs are believed to be the last cry of massive stars, an agonizing star cry that echo in the corners of the universe, holding valuable information, before ending into a deep cave where the cry might be heard. I think that; we, GRB astronomers; the only to hear such a voice, are blessed with one of the most moving jobs for the human heart.

About four years ago, the physics Noble prize went to a discovery that changed our understanding of the universe (Perlmutter et al. 1999). The universe is expanding, and the expansion is accelerated. As a consequence, in the very far future, galaxies would rush away with such speeds that it would not be possible to see them. Astronomers will see nothing but an entirely dark sky with no extragalactic objects; no GRBs. Based on that, astronomers would conclude that the universe is static and unchanging, a wrong, but physically justified picture. In other words, the cave they will live in is a totally locked. Sad as the future seems, and although this will happen in a very far future, I think this should be motivating, especially for extragalactic astronomy. We are living in a privileged epoch when some truth about the universe is within reach and can be heard, however this is not an eternal state[5]. Hence, GRBs, these cosmic telegrams journeying billions of years, before echoing in our detectors, deserve to be heard.

GRBs are of immense importance to astronomy. Although, enigmatic, GRBs are priceless to astronomers. Just the fact that GRBs are the farthest, oldest, and most luminous events ever observed would justify the human effort to understand them. In most cases, GRBs' light is coming from epochs closer to the big bang than to our time.

Their light holds information on the extragalactic environment, on the universe metalicity and even on the primordial universe nature (Savaglio et al. 2009 & Totani et al. 2014).

¹ Inspired from the Allegory of the Cave presented by the Greek philosopher Plato in his book "The Republic" (514a–520a)

² The Analogy of the Divided Line presented by the Greek philosopher Plato in his book "The Republic" (509d–511e)

³ "Whatever inspiration is, it's born from a continuous; I don't know" – By Wislawa Szymborska (1923 – 2012), she was awarded the Nobel Prize in Literature in 1996.

⁴ The Bible 26:4. The Quran, 6:75-79.

⁵ From Brian Greene TED talk: "*Is our universe the only universe?*" (02/2012)

ACKNOWLEDGEMENTS

hard times. I would also like to thank two precious friends, for the kind friendship and for the precious help: Aaron C. Bell and Pablo Morales, many thanks!

CONTENTS

LIST OF TABLES

LIST OF FIGURES

LIST OF ABBREVIATIONS AND ACRONYMS

AGN: Active Galactic Nucleus

AMR: Adaptive Mesh Refinement

BATSE: Burst And Transit Source Experiment (USA)

BeppoSAX: Beppo, in honor of the Italian scientist: Giuseppe Occhialini, detto Beppo; Satelite per Astronomia X-ray (Itally-Netherlands)

BH: Black Hole

CE: Central Engine

CGRO: Compton Gamma Ray Observatory (USA)

CPU: Central Processing Unit

CSM: CircumStellar Medium

EOS: Equation Of State

GRB: Gamma-Ray Burst

HETE: High Energy Transient Explorer (USA, France & Japan)

HN: HyperNova

HST: Hubble Space Telescope (USA)

LGRB: Long Gamma-Ray Burst

*ll*GRB: *low luminosity* Gamma-Ray Burst

MHD: Magneto Hydro Dynamics

NASA: National Aeronautics and Space Administration (USA)

NS: Neutron Star

SFR: Star Formation Rate

SGRB: Short Gamma-Ray Burst

SN: SuperNova

ULGRB: Ultra Long GRB

UV: UltraViolet

UVOT: UltraViolet/Optical Telescope

VLT: Very Large Telescope

WR: Wolf-Rayet

XRF: X-Ray Flash

XRT: X-Ray Telescope

LIST OF APPENDICES

1 GAMMA-RAY BURSTS

"To myself I am only a child playing on the beach, while vast oceans of truth lie undiscovered before me" — *Isaac Newton*

1.1 WHAT IS A GAMMA RAY BURST?

GRBs are very extreme and enigmatic events in almost every aspect, regarded as the most luminous explosions in the universe (Meszaros 2006). They are observed about once everyday in random positions in the sky. GRBs consist of a flash of energetic γ-photos, for a duration of ~ 0.1 - 100 seconds (called "prompt emission"), with an estimated total isotropic equivalent energies up to $~10^{54}$ erg! After the prompt emission a softer (from X-ray to radio) and longer emission is generally observed (called "afterglow"). GRBs are also the most distant objects ever observed, occurring at cosmological distances, billions of light years away in time and space, which makes them the oldest known objects/events (e.g: GRB090423 $z = 8.2$, i.e 13 billion light years old). Since their discovery by chance in 1967, very puzzling in every aspect, GRBs remained a highly debated topic.

Nowadays, the term "GRB" is increasingly vague, with the expanding diversity of GRBs revealed since the Swift era (2004 ~). Diversity has grown in duration (Long GRBs: LGRBs > 2 s and Short GRBs: SGRBs < 2 s) (Kouveliotou et al. 1993), in

energies (from Very Energetic to *low-l*uminosity GRBs, *ll*GRBs), and several other intrinsic properties. Although SNe and GRBs are closely related explosions, GRBs can be detected up to high redshifts (Figure 1.1). Furthermore, GRBs radiate over a wide spectrum (Figure 1.2). Thanks to their brightness GRBs are very powerful tool to study the early universe (up to 13 Gyr, e.g. Kawai et al. 2006), primordial galaxies and their evolution (e.g. Savaglio et al. 2009) the reionization epoch (e.g. Totani et al. 2014) etc. Their afterglow enables deriving precious information, such as the redshift, metalicity, dust extinction, SFR, etc. Also, as GRBs are closely related to the death of massive stars, they are windows to massive stars and their evolution.
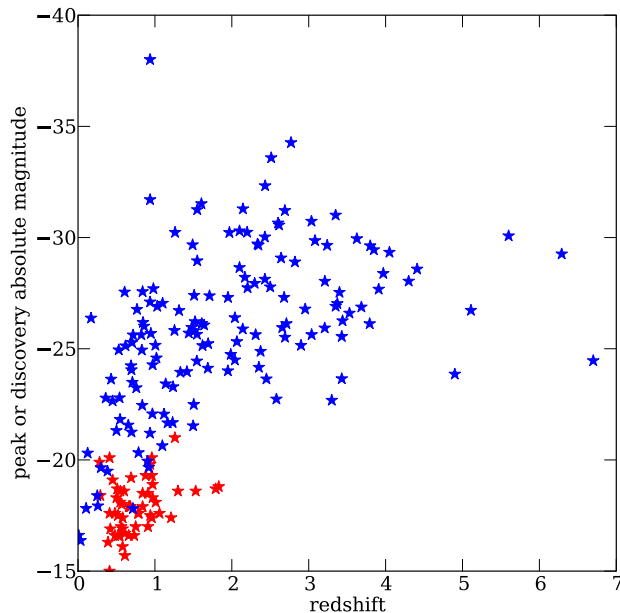
Figure 1.1: Comparison of absolute magnitudes of 153 known GRBs (optical afterglows; blue stars) with absolute magnitudes of core-collapse SNe (the peak of the absolute magnitude in the light curve in red stars). (Credit: Sevenson 2011).

Hamid Hamidani - February 2016
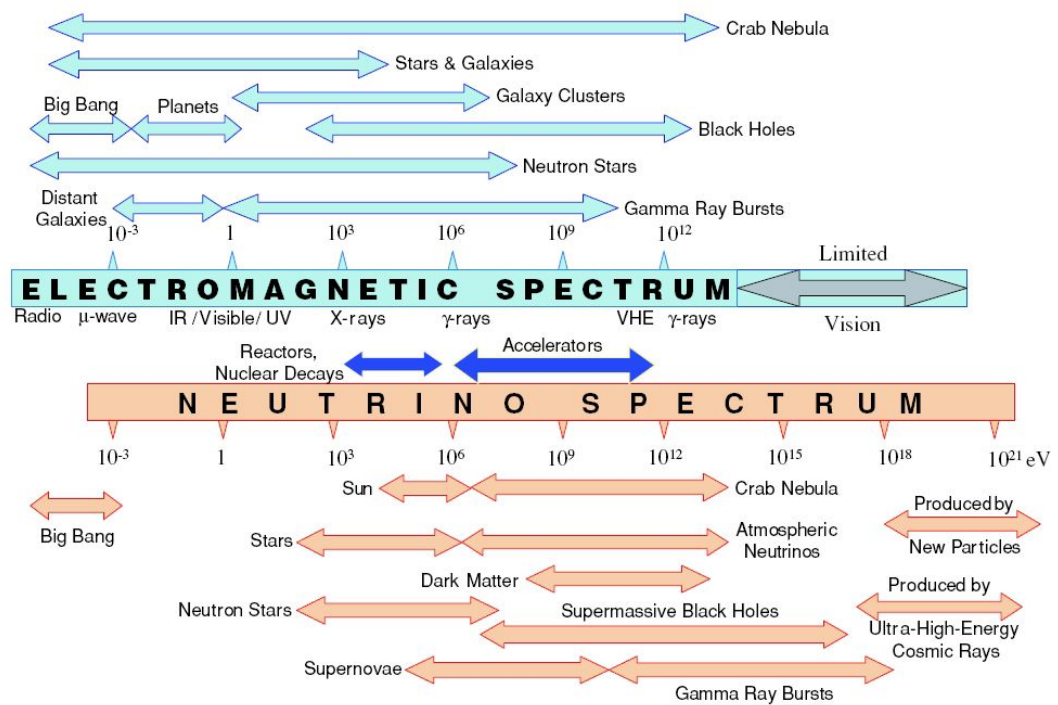
Figure 1.2: Gamma Ray Burst spectral regime in comparison with other astrophysical phenomena (Credit: Barish & Huchra et al. 2003)

1.2 THE DISCOVERY

A military mission, Vela, discovered GRBs in 1967 (Figure 1.3 & Figure 1.4). Vela mission consisted of satellites dedicated to the detection of γ-photons in a range ~ 0.2 − 1.5 MeV (emission from eventual Soviet illegal nuclear tests). The results were confusing: *Soviet nuclear tests violating international treaties, or the signs of an extraterrestrial intelligence?* The interrogation continued for several years; hence it was kept secret until 1973 were a first scientific paper was published (Klebesadel, et al. 1973).
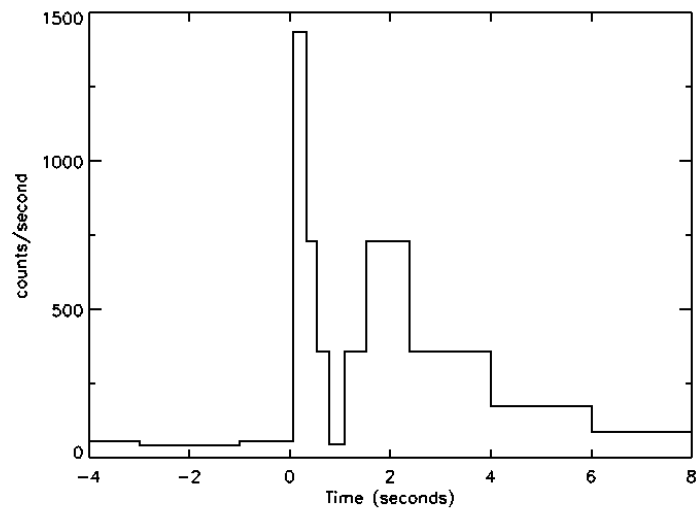
Figure 1.3: The first GRB detected in 1967 in Vela mission (Klebesadel, et al. 1973)

The mystery has just started, and soon after, as many as 100 different theoretical models were proposed to explain GRBs emission (Texas Symposium on Relativistic Astrophysics in 1975). No major breakthrough was possible until the end of 1990s, were sophisticated missions were finally devoted to GRBs, allowing the establishment of theoretical models (The fireball model Piran 2000; & the collapsar model MW99).

Hamid Hamidani - February 2016
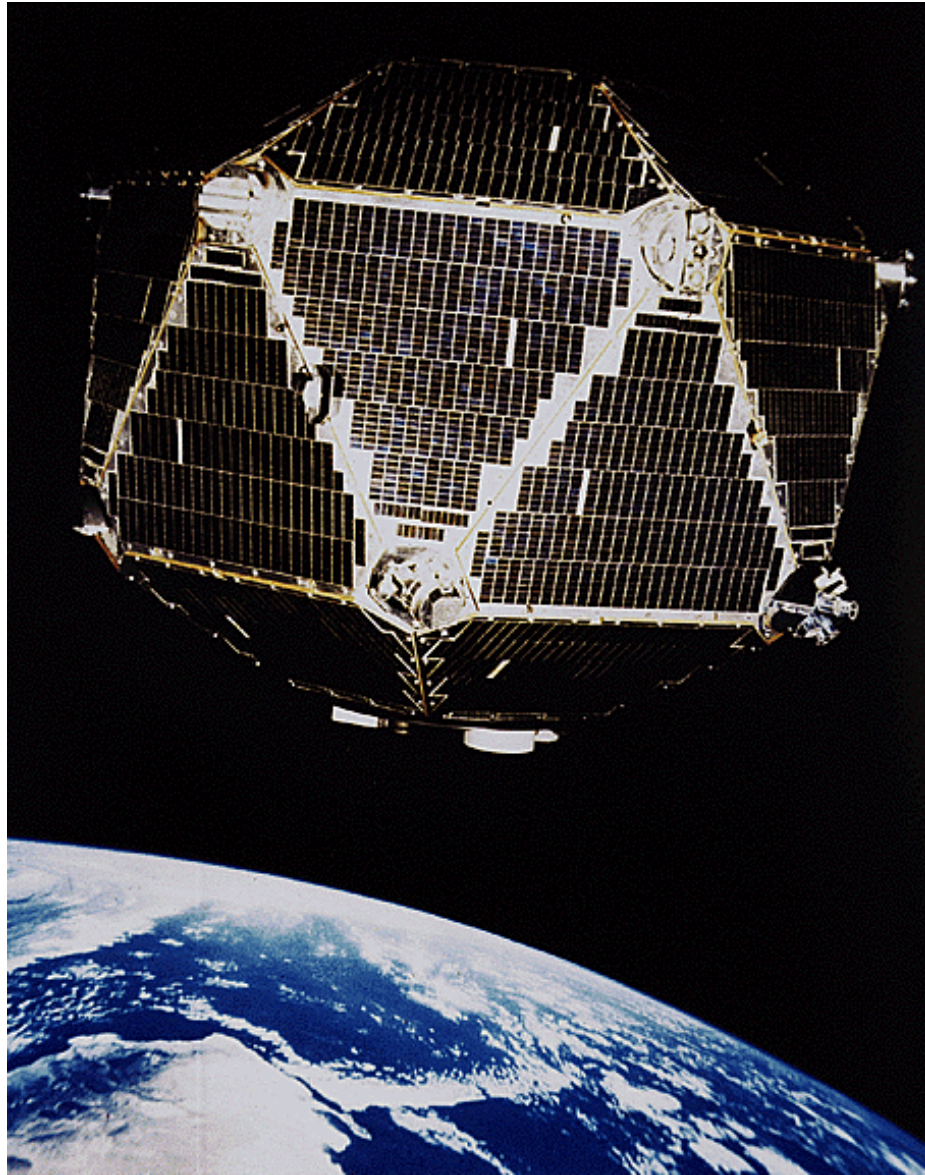
Figure 1.4: One of the Vela satellites thanks to which GRBs have been discovered (Credit: NASA).

1.3 MAJOR DISCOVERIES

1.3.1 EVIDENCE OF THE EXTRAGALACTIC ORIGIN

CGRO was a major NASA mission; one of its objectives was the understanding of GRBs' origin. Its instrument, BATSE, enabled a major discovery: GRBs occur randomly on the sky, without following the galactic plane (and hence are most likely not related to galactic objects) (Figure 1.5). This narrowed down the theoretical models, excluding most of the galactic models (except galactic halo models). The extragalactic origin was finally confirmed with the first redshift measurement thanks to BeppoSAX mission (Metzger et al. 1997).
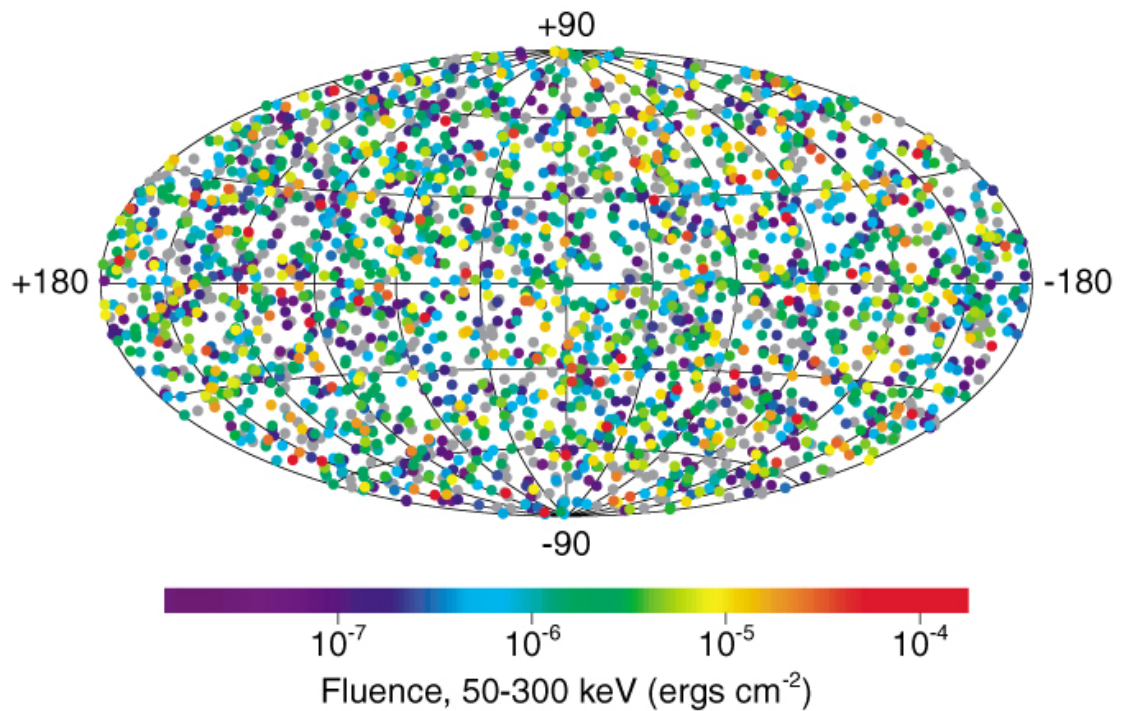
Figure 1.5: BATSE Sky Map showing the isotropic spatial distribution of GRBs, and hence revealing the extragalactic origin. (Credit: G. Fishman et al. BATSE, CGRO, NASA) (http://heasarc.gsfc.nasa.gov/docs/cgro/cgro/batse_src.html)

1.3.2 A BIMODAL DISTRIBUTION

1.3.2.1 DURATION DISTRIBUTION

BATSE instrument allowed one other major discovery: the duration distribution of GRBs revealed a bimodal distribution. There are two classes of GRBs: Short GRBs (SGRBs) with durations shorter than 2 seconds, and Long GRBs (LGRBs) longer than 2 seconds (Kouveliotou et al. 1993). This discovery initiated the debate on the origin of

each class. The short populations of GRBs observed in BATSE show a mean T_{90} of about 0.3 seconds, while the average duration for long GRBs is ~35 seconds (Figure 1.6).
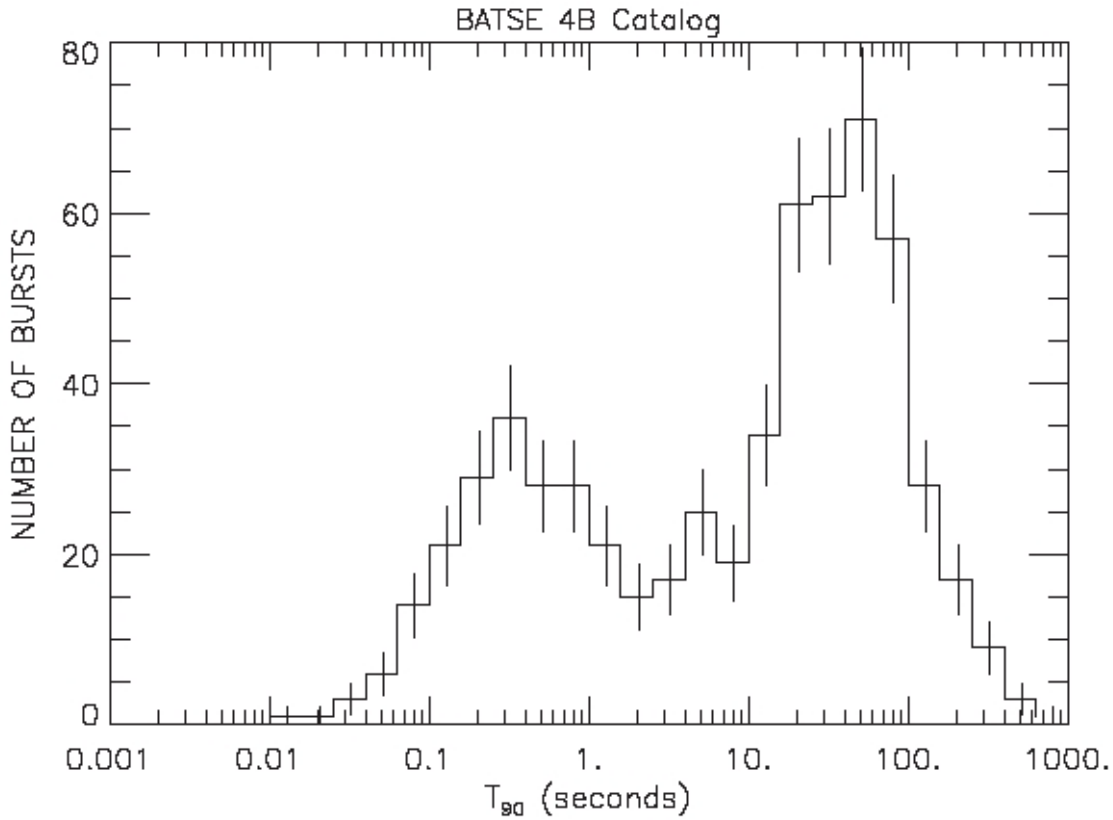
Figure 1.6: The bimodal distribution of GRBs as reviled by BATSE (CGRO). Long and Short GRB populations show durations (T_{90}) greater than and less than ~2 s, respectively. (Credit: BATSE, NASA). T_{90} is defined as the time interval over which 90% of the radiation has been detected.

1.3.2.2 HARDNESS-DURATION DIAGRAM

One other evidence of the bimodal distribution of GRBs can be found in the Hardness duration diagram. The ratio of the number of hard photons (100 − 350 keV) over the number of softer photons (50 − 100 keV), is the hardness. Plotted as a function of the duration of the prompt emission (T_{90}), it shows a bimodal distribution (Figure 1.7). This is also an illustration of the fundamental difference of the two classes; SGRBs are harder than LGRBs, which is most likely related to different origins.
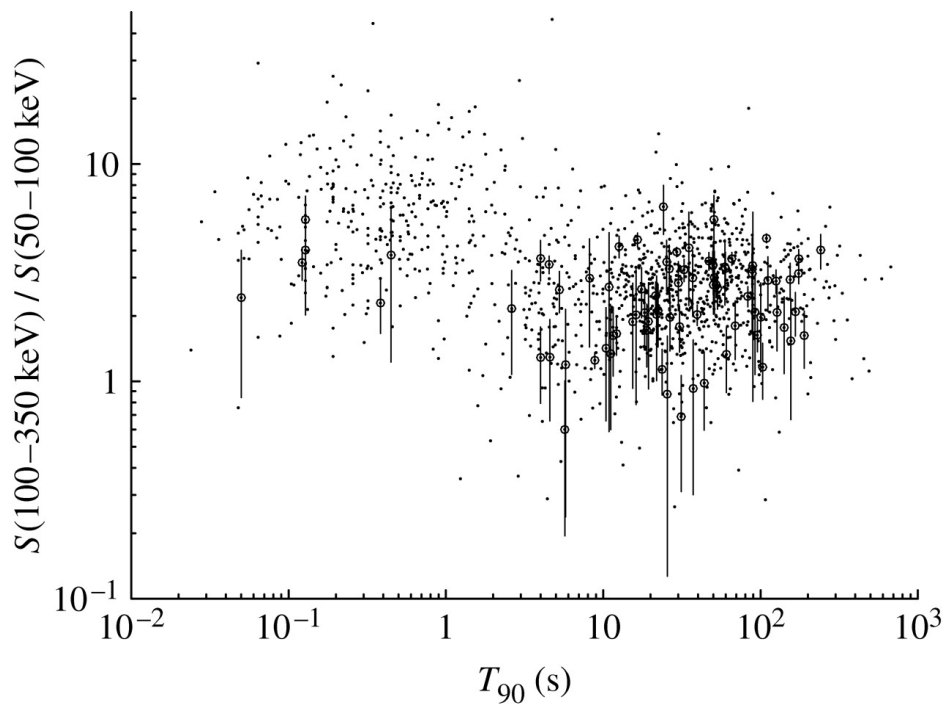
Figure 1.7: The Hardness-duration diagram up to 2006, confirming the bimodal distribution of GRBs population. Dots show BATSE 4B GRBs; circles show Swift/BAT GRBs. (Credit: Sakamoto et al. 2006)

1.3.3 THE SN CONNECTION

Observations revealed that GRBs are associated with stellar explosions (SN and HN). However, not all LGRBs could have been associated with SNe. The first case of GRB-SN association was SN 1998bw (Figure 1.8). SN 1998bw was associated with a particularly soft GRB (GRB 980425). Progressively other associations were found, although most of which were associations of relatively soft and low redshift GRBs with SNe/HNe (GRB011121/SN2001ke; GRB 031203/SN2003lw; GRB 030329/SN2003bh, etc. See Table 6-2 & Figure 6.8 for more details). GRBs' SNe are generally identified through bumps in the light curve, few days to few weeks after the prompt emission; SNe were also identified spectroscopically (Hjorth & Bloom 2011; Hjorth 2013). See Figure 1.11 for more information.

Hamid Hamidani - February 2016
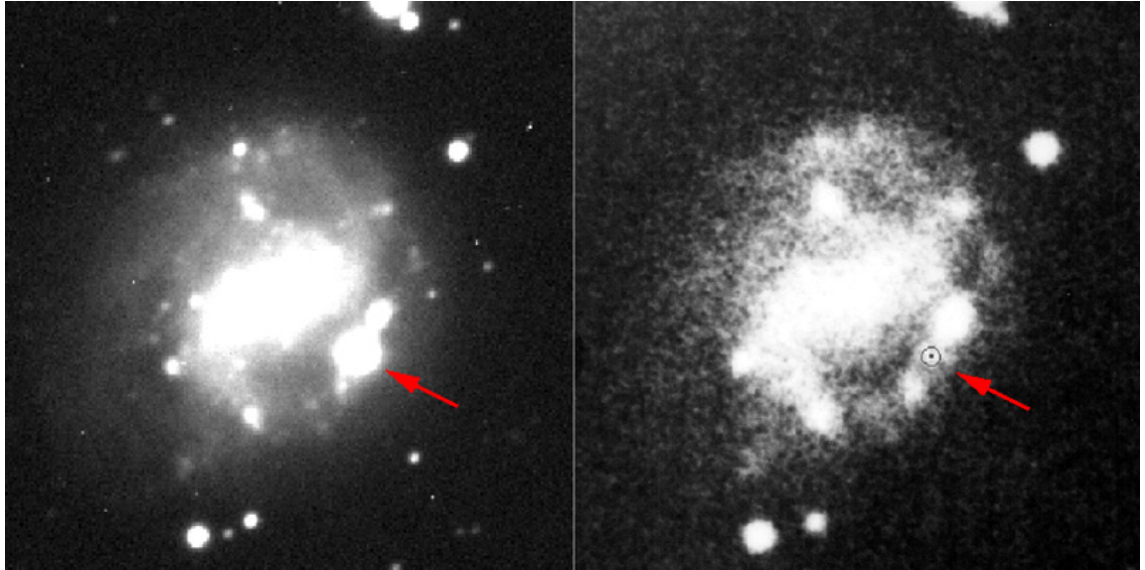
Figure 1.8: Images showing the discovery of the first SN associated with a GRB (GRB 980425 / SN 1998bw). The SN was discovered is a spiral galaxy ESO 184–G82. From the right to the left shows before and just after the occurrence of the SN. (Credit: Galama et al. 1998 & Gomboc 2012).

1.3.4 LOCAL ENVIRONMENTS

GRB host galaxies have increasingly been identified, reveling the environment of GRBs. Unlike SNe, LGRBs generally occur in specific regions, with a young stellar population rich in massive stars; LGRBs are in particular found in dwarf galaxies or in the arms of spiral galaxies (see Figure 1.9). The typical SFR of LGRBs hosts is in the range $1 - 10$ M$_\odot$yr^{-1} (Hjorth et al. 2005 & Savaglio et al. 2009). The low metalicity and high SFR confirms that LGRBs are related to the death of rapidly rotating massive stars (the collapsar model; MW99).

On the other hand, the situation is more complex for SGRBs, as the afterglow emission has rarely been observed, making it difficult to accurately localize them. Still, some SGRB host galaxies have been identified. However, at the difference of LGRBs, SGRBs are found in both late-time, red, elliptical galaxies and as well as star forming galaxies. The SFR of SGRB hosts is typically in the range $0.1 - 0.2$ $M_\odot yr^{-1}$, about one order of magnitude smaller that of LGRB hosts (Hjorth et al. 2005). This doesn't conflict the notion that SGRBs originate from compact objects merging (NS-NS or NS-BH), a scenario that doesn't necessarily require a high SFR or a low metalicity (Savaglio et al. 2009).
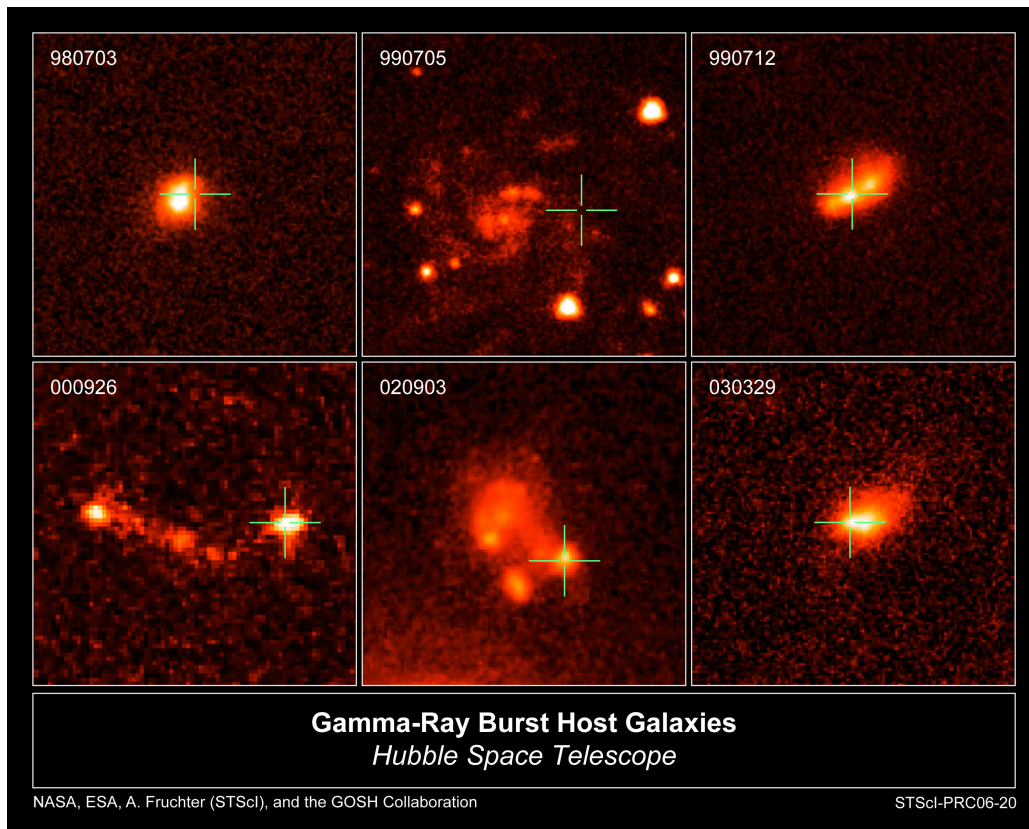
Figure 1.9: Sample of LGRB host galaxies. LGRBs are found in low metalicity high SFR regions: in the irregular dwarf galaxies, or in the arms of spiral galaxies, rich in young massive stars. (Credit: Fruchter, NASA HST)

1.4 THE FIREBALL MODEL

The fireball model explains Short and Long GRBs in a general picture of a highly relativistic and beamed jet. A system of a stellar BH surrounded by an accretion disk is assumed to power the jet (the engine). In the case of SGRBs, the system might be the product of compact objects merging (NS-NS or NS-BH). While in LGRBs, the situation is clearer; the system can be found during the gravitational collapsar of massive stars (The collapsar model; MW99: see § 1.7). The main radiative process is synchrotron emission of relativistic electrons (Piran 2000). Internal shocks in the jet are assumed to produce the prompt emission, while the external shocks produce the afterglow (Figure 1.10). The light curve, decay, spectrum, energy output, variability and other basic properties of GRBs can be well explained with this scheme (Piran 2000). The research plan of this work is not related to SGRBs, and therefore the focus is on LGRBs only.
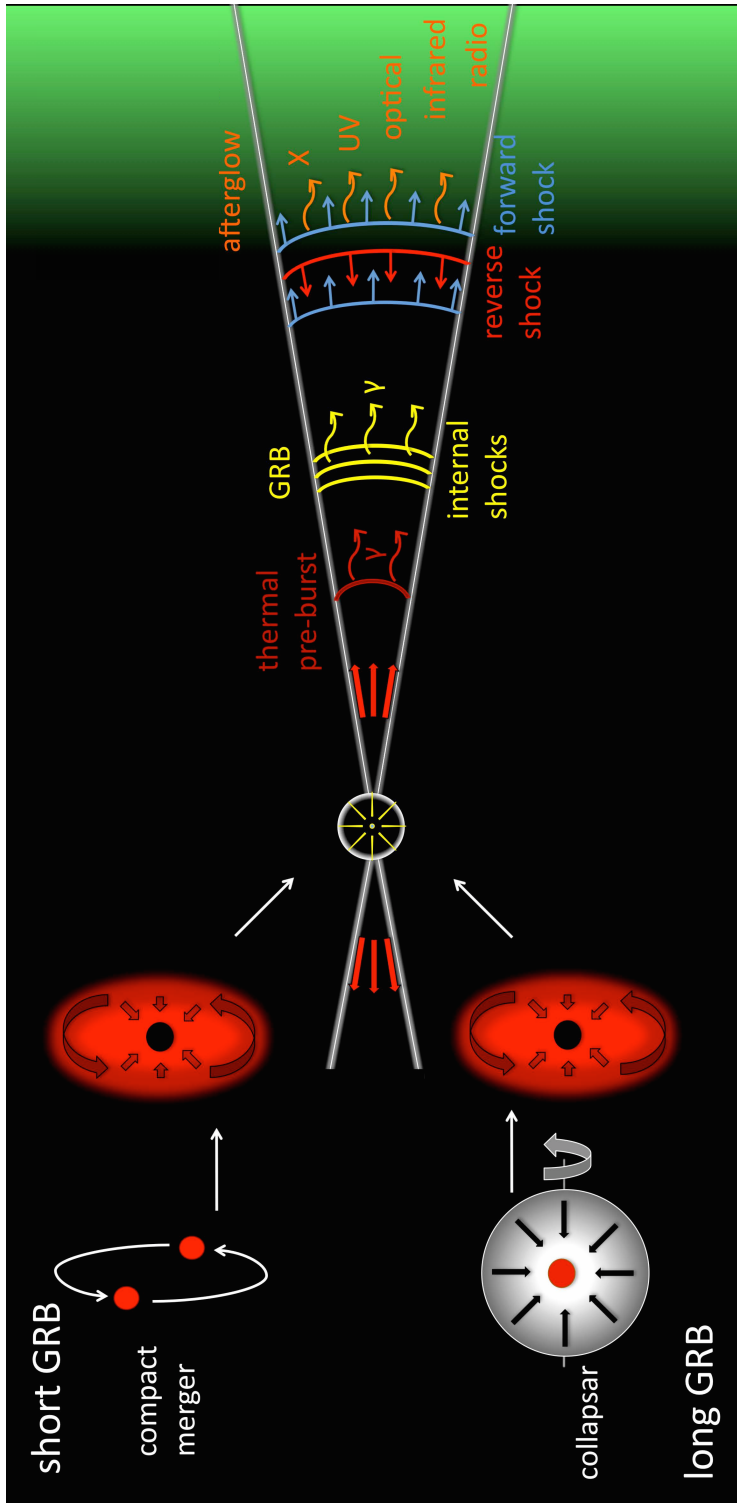
Figure 1.10: The fireball model and the systems to explain SGRBs & LGRBs. The relativistic jet and the sites where the prompt emission (γ-photons) and the afterglow are shown. (Credit: Gomboc 2012)

1.5 LONG GRBS LIGHT CURVE

In Figure 1.11 is the scheme of a typical LGRB light curve. The illustration shows the prompt emission, the afterglow (which could be from X-ray down to radio frequencies), and the SN bump (up to few weeks after the burst). The light curve is composed of the following phases (Nousek et al. 2006 & Gomboc 2012):

- *The prompt emission*: very short, bright, variable and energetic.

- *A steep decay*: The low-energy tail of the prompt emission. There have been several interpretations of this segment (high latitude emission observed at latter times, "curvature" effect, etc.)

- *The plateau*: Interpreted as times when the external shocks become dominant over internal shocks, although its spectra is not always consistent with the standard model. Therefore, some interpreted it as an energy injection phase. Flares are found in this phase, in about half GRBs (Willingale et al. 2007).

- *Afterglow and the jet breakout*: This part is much consistent with the fireball model. It shows a "jet break" which is due to the jet slowing down (see § 1.5.2).

- *SN bumps*: It is the signature of a SN/HN explosion. It can be observed few days to about one month after the prompt emission.
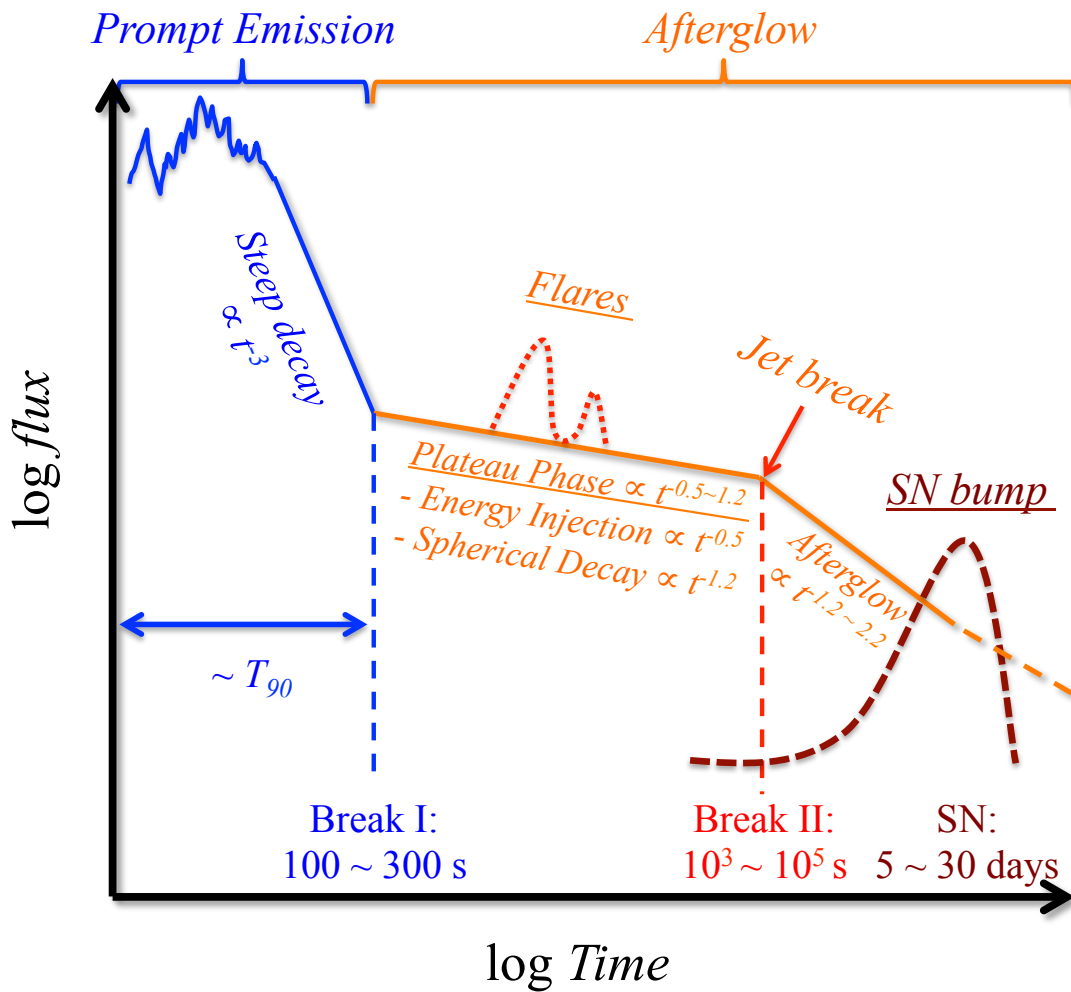
Figure 1.11: Illustration of canonical light curve in a typical Long GRBs. The prompt emission is in blue and X-ray afterglow is in orange. The jet break is shown in red, and the SN bump in dark red. The power law segments are not always present, in particular the underlined components: plateau phase, energy injection phase, spherical decay, flares and SN bump. (From more details, see: Nousek et al. 2006)

1.5.1 THE PROMPT EMISSION

The prompt emission is a very hard and variable phase. It consists of a combination of a number of pulses overlapping. In order to define the duration of the prompt emission, the term T_{90} have been introduced to define the time interval over which 90% of the radiation has been detected.

In many cases the variability is down to milliseconds, which suggest that the engine is a stellar sized object. In the fireball model, the prompt emission (and the temporal variability) is generally related to the engine activity time. However this might not be the case for some particular events, such as: GRBs showing a thermal spectrum, and the *low luminosity* GRBs (*ll*GRBs). For instance, in *ll*GRBs the duration would be explained by a mildly relativistic shock breakout (Campana et al. 2006; Nakar et al. 2012 & Nakar 2015).

Figure 1.12 shows a sample of BATSE prompt emissions. Each of the prompt emissions is unique. The variability and the number of bulks differ from a burst to another (single peak or multiple peak). The light curves below are one illustration of the huge diversity of GRBs.
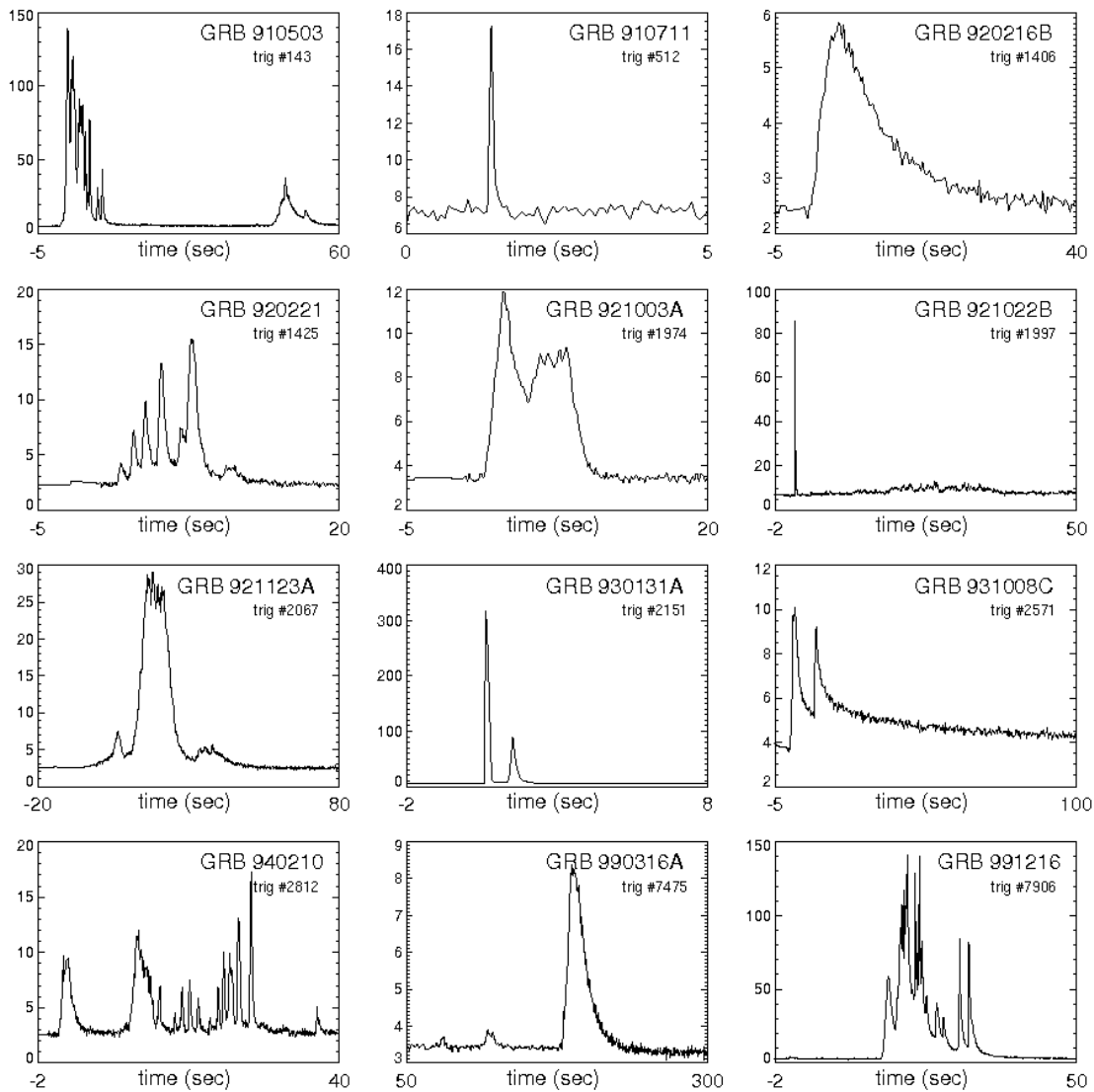
Figure 1.12: A sample of 12 BATSE short and long GRBs, illustrating the uniqueness of each burst and the huge diversity. This sample, made by, includes different events: short, long, smooth and variable. (Credit: Daniel Perley. Source: NASA, BATSE http://gammaray.msfc.nasa.gov/batse/grb/catalog/)

Hamid Hamidani - February 2016

1.5.2 AFTERGLOW AND JET BREAK

The jet break is a natural consequence of a relativistically expanding jet. As it slows down to relativistic speeds where the relativistic beaming gives an angle larger than the jet-opening angle, the radiation is more widely spread steepening the decay of the light curve (Figure 1.13). Although not all GRBs show a clear jet breaks, breaks are generally observed in the X-ray afterglow. The breakout time is from 10^3 to 10^5 seconds. It's detection allowed the measurement of GRBs' opening angle and the beaming factor, by which estimation of the true energy of GRBs, the corrected energy, could have been made (Frail et al. 2001). The jet break time helped also estimating the radiative efficiency of some GRBs (Zhang et al. 2007b; for more derails see § 1.6.2).

1.5.3 SN BUMP

The signature of a SN explosion can be detected in the decaying light curve of GRBs. From few days to few weeks after the burst a bump is often detected in the light curve, which cannot be explained by a canonical decay of the afterglow alone. The bump is interpreted as a SN, which is would peak few days to few weeks after the burst. In some cases a spectral signature could also be detected. The SN bumps are mostly observed in *ll*GRBs, most likely due to their low redshifts. While in the standard GRBs, SN bumps are rarely found, although there are some exceptions (Figure 1.14). Whether it is due to the high redshift, afterglow and host galaxy contamination, or to the brightness of the explosion itself, the absence of SN bumps in many typical GRBs is debated (Hjorth 2013).
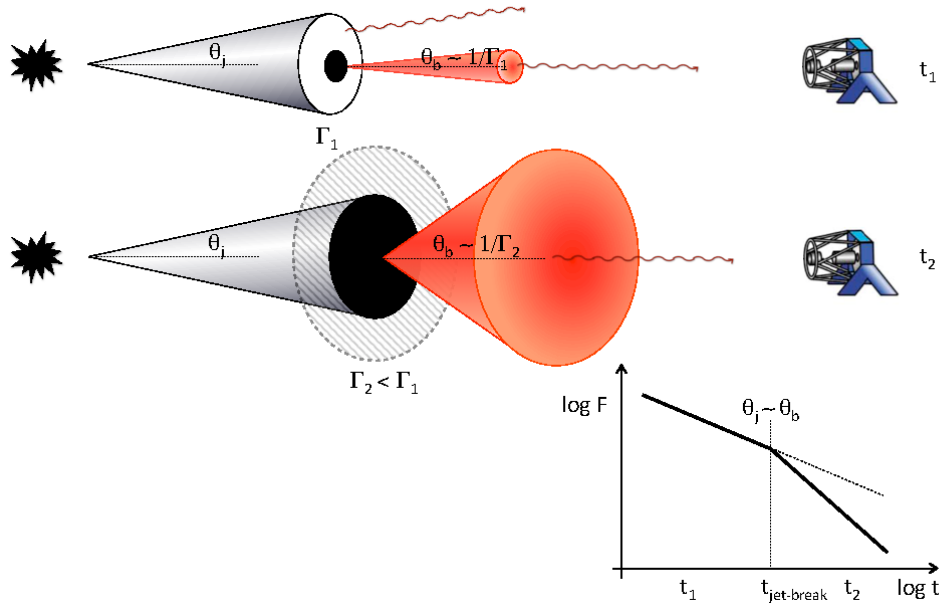
Figure 1.13: Illustration showing the jet-break time and the steepening of the light curve decay. When the a relativistic jet (with Γ_1) is relativistically beamed in a narrow angle ($\theta_b = 1/\Gamma_1$) and is slowing down, a jet break will appear in the light curve as the jet slows down to a relativistic Lorentz factor where $\theta_b = 1/\Gamma_2$ is larger than the jet opening angle θ_j. The light curve steepening is a consequence of the observer missing the emission from the dashed area as shown above. (Credit: Gomboc 2012)
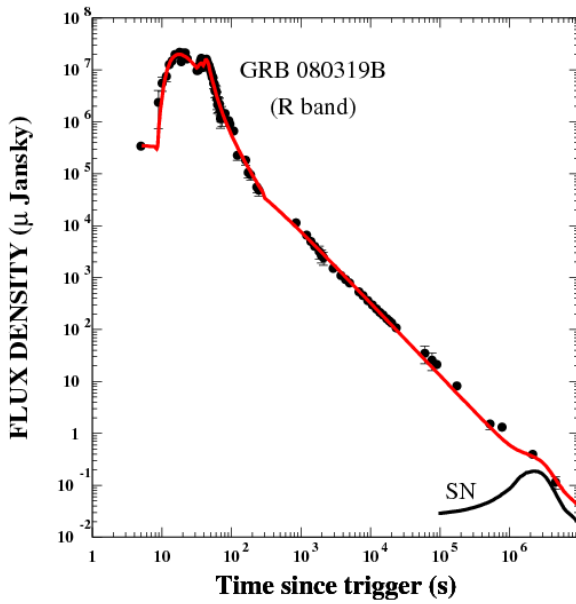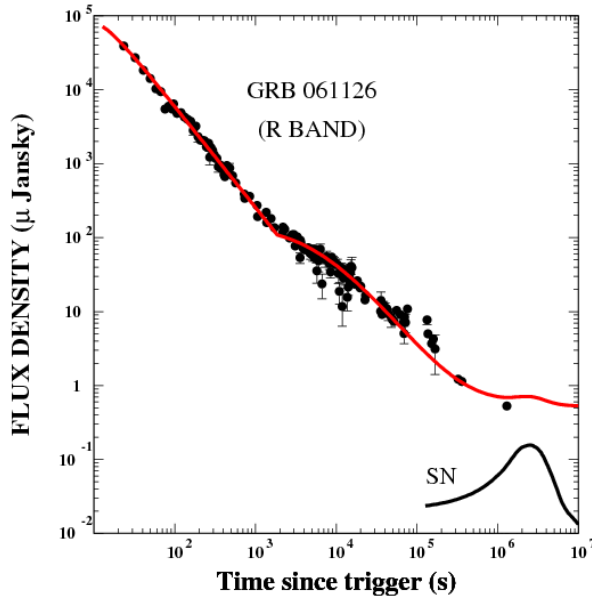
Figure 1.14: Swift X-ray light curve of GRB 061126 and GRB 080319B, suggesting SN bumps. The red line is a fitting of Swift data (black circles) using the cannonball model. (Credit: Gomboc 2012)

1.6 OTHER PROPERTIES OF LONG GRBS

1.6.1 THE SPECTRUM

The prompt emission of GRBs is mostly non-thermal emission. It can be fitted with the Band function (Band et al. 1993). However, thermal components are regularly detected in GRBs, especially with the recent Fermi telescope. The non-thermal emission has classically been interpreted as synchrotron emission of electrons, in a highly magnetized and relativistic plasma's internal shocks (Sari et al. 1998; Piran 2000 & Piran 2004). The thermal emission is interpreted as thermal photons escaping at the photosphere of a highly relativistic jet (Ryde 2004). Figure 1.15 shows a sample of three different spectrums, from left to right: non-thermal, thermal, and non-thermal with a thermal component.
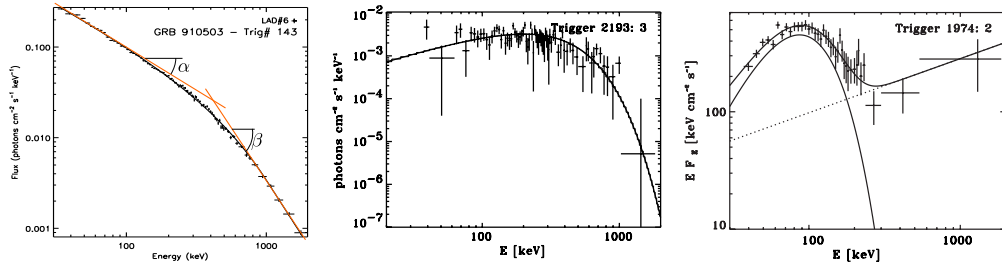
Figure 1.15: Three spectrums of GRBs. (Left) Spectrum showing a non-thermal emission (the power law indexes: low energy index α = -1 and the high energy index β = -2.4). (Center) A thermal spectrum well fitted with a blackbody model. (Right) A spectrum displaying both a thermal component (solid line), and a power law non-thermal component (dotted line). (Credit: Kaneko et al. 2005; Ryde 2004 & Pe'er et al. 2008).

1.6.2 GRB RADIATIVE EFFICIENCY

The radiative efficiency (η_γ) is a very important and useful parameter to understand GRBs. It is a measurement of how efficiently the jet kinetic energy is converted to radiation (γ-photons in the prompt emission). It is defined as (Zhang et al. 2007b):

$$\eta_\gamma = \frac{E_\gamma}{E_\gamma + E_K}$$

Where E_γ is the energy of the prompt emission radiation, and E_K is the kinetic energy that remains in the afterglow after the prompt emission phase. This definition assumes that after the prompt emission there is no engine activity and hence no additional energy injection. In Zhang et al. (2007b) η_γ was estimated for 31 Swift GRBs. The efficiency varies from a burst to another but is found < 10% in general (Zhang et al. 2007b. More details on η_γ can be found in § 4.4.4)

1.7 THE COLLAPSAR MODEL

A highly relativistic outflow and a huge isotropic equivalent energy output are two essential requirements to explain the prompt emission. One privileged structure to explain the two above is a well-collimated (5 – 10º), and highly relativistic jet ($\Gamma > 100$) (the standard model, Piran 2000). Such a structure can be found in accretion disks (Stellar BHs and AGNs). However, the short time scale of GRBs excludes any AGNs, and implies a stellar size object. In SGRBs, the very short timescale (often in the order of milliseconds) is puzzling, but is generally explained by compact objects merging, such as NS-NS or NS-BH systems, although this presents serious limitations (Zhang et al. 2007 & 2009) (see Figure 1.10). LGRBs requires an engine of a longer duration, from 2 ~ 1000 seconds. The answer was in the core-collapse of massive compact stars (Wolf Rayet), it is the collapsar model (Woosley 1993; MacFadyen & Woosley 1999, hereafter MW99). The collapsar model uses a common stellar object (WR stars) to explain LGRBs emission and rate.

The highly rotating BH, born in the center of a massive rapidly rotating Wolf-Rayet, star after its iron core gravitationally collapses, can power the well-collimated highly relativistic jet: The accretion onto the BH produces a considerable amount of energy (through MHD or neutrino annihilation process), which powers two polar jets, and as the jets breakout out from the progenitor it will accelerate to reach highly relativistic Lorentz factors (MW99). Thus, prompt emission features and the energy output can be explained by an on-axis observation of a highly relativistic jet breaking out a massive star (Figure 1.16).

This model has two essential requirements: i) LGRBs must be associated with high SFR regions in the universe, as they must be related to massive stars death, and ii) the metalicity should be low, in order to keep the rotational momentum of the star and produce the rapidly rotating BH. Both requirements have been confirmed by observations of LGRB host galaxies (Savaglio et al. 2009), although there have been few rare exceptions (such as GRB020127; Berger et al. 2007). Furthermore, observations of LGRB sites confirmed their link to SNe explosions, and thus to massive

stars death phenomena (i.e: GRB980425/SN1998bw, Iwamoto et al. 1998; and GRB030329/SN2003dh, Hjorth et al. 2003). Such SNe were categorized into a sub-class, called Hypernovae whose explosion energy is ~10^{52} ergs (Nomoto et al. 2006a and the references within).

Finally, special-relativistic numerical calculations on massive WR star models did confirm the collapsar scenario and its capacity to explain GRBs, in particular the successful launch of the required highly-relativistic and well-collimated jet (MW99; Aloy et al. 2000; Zhang et al. 2003). Thus, the above statements justify the general popularity and acceptance of the collapsar model in GRB community, which this thesis is based upon.
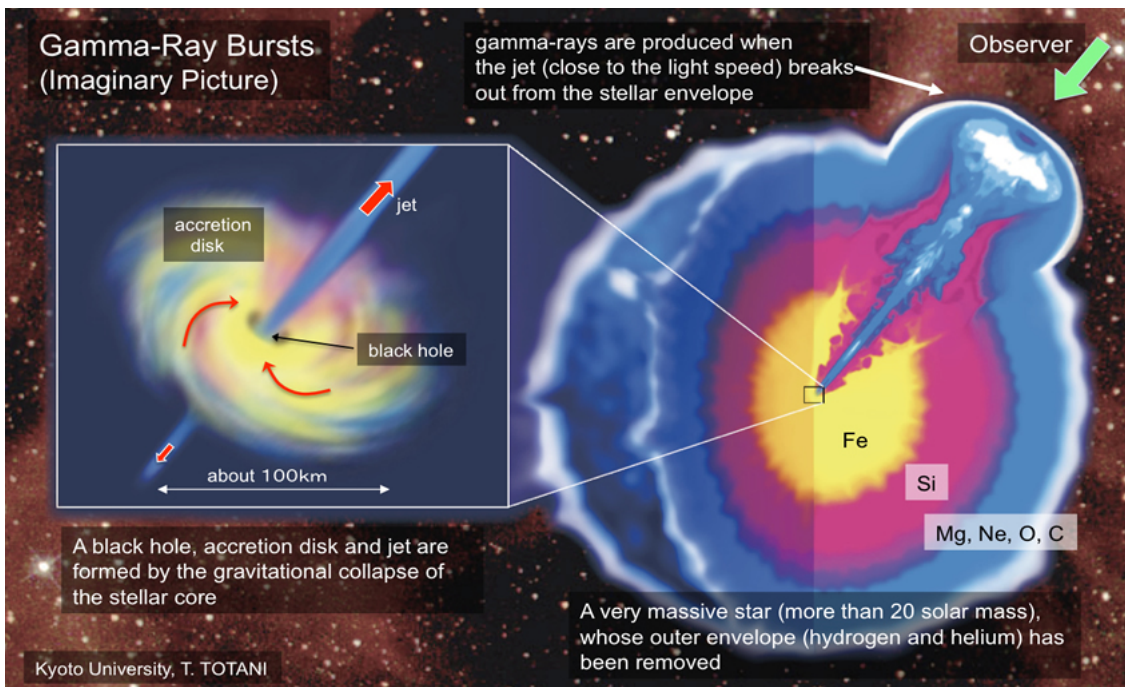
Figure 1.16: Imaginary illustration of the collapsar model and its key elements: A massive star that has lost its stellar envelopes (~ 20 solar masses WR), a rapidly rotating BH-accretion disk system – the engine – in the center of the iron core (2~3 solar masses) and two relativistic polar jets (Credit: Totani T., University of Tokyo)

1.7.1 DIVERSITY OF GRBS

Although our knowledge on GRBs has increasingly improved with the fireball and collapsar models, hence LGRBs origin could be explained; but many questions remain unsolved. Among the remaining issues is GRBs' diversity and irregularity. Since the launch of Swift the population of GRBs have significantly increased. With the improving statistic, more and more irregular GRBs are found. In this context, it became difficult to define all GRBs in one pattern and some suggestions for variant models have arisen (such as the "magnetar model"). GRBs are exclusively diverse compared to other astronomical events (i.e: as SNe). A diversity and irregularity in:

- *Light curves*: Especially in the prompt emission, GRBs are very diverse always-presenting unique shapes (Figure 1.12).

- *The total energy (and luminosity)*: From Very-Energetic ($E_{iso} \sim 10^{54}$ erg), to soft/weak *ll*GRBs ($E_{iso} \sim 10^{47\text{-}49}$ erg). A good illustration of this energetic diversity is the Amati relation where GRBs are spread over $5 - 6$ orders of magnitude (Figure 1.17: Amati et al. 2009 & 2010).

- *Diversity in duration and timescale* (Figure 1.18): From few seconds to the newly discovered Ultra-Long (ULGRBs, $\sim 10^4$ s) (Levan et al. 2014).

- *And other irregularities*: thermal and non-thermal components, strange GRBs inconsistent with the standard model (e.g: GRB 100316D) or showing a plateau (magnetar?), dark GRBs, GRBs showing dead times etc.

With the increase of such peculiar GRBs, their nature/origin is challenging the collapsar and implies an ultimate question *"How would the collapsar model explain all this irregularities?"* This thesis will explore a diverse version of the collapsar model in order to investigate this issue.
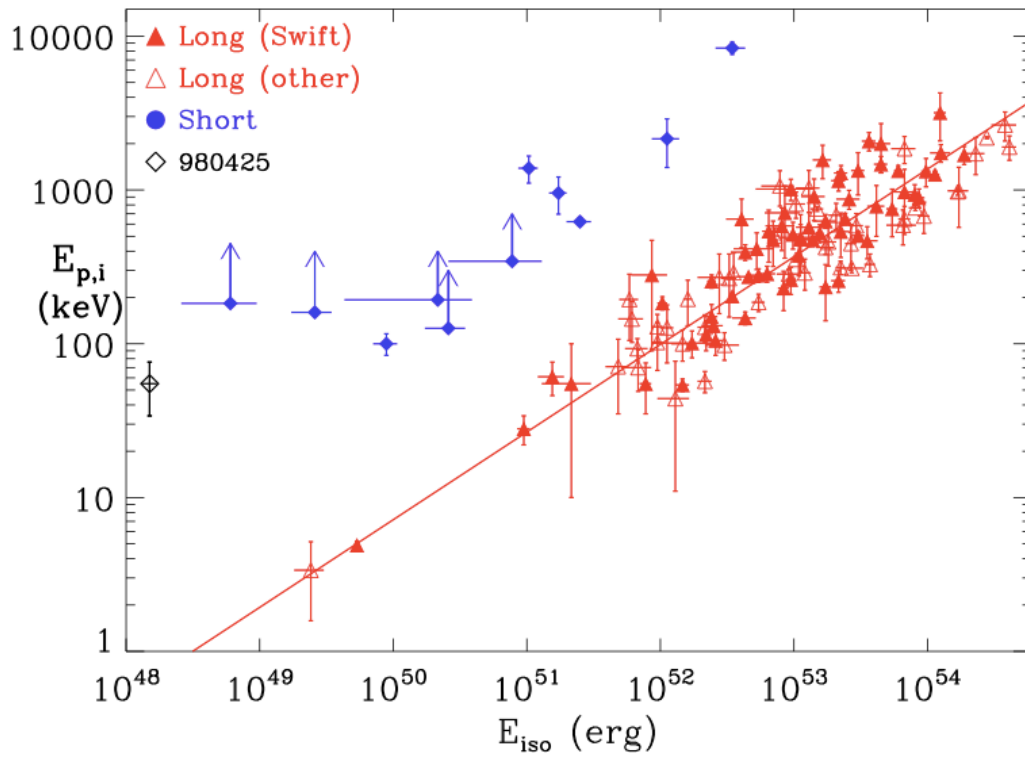
Figure 1.17: The Amati relation, a correlation of the energy at which the spectrum peaks $E_{p,i}$ with the isotropic equivalent energy E_{iso} (both in the rest frame of the GRB). 108 LGRBs are shown, Swift and other detections, in filled and unfilled red triangles respectively. SGRBs, in blue, are outliers. (Credit: Amati 2010)
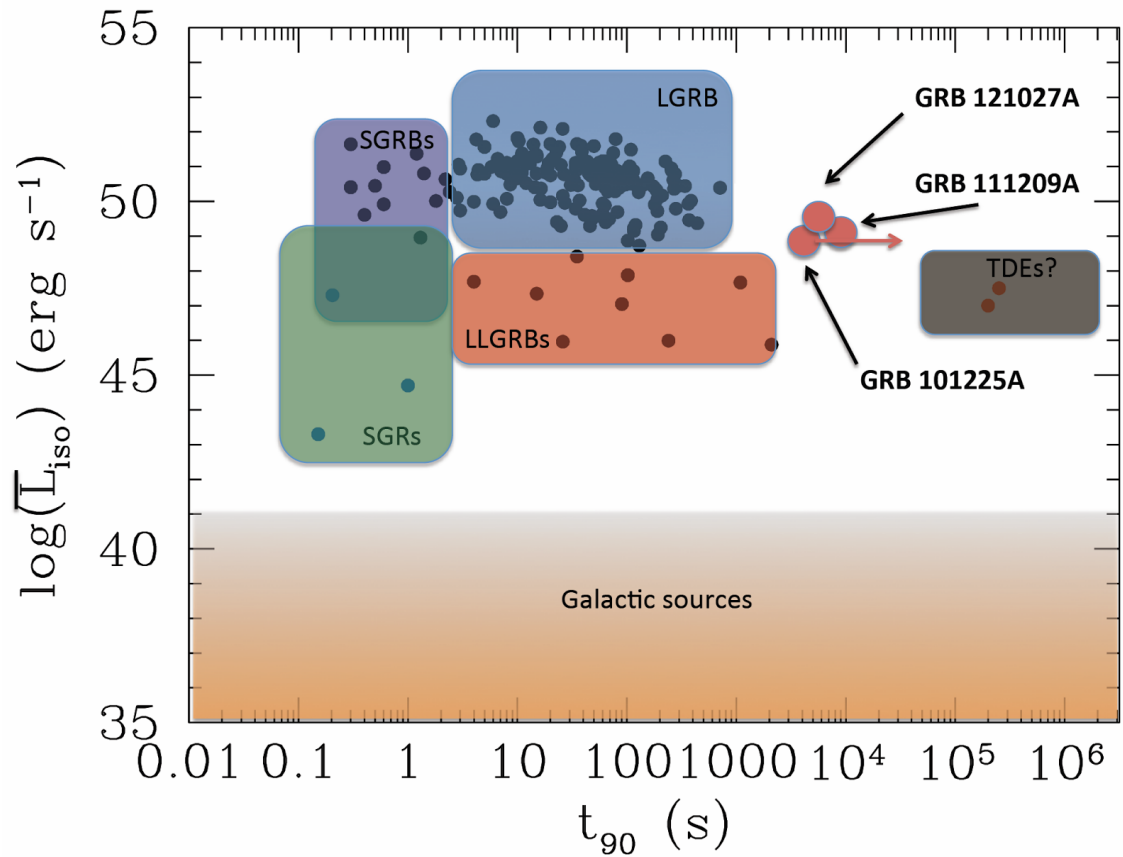
Figure 1.18: The different classes of GRBs, as a function of duration T_{90}, and the average luminosity. From left to right: SGRBs, LGRB, *ll*GRBs, and 3 ULGRBs. (Levan et al. 2014)

1.8 ORGANIZATION OF THE THESIS

After the Swift revolution, GRB detection has increased qualitatively and quantitatively, and with it the GRB diversity and questions on its origin. Here, I will address this issue with numerical simulations on the collapsar model. I analyze the effect that diverse collapsar engines, in terms of duration (and opening angle later on), would have on the GRB, and investigate how this would account for some of GRB diversity in nature.

This thesis is organized as follows: In § 2 I summarize the properties of a specific class of GRBs (*ll*GRBs), which this study findings might explain the very debated features. In § 3, I review the previous numerical studies on the collapsar model, and explain my motivation, the originality, and the research plan. In § 4, I explain the stellar model, the grid system and the jet initial conditions for a series of engine models. I also explain the procedure used to derive the angular and temporal properties from the data. The results are analyzed in § 5. The astrophysical implications for GRBs and *ll*GRBs, as well as the SN emission are discussed in § 6. Then, in § 7, I investigate the effect of the initial opening angle on the findings. Finally, the conclusions are presented in § 8. After the bibliography in § 9, and for more information about the code, § 10 presents some tests, to show its consistency.

2 LOW LUMINOSITY GAMMA-RAY BURSTS

"The treasures hidden in the heavens are so rich that the human mind shall never be lacking in fresh nourishment." — *Johannes Kepler*

2.1 THE PROBLEMATIC LOW LUMINOSITY GRBS

Since its discovery, *ll*GRBs class is at the center of attention of GRB astronomers. The study of *ll*GRBs allows understanding the universal picture of GRBs phenomena in the universe on a larger and generalized scale; from low redshift to high redshift; and from soft to hard & high-energy domain. *ll*GRBs present several peculiar features that make them debated. Apart from their softness, *ll*GRBs present two features differentiating them from the standard GRBs: High rates and strong SN connection.

2.1.1 LLGRBS' HIGH RATE

The considerably low redshifts of the observed *ll*GRBs suggest a huge density of these events, about 100 to 1000 times those of standard GRBs (Bromberg et al. 2011a and the references within). Below is a summary of major studies where the rate of *ll*GRBs has been estimated. Note that the rate of the standard GRBs is ~1 Gpc^{-3} yr^{-1} (Piran et al 2006 & Liang et al. 2007):

- Coward 2005: ~220 Gpc^{-3} yr^{-1}

- Piran et al. 2006: ~110^{+180}_{-20} Gpc^{-3} yr^{-1}

- Soderberg et al. 2006: ~260^{+490}_{-190} Gpc^{-3} yr^{-1}

- Cobb et al. 2006: ~300 times GRBs

- Liang et al. 2007: ~325^{+352}_{-177} Gpc^{-3} yr^{-1}

- Guetta & Della Valle 2007: ~380^{+620}_{-225} Gpc^{-3} yr^{-1}

Figure 2.1 shows the rates of *ll*GRBs and the standard GRBs as a function of redshift, estimated from the observations. According to Liang et al. (2007) and the studies cited above, the observation suggests that the rate of *ll*GRBs is, at least, about 100 times higher than that of the standard GRBs! This would imply that *ll*GRBs are much more common than GRBs, at least at low redshift, and that GRBs are the minority and probably the exceptional collapsar case. Hence, *ll*GRBs and their origin is a very important issue in GRB astronomy.
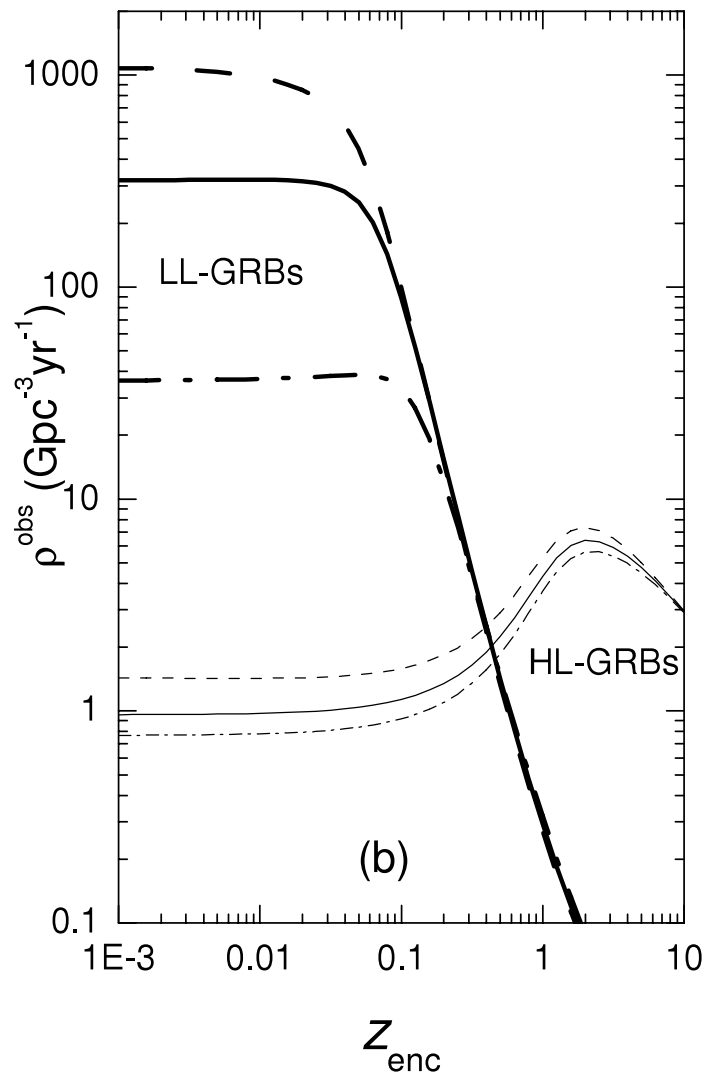
Figure 2.1: The estimated event density (according to the observations) for both *ll*GRBs and the standard GRBs, considering the volume enclosed by the redshift $z_{enclosing}$. The different line styles are for different adopted model parameters. *ll*GRBs largely dominates at low redshift. (Credit: Laing et al. 2007)

2.1.2 THE STRONG SN CONNECTION

*ll*GRBs always hold a high level of evidence for a SN explosion, at the contrary of standard and energetic GRBs that are generally SN-less (see more details see § 6.3: Figure 6.8 and Table 6-2). This might be related to *ll*GRBs relatively low redshift

(Hjorth & Bloom 2011), or to nucleosynthesis and ^{56}Ni abundance (Tominaga et al. 2007). However, there are few cases where no SN emission could have been detected for typical GRBs, down to very deep limits (GRB 060505 & GRB 060614, see: Figure 2.2). Such SN-less LGRBs represent the evidence that not all LGRBs are associated with SN/HN explosions, in contrast with *ll*GRBs. Hence, the SN is one of *ll*GRBs peculiar, and highly debated, features (Hjorth 2013). Why? In § 6, I will present one possible explanation.
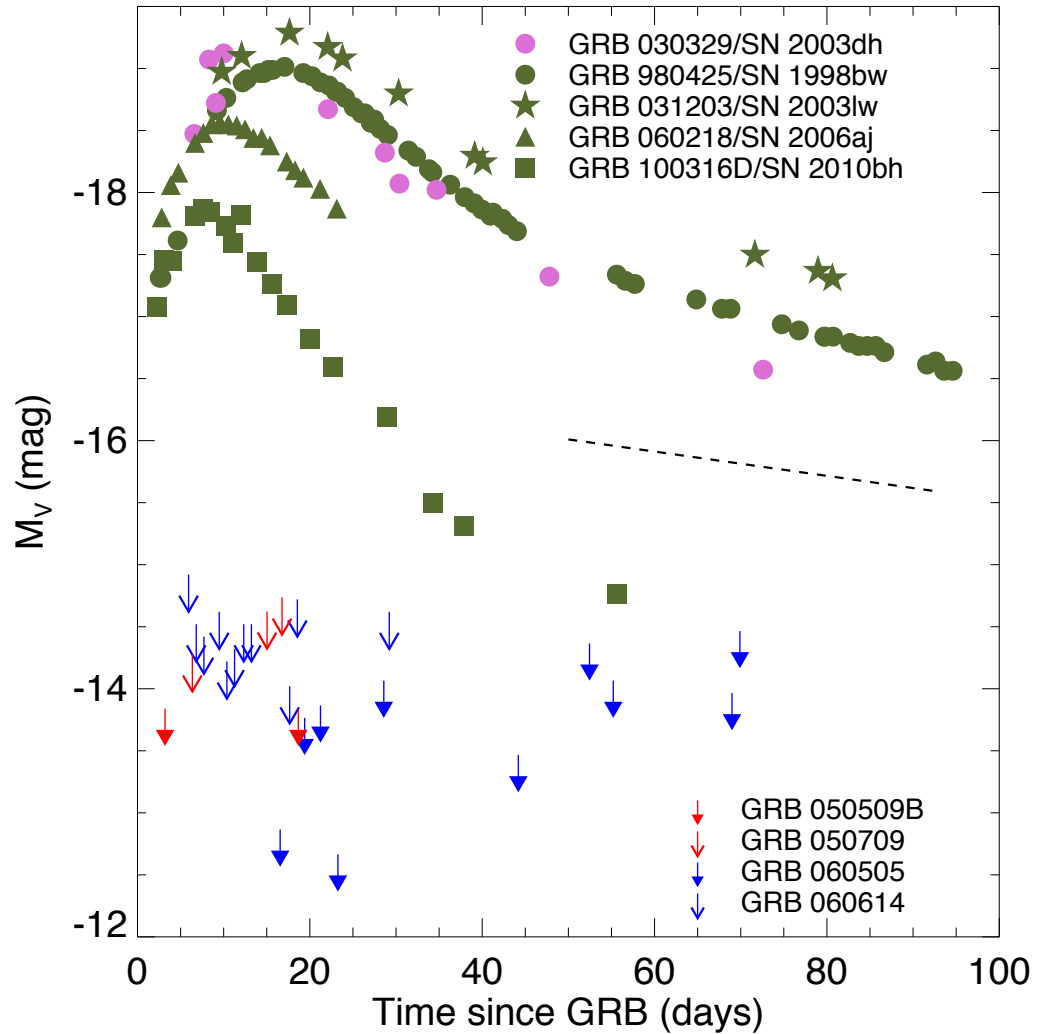
Figure 2.2: Light curves for the clearest supernovae associated with gamma-ray bursts (all grade A, apart from SN 2012bz). In olive are supernovae associated with *ll*GRBs. On orchid is SN 2003dh, associated with the standard and energetic GRB 030329. Upper limits on supernova emission are also shown: for LGRBs (blue) and SGRBs (red). (Credit: Hjorth & Bloom 2011; Hjorth 2013)

2.2 OTHER PROPERTIES

2.2.1 LIGHT CURVE & SPECTRUM

As well illustrated in Margutti et al. (2013) & Schulze et al. (2014), *ll*GRBs' light curves largely differ from those of the classical/fireball GRBs (see: Figure 2.3). *ll*GRBs are much smoother, and much softer (up to ~10 000 times softer), lacking the high energy hard tail (thus no compactness issue, and a low Lorentz factor). It is a very rare type of features among the standard GRBs. As only few events have been detected so far, the statistic of *ll*GRBs is not very good yet. But, compared with the light curves of the standard GRBs – which are anything but smooth – the chance that the few known *ll*GRBs are smooth by chance is almost zero (Nakar 2012).
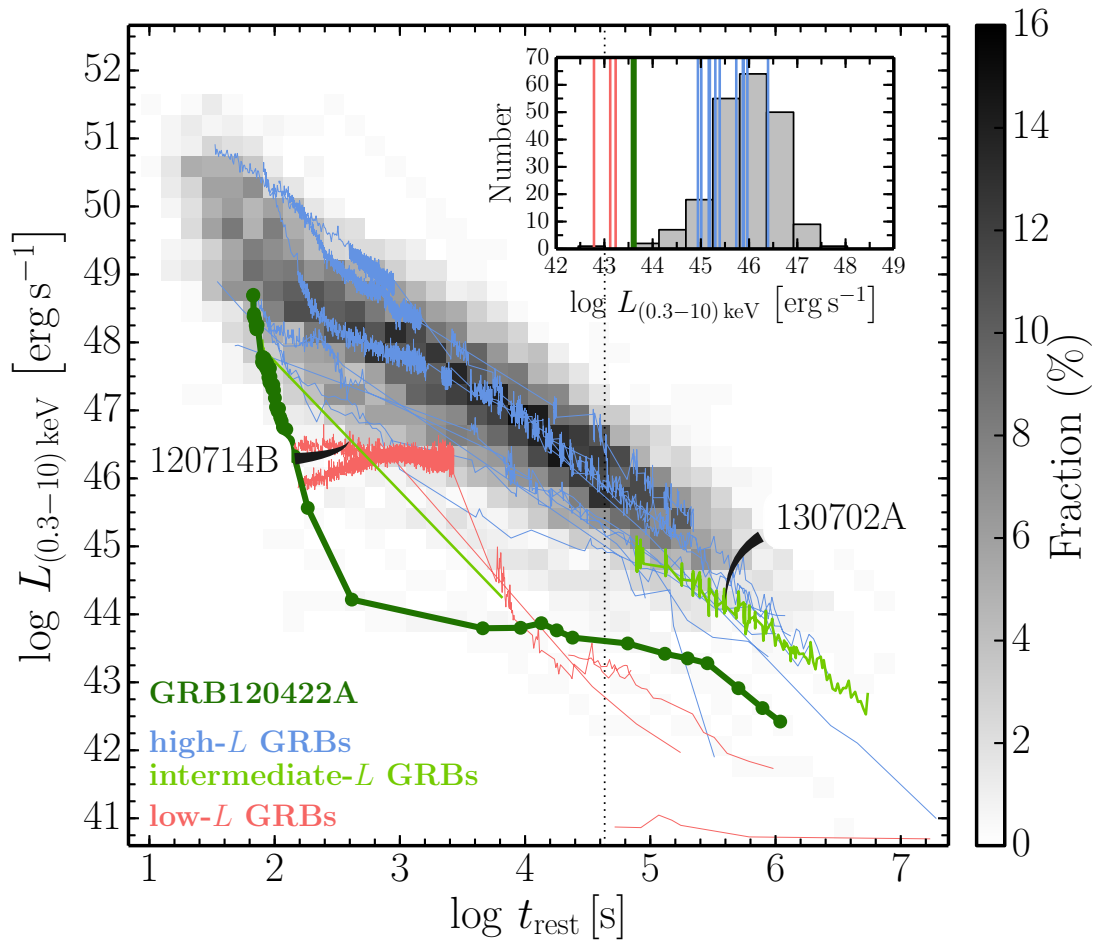
Figure 2.3: Light curves (X-ray) of sub-energetic GRBs (low and intermediate luminosity), in comparison with the classical high-luminosity GRBs in the background (273 Swift SN-less GRBs). The inset shows the luminosity at 12 hours after the burst (dotted line). In the inset, the luminosities are shown, in particular for 3 *ll*GRBs (GRB 031203, GRB 060218 & GRB 100316D), much fainter than typical Swift GRBs. (Credit: Schulze et al. 2014)

2.2.2 EJECTA

The modeling of optical, and radio emissions, allows estimations of the kinetic energy and ejecta velocity at different times. This have allowed the estimation of the energetic and relativistic properties of a large number of events; non-relativistic events (SNe), mildly relativistic (*ll*GRBs), and highly relativistic (GRBs). Margutti et al. (2013), presented an interesting "energy – velocity" picture (see: Figure 2.4). The profiles, suggests (with the help of numerical simulations; Lazzati et al. 2012), that the degree of collimation is dramatically different; from high to low: GRBs, *ll*GRBs and SNe. This was a very interesting result, as it links the three events tightly, and put the *ll*GRBs as an intermediate event, between SNe & GRBs.
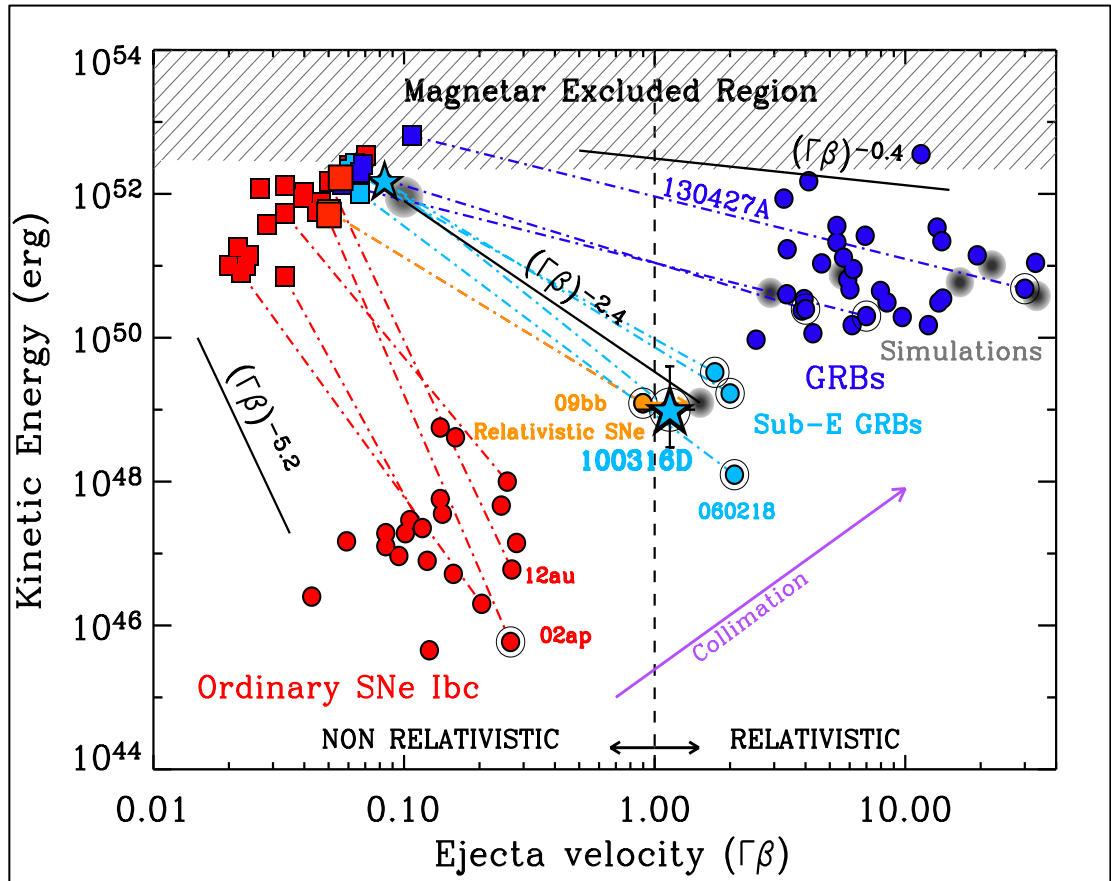
Figure 2.4: Kinetic energy – velocity profile, for a diversity of events: SNe (red), *ll*GRBs (light blue) and GRBs (blue). The different types of events show different slopes, and suggest different collimation levels (Credit: Margutti et al. 2013).

2.3 THE ORIGIN OF LLGRBS

In the context of the peculiar features above, questions on the origin of *ll*GRBs arise: "What origin can explain *ll*GRBs features?" "What makes them different from the standard GRBs?" "How *ll*GRBs are related to the standard GRBs?" Two major concepts have been suggested to explain the origin of *ll*GRBs.

2.3.1 THE UNIFICATION MODEL AND LLGRBS

Soon after the identification of the sub-energetic *ll*GRBs, named XRFs, Nakamura (2000) & Yamazaki et al. (2002 & 2004) proposed a model to unify all GRBs (SGRBs, LGRBs and XRFs/*ll*GRBs) in one general picture. Ramirez-Ruiz et al. (2002) & Lamb et al. (2003 & 2005) proposed a similar unification model as well. The main idea of the unification model is similar to that of AGNs (Antonucci 1993):

> *"Observation of the same source by different observers, on different lines of sights, produces different properties and hence different events"*

The unification model claims that *ll*GRBs and GRBs are the jet-explosion viewed at different angles. Hence, according to this model GRBs and *ll*GRBs origin is the same (Nakamura 2000; Yamazaki et al. 2002, 2004; Lamb et al. 2005): Typical collapsar events, with the same engines as in MW99: $T_{inj} >> T_{breakout}$ (see Figure 3.6). The unification model is an attractive option to explain *ll*GRBs, but *"could off-axis observation of standard GRBs, alone, explain llGRBs high rates?"* One serious limitation is that this model implies a maximum rate (Cobb et al. 2006). As jet break observations, in afterglow light curves of standard GRBs, implies a jet opening angles of ~10º (Frail et al. 2001), the maximum rate of *ll*GRBs to GRBs in the unification model would be $1/(1 - cos\theta_{jet\ GRB}) \approx 65$ (Cobb et al. 2006). This is far below *ll*GRBs rates, above. Hence: *"are llGRBs from standard GRBs engines? if not what alternative model would explain them?"*

2.3.2 LLGRBS FROM FAILED JETS

Bromberg et al. (2011a & 2012), by analyzing the breakout times, proposed a different origin for *ll*GRBs (for more details see § 3.3.2.3):

> *"At the opposite of typical GRBs arising from successful collapsars, llGRBs are from collapsar-failed jets with: $T_{inj} \leq T_{breakout}$"*

This is in agreement with the observation suggesting that *ll*GRBs are from considerably weaker jets (than GRB jets) that fail to breakout (e.g: Campana et al. 2006 & Mazzali et al. 2008). This would suggest that GRBs engines/jets are significantly different from that of *ll*GRBs.

Lazzati et al. (2012) who used different engine durations found that, indeed, engines with $T_{inj} \leq T_{breakout}$ would produce *ll*GRB-like ejecta. But unfortunately no conclusion could be made on the rates or SN connection.

Nakar et al. (2012) showed that *ll*GRBs prompt emission can be explained with a shock breakout of a failed jet, supporting Bromberg et al. (2011a & 2012) results. In a very recent study, Nakar (2015) proposes that an extended mass around the progenitor might bump the jet and produces a shock breakout that explains *ll*GRBs spectra and light curve. Nakar (2015) theoretical model would be interesting to investigate numerically, in the future. Hence, a failed jet, for whatever reasons, is the attractive model to explain *ll*GRBs. However, the extent to which failed jets would explain llGRBs' peculiar features, mentioned previously, have not been studied numerically yet.
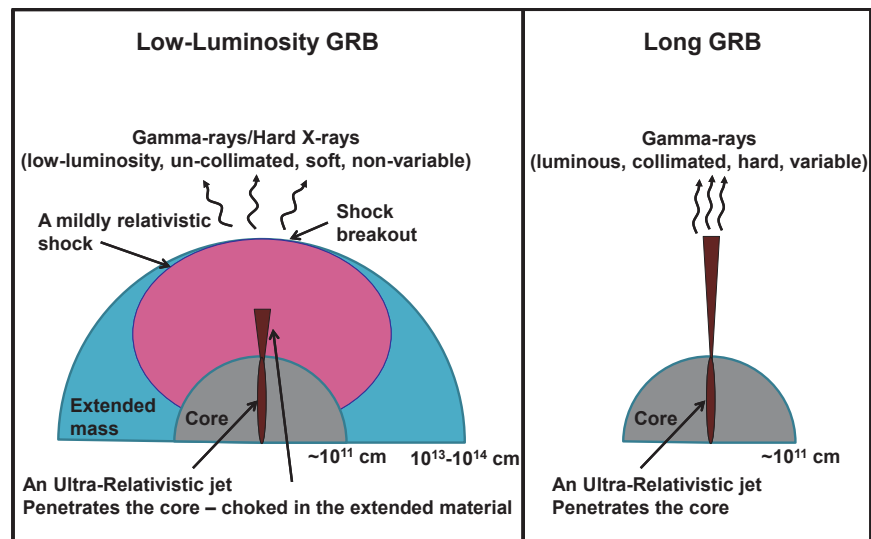
Figure 2.5: A recently published illustration on how GRBs and *ll*GRBs might be related, and hence unified in a general collapsar picture, based on the presence or not of an extended mass. (Credit: Nakar 2015)

2.3.3 THE OPEN QUESTION

In this chapter I presented the two main models, which debate on the origin of *ll*GRBs. The unification model is purely theoretical, while the failed jet model relays on estimated breakout times and the observed GRB durations. Having two models within reach – and not simply one model – my ultimate interrogation was, still, what is the origin of *ll*GRBs? Could one model be wrong? Or is it rather, the combination of the two models?

In this thesis, I put both of the models to a numerical test, in order to find a clear answer of the questions above.

3 PREVIOUS NUMERICAL COLLAPSARS

"The only feature that all but one (and perhaps all) of the very many proposed models have in common is that they will not be the explanation of γ-ray bursts. Unfortunately, limitations of time prevent me from telling you which model is the exception. (If I did so, I would suggest Black Hole ridden by Accretion as the favorite in the race with Glitch as a dark horse if only because so many different horses and jockeys are riding under that name.)"
– Mal Ruderman, Texas Conference, 1974

3.1 OVERVIEW OF THE APPROACH

Immediately after the theoretical establishment of the collapsar model (MW99), numerical studies have been considered as a basic approach to explore the model, and its consequences (Aloy et al. 2000 & Zhang et al. 2002). Since then, numerical investigations of the collapsar model using 2D Special Relativistic Hydro-Dynamic codes (2DSRHD) have flourished. Many ideas have been investigated, below is a list of some of major works:

- GRBs and SN energy (Zhang et al. 2003),

- Jet hydrodynamics and phases (Lazzati et al. 2007 & ML07)

- GRB precursors and dead times (ML07)

- GRB progenitors (Mizuta et al. 2009)

- GRB variability (Morsony et al. 2010)

- Photospheric emission from the collapsar jet photosphere (Mizuta et al. 2011 & Nagakura et al. 2011)

- Engine duration and GRBs diversity (Lazzati et al. 2012)

- Ultra-Long-GRBs (Nakauchi et al. 2013)

- The duration distribution of GRBs (Lazzati et al. 2013b)

- Amati relation (Lazzati et al. 2013a)

- Non-thermal emission and polarization: Using complex jet structure (stratified jets and precession) (Ito et al. 2014 & 2015)

In general, two main issues have been given a particular importance: i) the central engine, its mechanism, its environment, and its relation to the prompt emission; ii) the relativistic jet radiative process and how does it produce the prompt emission properties: hard emission, variability, timescale, polarization etc. This thesis would investigate GRBs through the former issue (i). In this chapter, I will summarize the previous numerical studies, and explain how they contribute to the understanding of GRBs. Then, I present my motivation and the research plan.

3.2 PREVIOUS STUDIES AND THE NUMERICAL PROCEDURE

GRBs and their central engines have been progressively studied in both analytical and numerical approaches using the collapsar model. In one major work, Matzner (2003) analytically investigated constraints on the progenitors in the collapsar model, in terms of GRB duration and driving mechanisms. He argued that He or CO Wolf-Rayet stars are plausible GRB progenitors, as the duration of many LGRBs necessitates a compact progenitor $\sim 10^{10}$ cm. Nagataki (2010) carried out general relativistic Magneto-Hydro-Dynamical (MHD) simulations. He studied collimated jets launched from a rotating BH via MHD process. Nagataki (2010) confirmed that more rapidly rotating progenitors would launch more energetic and powerful jets. Many similar (and different) studies have since been undertaken, but the detailed properties of the central engine are still far from understood.

On the other hand, by assuming that the engine is capable of producing some relativistic outflow, deep in the progenitor, GRB jets have been investigated independently from the central engine specific mechanism. Many studies have been carried out in this way considering a certain injection nozzle (e.g. Aloy et al. 2000; Zhang et al. 2003; Umeda et al. 2005; Mizuta et al. 2006, 2009; Morsony et al. 2007, 2010; Woosley et al. 2007; Lazzati et al. 2009, 2010, 2011, 2013a; Nagakura et al. 2011; etc.). These studies investigated the dynamics of a collimated and relativistic jet drilling stellar mantle. This widely used simplified method allows us to compare jet properties with basic observational GRB properties. Thus, one may constraint central engine temporal, angular, and energetic properties.
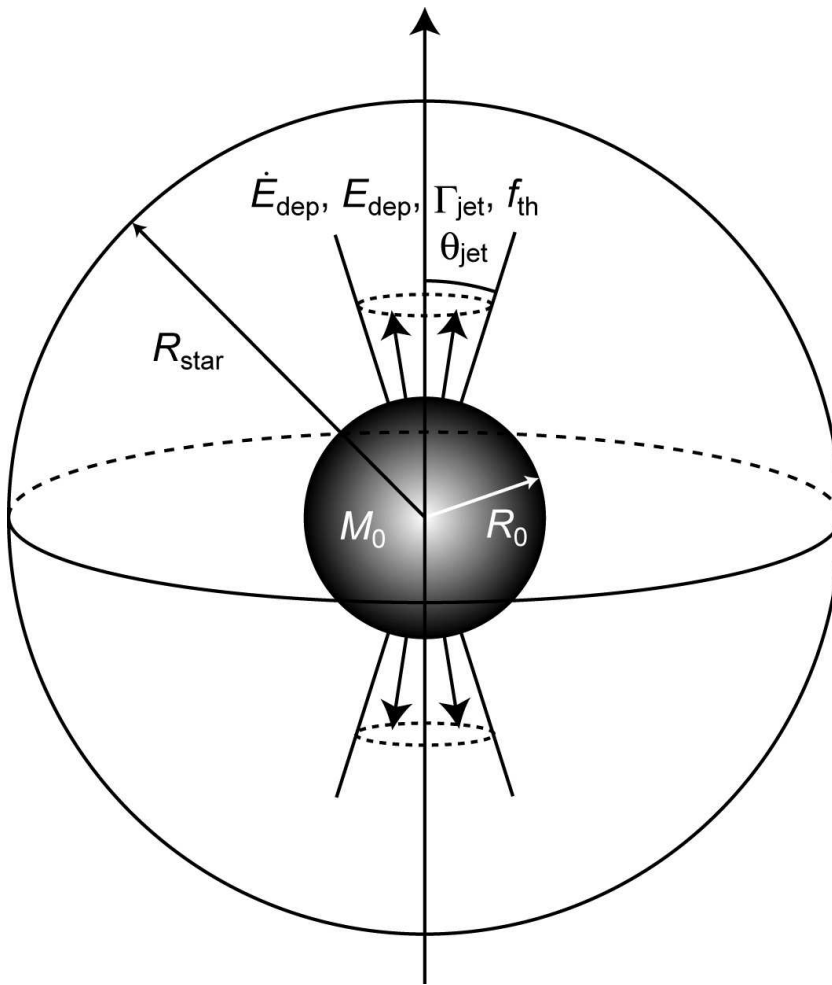
Figure 3.1: Illustration of a collapsar explosion, with the inner core and the two polar jets. Assuming a spherical symmetry the explosion can be simulated in 2D. The key elements to the numerical modification of the explosion are indicated: stellar radius, the injection nozzle, the energy deposition, the jet Lorentz factor, opening angle and thermal energy fraction (Credit: Tominaga et al. 2007)

3.3 The Engine Duration

3.3.1 In Major Numerical Studies

Most major works using 2D hydrodynamic simulations have focused on relatively long engine duration models, in the range of ~10 - 100 seconds, with many engine duration models $\geq$ 50 seconds. Zhang et al. (2003) used engines with durations > 10 sec, and studied the initial parameters for jet propagation inside the progenitor star. Umeda et al. (2005) used a 9 sec engine to investigate Hypernova GRB. Mizuta et al. (2006), considering a 10 sec injection duration, studied the effect of the initial Lorentz factor and the initial specific internal energy on the jet properties, such as angular and relativistic properties. They pointed out that transition from GRBs to XRFs (or *ll*GRBs) could be due to different initial specific energies. Morsony et al. (2007) (hereafter ML07), one major study, considered a 50 sec injection in order to study temporal and angular properties of the jet. The jet propagation was divided into three phases: precursor, shocked and unshocked. ML07 considered the possibility of observing dead times in the GRB light curve, as the shocked phase is narrow and can not be observed at some specific viewing angles. Lazzati et al. (2009), considered the same jet initial conditions of ML07, including the same 50 seconds engine duration, to study the efficiency of the jet using the photospheric model. Morsony et al. (2010) considered, again, the same 50 seconds duration to explain GRBs variability using, variable entropy and variable baryon load engines, and compared them to a uniform engine. Lazzati et al. (2010) used the same engine as well (50 seconds), to consider possible SGRBs from the collapsar jet at 45º off-axis. Nagakura et al. (2011) focused on the timing of the jet injection in a rapidly rotating massive star, and its effect on the prompt emission, using a 30 sec engine, and the photospheric model to derive a thermal prompt emission. Mizuta et al. (2011) & Lazzati et al. (2011), both used the photospheric model to derive the GRB emission, for an engine of 100 seconds. Lazzati et al. (2013a) used different models, most of them with 100 seconds injection duration. Combined with different progenitors and viewing angles, Lazzati et al. (2013a) could successfully populate the same region of the Amati relation (Amati et al. 2002).

Lazzati et al. (2013b) studied the duration of the produced prompt emission, in relation to the duration of the engine using central engine duration > 10 seconds. They considered some reasonable assumptions on the SFR, redshift, and on the observed prompt emission. One of their most interesting results is that BATSE LGRBs might be explained by engines of an average duration of ~ 20 seconds, and that long engines ~100 seconds, must be rare. Lazzati et al. (2013b) also concluded that even shorter engines might be contributing to some of the observed GRBs. Accordingly Lopez-Camara et al. (2014) considered a uniform 20 seconds engine (with a 40 seconds variable engines), to study the effect of variable engines and how it can justify the observed variability observed in GRB light curves.

Although most of the hydrodynamical simulations focused on long injection duration, a few short engine models have been studied. One rare study is Mizuta et al. (2009) where the injection duration was less than 10 sec (4 sec) to investigate the angular energy distribution of a GRB jet, using different progenitors. Another case is Lazzati et al. (2012) who studied the kinetics of the ejecta by carrying out simulations with injection durations from ~3 to 10 sec.

Figure 3.2 summarizes major numerical simulations of collapsar jets, showing the engine luminosity as a function of the engine duration. Although the central engine and its duration is one very important and not a well-understood ingredient in GRB theory, effects of the duration have not been widely studied (least of all, in the range of ~ 0.1 - 10 seconds). Furthermore, the considered engine energy was often very high (> 10^{52} ergs). The collapsar model claims that an output of ~10^{52} ergs is already very energetic phenomenon requiring a hyperaccreting black hole (MW99). However, such high energies (possible only in even much extreme and rare conditions) have been largely considered. Considerations of such high energies and long durations reflect the focus on the extreme GRBs (although extreme GRBs are rare events).
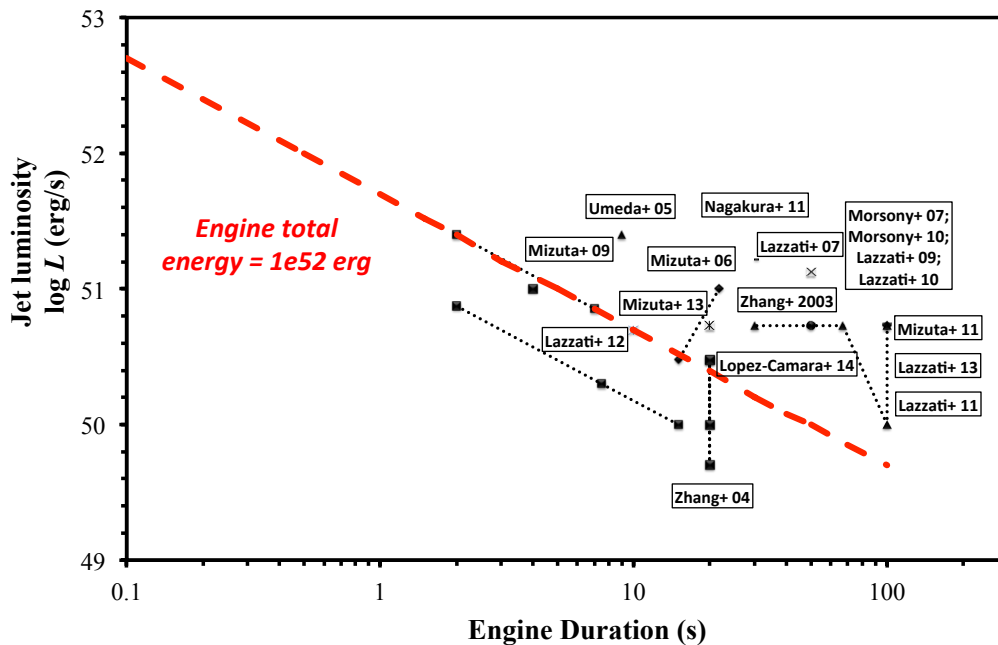
Figure 3.2: Major previous 2D simulation using the collapsar scenario, in terms of engine duration and luminosity. Black symbols with dotted lines show the domain of previous studies. The red dashed line shows region of an engine with a total energy of 10^{52} ergs.

3.3.2 Evidence Of Diverse Engines

Although short engine durations are very rare in the previous studies, it is most likely the case that they are rare event in nature. There is evidence that not all collapsars are long engines, and that long engines as those cited above are just an exception and an extreme case. Here are some arguments that support this statement.

3.3.2.1 The Collapsar

Many of the previous numerical collapsars considered durations in the domain of ~50 – 100 seconds. This choice of long durations was considered as it favors the launch of the

energetic and highly–relativistic jets (thus explains some particularly extreme GRBs). In fact, the collapsar model original idea was to explain the mysteriously energetic GRBs (such as GRB 971214; MW99), as the general understanding of GRBs at the time of the collapsar model was about extreme and energetic events, only. The collapsar model explains such extreme events but only with extreme conditions – assuming extreme engine conditions – that would produce and explain the origin of such "energetic/cosmological" GRBs. I quote here from MW99's conclusion:

"We believe that the collapsar produces strong, hard GRBs like GRB 971214 only in the most extreme cases of high accretion rate and long duration - perhaps only for the most massive stars or those that have just the right angular momentum distribution". *"Our standard model gives about 10^{52} ergs; focused into ~1% of the sky and a duration of ~15 s; this matches the observed properties of GRB 971214 pretty well"*

The collapsar model focus on the "standard/cosmological/energetic GRBs" relating them to extreme conditions where long engine can be activated. However, it does not mention about the less extreme conditions, such as short duration engines, nor exclude them. The collapsar model states simply that GRBs' engines/jets are *"an extreme case, in extreme conditions"*, thus one would expect that these extreme engines/jets are one exceptional and most likely rare case, and much diverse engine durations exist in the universe (Lazzati et al. 2012).

Moreover, the collapsar model (MW99) relates the engine duration to the accretion time of the torus surrounding the BH and thus to very complex parameters, such as rotation, metalicity, magnetic field, etc. Thus, diverse engines in a wide duration range are theoretically expected considering the complexity of jet production mechanism and reflecting the diversity of these parameters in nature.

3.3.2.2 ROTATING COLLAPSARS

GRB, progenitors, before going through the gravitational collapse, are suppose to be very diverse, reflection diversity in the universe. As instance, the angular momentum must be different, from a progenitor to another, most likely related to the strength of stellar wind, and thus to the metalicity of the star. As the magnetic field, is strongly

related to the rotation of the core, the magnetic field will also differ for different rotating stars. This would lead to significant difference in the central black hole dynamics, spin and geometry (MW99). Thus, different rotations might have a strong effect on the engine and its intrinsic properties, such as the duration and the jet-opening angle (Harikae et al. 2009).

Harikae et al. (2009) shows clearly how progenitors with different rotations and different magnetic fields, result in different accretion disks, and different energy depositions: jet luminosity and jet collimation. This two means, in numerical simulation, the engine duration T_{inj} and the initial opening angle θ_0, respectively (see table 2 in Harikae et al. 2009). Harikae et al. (2009) findings suggest that slow rotation leads to high accretion rates – short-intense engines – while fast rotations produce lower accretion rates & more stable accretion disks, long-mild engines (Figure 3.3).

In other words, the diversity in metalicity, rotation and magnetic field in GRB progenitors, calls for diversity in the engine duration T_{inj} (and θ_0). To study collapsar events properly, as they take place in the universe, one should not be limited to certain engine durations (and certain opening angles), otherwise the study would be biased.
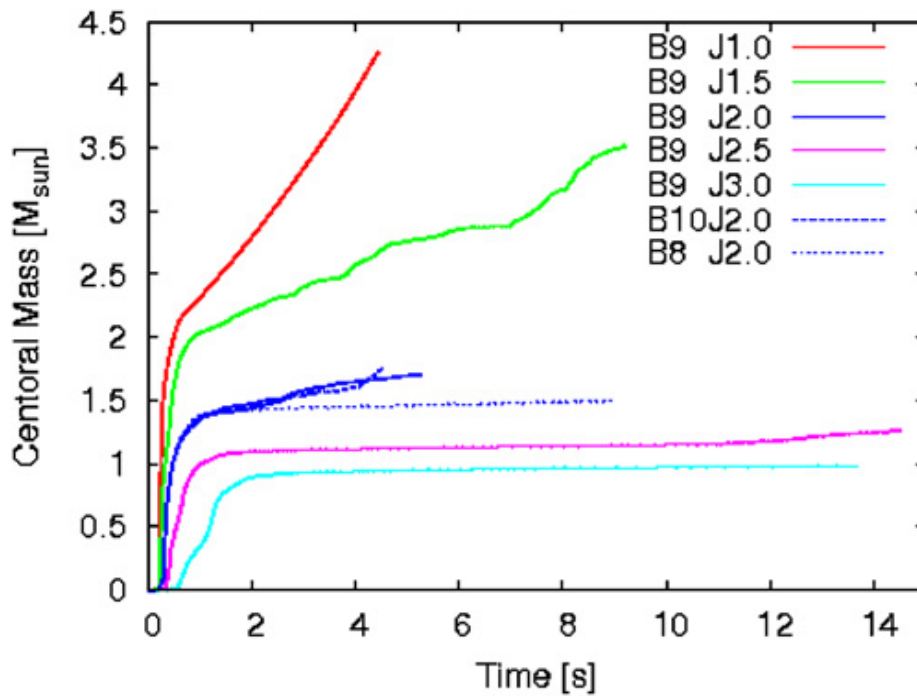
Figure 3.3: Numerical study on the effect of the angular momentum (J), combined with the magnetic field (B), on the accretion rate. The trend is that small rotation gives short intense engines, while large rotation leads to mild-long engines (Credit: Harikae et al. 2009)

3.3.2.3 FROM GRB BREAKOUT TIMES

3.3.2.3.1 FAILED JETS IN GRB POPULATION?

Bromberg et al. (2011a) is a unique study. By considering the assumption relating the duration of the prompt emission to the difference between the engine duration and the jet breakout time:

Prompt emission duration (T_{90}) ≈ Engine activity time (T_{inj}) – Jet breakout time (T_b)

Moreover, by developing an analytical model for relativistic collapsar jets (Bromberg et al. 2011b), and relating the jet breakout time (t_b) to some measurable parameters, an estimation of the breakout time for many GRBs could be developed using the following formula:

$$t_B \simeq 15\,\text{s} \times \epsilon_\gamma^{1/3} L_{\gamma,50}^{-1/3} \theta_{10^\circ}^{2/3} R_{11}^{2/3} M_{15\odot}^{1/3},$$

From light curves

llGRBs: 30°
LGRBs: 10°

$\rho \propto r^{-2.5}$

Taken as 0.2

llGRBs: from the SN
LGRB: 10^{11} cm & 15M$_{sun}$
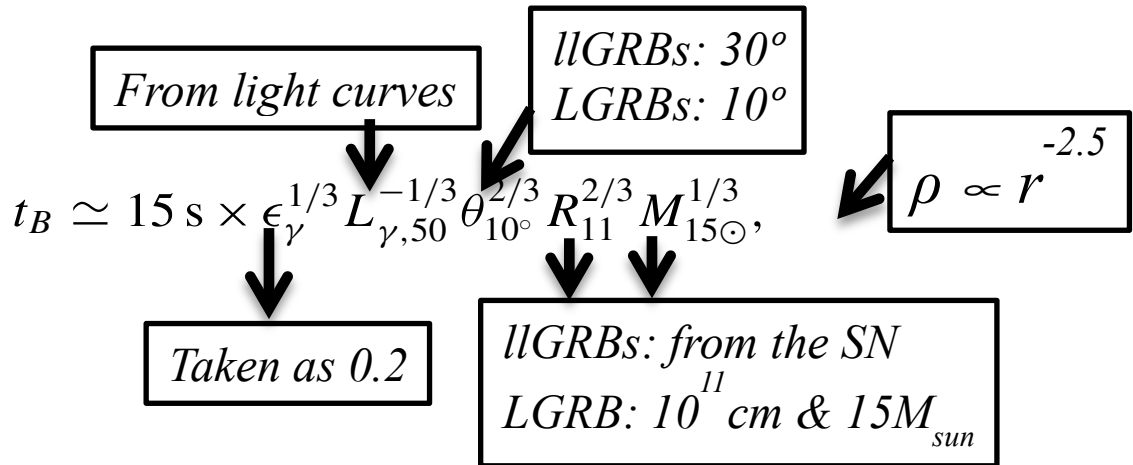
Bromberg et al. (2011a) compared the ratio of T_{90}/t_b. The finding (see Figure 3.4) was that the standard GRBs show an engine activity much longer than the breakout time ($T_{inj}/t_b \gg 1$). While *ll*GRBs, show instead engines shorter, in several cases shorter than the breakout time ($T_{inj}/t_b < 1$). This finding restarted the debate on llGRBs and their origin. However, more importantly it allows imagining collapsar engines different from the classical engines proposed by the collapsar model; shorter engines to explain the *ll*GRBs that posed huge rates (Soderberg et al. 2006 etc.).

Figure 3.4: The distribution of the ratio T90 over the breakout time (tb) for differnet type of GRBs (after Bromberg et al. 2011a).

3.3.2.3.2 A COLLAPSAR PLATEAU

Using the same assumption as in the previous section, one other work of Bromberg related to the engine duration showed that the distribution of GRBs for different instruments shows a plateau (see Figure 3.5). According to Bromberg et al. (2012) the plateau is a potential signature of the breakout time, since the engine duration distribution at the vicinity of the breakout time has to be flat. The plateau is discussed as a confirmation of the collapsar model.

A very interesting consequence of the plateau is that the distribution of GRBs at times longer than the plateau (where $T_{90} >> t_b$) would be dominated by the engine true duration distribution. The duration distribution at long duration (≥ 100 seconds) shows a steep decrease in events, and was fitted with a power law index $-4 < \alpha < -3$. This indicates that:

i)   Long engine durations (~100 seconds), must be rare and doesn't reflect the observed GRBs.

ii)   An extrapolation of the distribution at long duration (with the index $-4 < \alpha < -3$), would give an estimation of the total engine duration distribution. According to Bromberg et al. (2012), the extrapolation suggests that the there is a huge number of engines with short duration (failed jets, with $T_{inj} < T_b$).

Therefore, this is an additional evidence of the existence of a large population of collapsars with short engine durations, likely to be related to failed GRBs and most likely *ll*GRBs and their high rates (Bromberg et al. 2012).

Thus, the observed GRBs show some evidence of short engines, shorter that numerically considered so far. Such short engines' study might help understanding llGRBs.
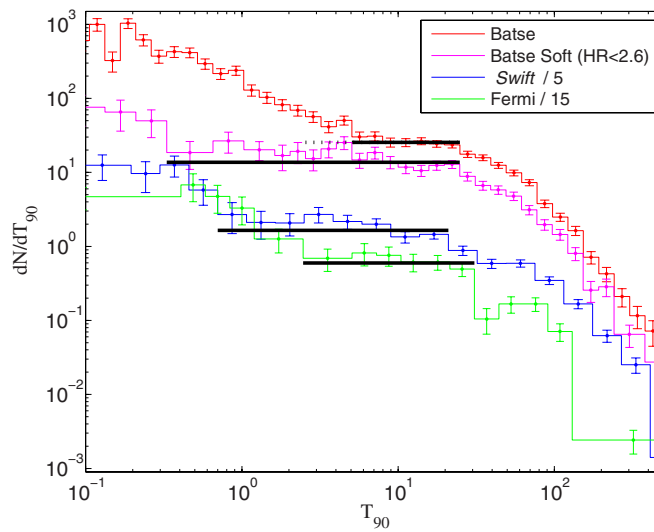
Figure 3.5: The duration distribution of the GRBs from different instruments as a function of the events duration (T_{90}). (After Bromberg et al. 2012)

3.3.2.4 BATSE GRBs AND THE ENGINE DURATION

As cited in § 3.3.1 Lazzati findings clearly suggest that the previous numerical collapsars used exaggeratedly long durations. Lazzati et al. (2013) study on the engine duration distribution, indicates that the diversity in GRBs (and their light curves), suggests that the average duration of the engine would be ~ 20 seconds, and shorter engines are likely, while engine durations of ~ 100 seconds must be rare. Lazzati et al. (2013), used the same as previously explained, relating T_{90} to the difference between the engine duration (T_{inj}) and the jet breakout time (t_b) (Bromberg et al. 2011a; 2012 & 2015). The parameter T_{90} could be taken from the light curves.

By considering BATSE light curves, and comparing with different numerical simulations, using different engine durations, and considering different viewing angles, and redshifts, T_{inj} = 20 seconds was the best at fitting BATSE T_{90} distribution. Engines with longer durations were not good at fitting BATSE GRBs results. For the cosmological GRBs (only) the average duration is ~10 – 20s.

Therefore, Lazzati et al. (2013b) argued that long engine duration, as considered in many previous studies, is too long and does not reflect the real GRBs. While shorter duration, might be more likely. Hence, the GRB population was found populated by engines shorter than previously believed and investigated.

3.3.2.5 THE GROWING DIVERSITY IN THE OBSERVED GRBs

The increasing diversity of GRBs after Swift entered full service, and the uniqueness of each GRB, suggest a more diverse and complex origin for GRBs. In pre-Swift era GRBs referred to energetic, cosmological, and highly relativistic events ($\Gamma > 100$) (Piran 2005). Nowadays, and after a decade of Swift service, the term GRB is much more diverse, and the "standard/cosmological/energetic GRBs" are just one class of GRBs among many others (§ 1.7.1).

For instance, in terms of the isotropic equivalent energy, GRB energies are spread over 6 orders of magnitude (Amati et al. 2008 & 2009). Among the newly discovers classes, is *low luminosity* GRBs "*ll*GRBs" class (Soderberg et al. 2004b). *ll*GRBs are several orders of magnitude less energetic than the classical GRBs, with the isotropic equivalent energy $E_{iso} \leq 10^{49}$ erg (Laing et al. 2007 & Bromberg et al. 2011a). Due to their low redshifts, these *ll*GRBs suggest huge rates; at least 100 times higher rates than that of standard GRBs (see: Coward 2005; Piran et al. 2006; Soderberg et al. 2006; Cobb et al. 2006; Liang et al. 2007; Guetta & Della Valle 2007; Bromberg et al. 2011a and the references within). Such rates suggest that the cosmological GRBs are a minority in numbers in nature, compared to *ll*GRBs, thus the importance of the study of *ll*GRBs. *ll*GRBs are highly debated, in particular about their origin, and whether they do arise from the classical collapsars and about their link to classical GRBs (Yamazaki et al. 2004 & Bromberg et al. 2011a).

There have been some attempts to use the collapsar to explain *ll*GRBs and their high rates, but a classical collapsar ($T_{inj} >> T_{breakout}$) shows serious limitations (Cobb et al. 2006). A more diverse collapsar is therefore needed to explain the origin of *ll*GRBs and investigate a possible unification with the traditional GRBs.

Hence, considering the various observed GRBs, and various possibilities for collapsars in nature, the engine duration must be considerably diverse. A deep numerical investigation on a wide range of the engine duration is justified. In particular investigating short duration, not deeply investigated yet, in order to explain the origin of peculiar GRBs (such as *ll*GRBs) under the collapsar scenario.

3.4 THE MOTIVATION

The main motivation of this thesis is:

> ***In general***: *To explore a more diverse version of the collapsar model, which would reproduce, and explain, the diverse nature of GRBs, increasingly apparent in the observation.*

In particular: To investigate on the origin of llGRBs, by testing the previously suggested theoretical models (§ 2.3.1 & § 2.3.2), and to which extent llGRBs peculiar features (High rate and SN connection) can be explained

3.5 THE RESEARCH PLAN

In order to produce diverse collapsar events, and investigate the origin of *ll*GRBs, I use a varied numerical version of the collapsar model. I aim to produce not all classical events of the collapsar model, but diverse collapsar events as the observations suggest.

I keep all the jet properties constant except the engine duration T_{inj}. I choose the collapsar engine duration as the main parameters because the engine is poorly understood, as the BH surrounding environment is very complex and poorly understood. Hence this might contribute to exploring the mysterious nature of collapsars' engine. Such different engine duration can be linked to, and justify by, parameters widely diverse in nature: Rotation, magnetic field, metalicity, and other such physical parameters. The different engine durations produce long and successful jets, as well as very short and failed jets.

Assuming the collapsar scenario for *ll*GRBs, I search for an engine specific duration domain that explains *ll*GRBs' peculiar features of: i) a high rate relative to standard GRBs, and ii) a strong SN connection. In other words, I numerically test the scenarios proposed above for *ll*GRBs and which scenario would reproduce i) & ii) (as shown in Figure 3.6): a) the scenario of failed jets (Bromberg et al. 2011a: $T_{inj} \leq T_{breakout}$); and b) the scenario of successful jets (unification model: $T_{inj} >> T_{breakout}$). That is, I will answer the following ultimate question:

"What origin would explain llGRBs' i) & ii): off-axis observation of GRBs successful jets, or instead, off-axis observation of short/failed jets?"

I believe that exploring this question numerically would make a contribution to the scientific debate in *ll*GRBs.
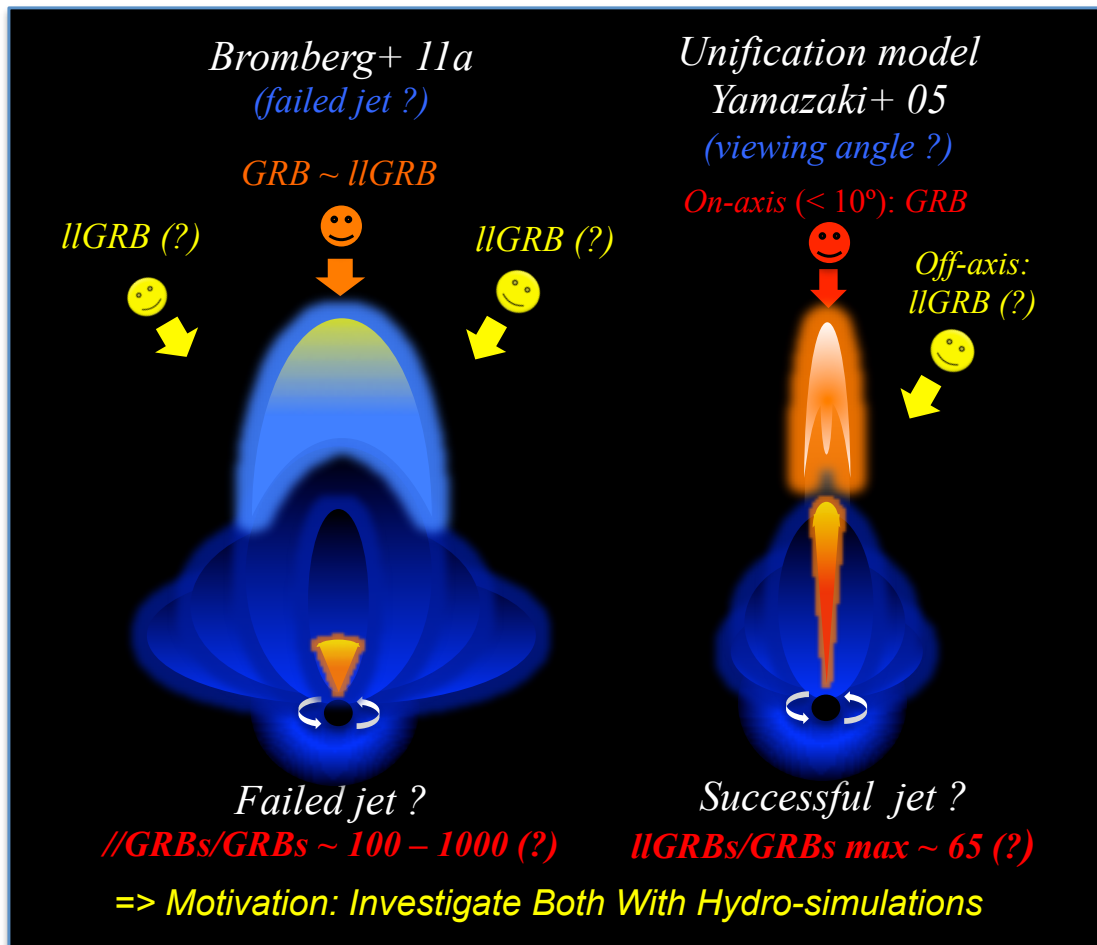
Figure 3.6: Illustration showing the two major scenarios of *ll*GRBs and their dilemma. The motivation of this thesis is to explore the questions (?) numerically.

3.5.1 DESCRIPTION OF THE RESEARCH PLAN

In this thesis, I consider a series of numerical simulations, using a very wide variety of engine durations (0.1 – 100 sec). This domain is justified by the two studies previously reviewed: 1) Lazzati et al. (2013b) showing that BATSE GRBs are from *intermediate* engine duration (~ 20 seconds), and that long engines (~ 100 seconds) are unlikely, & 2) Bromberg et al. (2012) suggesting a power law distribution for collapsar engine

duration, with a steep index ($-4 < \alpha < -3$); in other words, indicating that long engines are very rare relative to short engines (and thus to failed jets). For an illustration of the choice of initial conditions, and how it is justified with other studies, see Figure 3.7.

I explore some collapsar engines that have not been numerically investigated yet. For the different engines, I consider the same total injected energy, 10^{52} erg, (in the reasonable range of typical Hypernovae explosion energy and not very extreme; Nomoto et al. 2006a).

For this, I use an Adaptive Mesh Refinement (AMR) two-dimensional special relativistic hydrodynamical numerical code. I use deeper injection nozzle position, 10^8 cm instead of the 10^9 cm used in ML07 and most previous studies. Injection nozzle in 10^8 cm is more realistic, increasing the star-jet interaction, although such a calculation is about one order of magnitude more time-consuming. I investigate how the jet phases, precursor, shocked and unshocked, and other temporal, angular and energetic properties, depend on the injection duration, and how diversity can be produced to explain GRBs' diversity (extending the study in Lazzati et al. 2013b & ML07).

I finally analyze the GRBs and *ll*GRBs estimated from different engine models. I compare the rates of both GRBs and *ll*GRBs for different models, and compare to the observational predictions (Soderberg et al. 2006; Piran et al. 2006; etc.). I also estimate the SN explosion energy and in which models SN can be clearly identifiable, as in the case of *ll*GRBs.

The numerical simulations were carried-out using a super computer account (CFCA X30). In total, the numerical calculations consumed over ~1 000 000 core-hours of computing time.
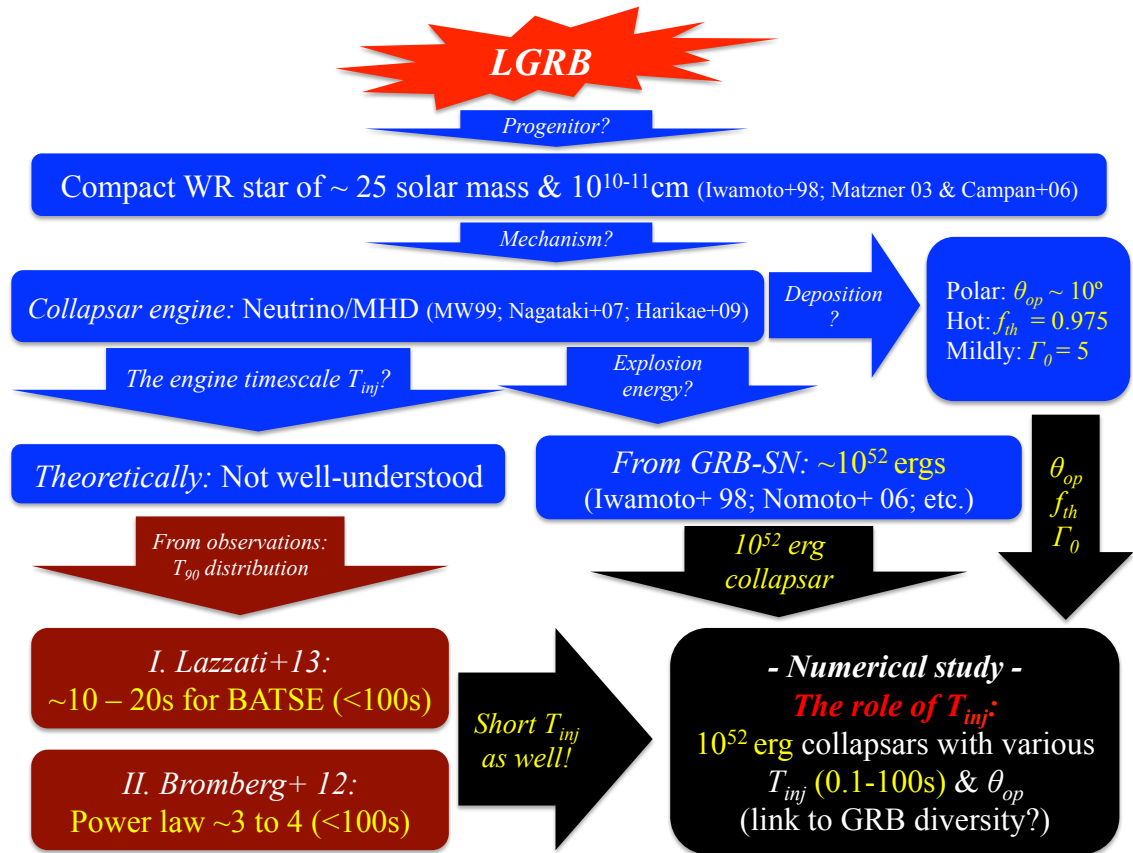
Figure 3.7: Initial conditions of the considered series of simulations and the arguments behind the considered values.

3.5.2 ORIGINALITY

As short engine duration are linked to fail-jets, they fail to power standard GRBs. Hence short engines have rarely been considered in numerical studies (except Mizuta et al. 2009 & Lazzati et al. 2012). The study here is an exception as one deep study on short engines as well as long engines.

Lazzati et al. (2012) compared engine duration and suggested that *ll*GRBs are well produced by short engines. However, no solid conclusion could be reached on llGRBs

rates or on their SN connection. I extend Lazzati et al. (2012) study and consider the widest duration range ever for collapsar engines. Another original point is that I derive the rates of GRBs and *ll*GRBs, considering the viewing angle. I derive the energy of SN explosion as well. This two estimation would allow an interesting discussion on the engines of *ll*GRBs.
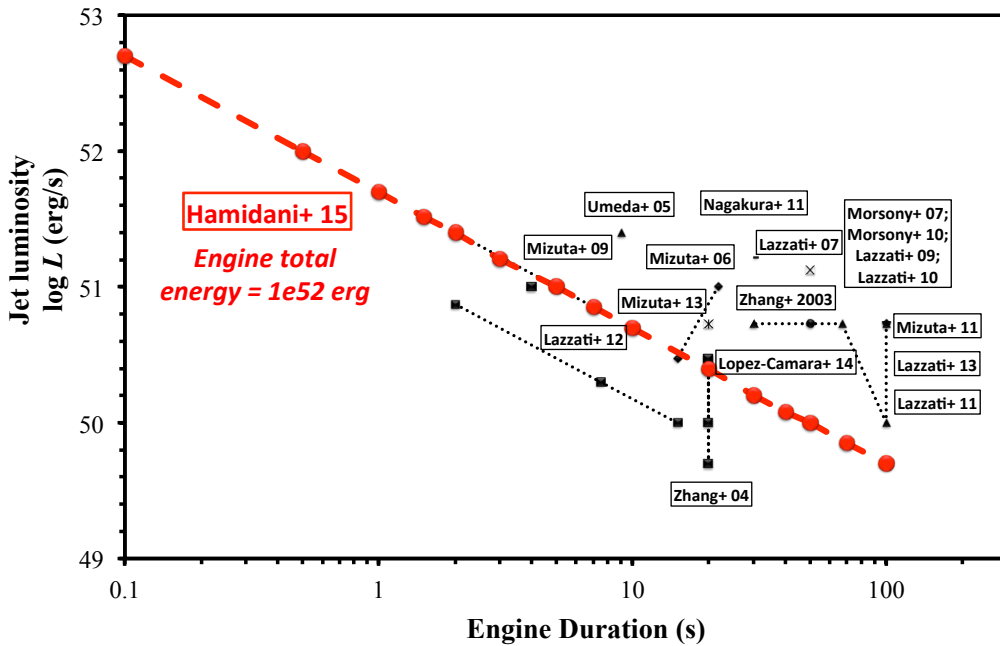
Figure 3.8: The wide duration domain considered in this study, in comparison with previous major 2D simulation of the collapsar.

4 NUMERICAL METHOD

"A scientist in his laboratory is not a mere technician: he is also a child confronting natural phenomena that impress him as though they were fairy tales. " — *Marie Curie*

4.1 OVERVIEW

After overviewing the phenomenology of GRBs, and its popular model (the collapsar; § 1.7), a summary of how numerical studies used this model to explain several of GRBs' peculiar properties was presented (§ 3). As distance makes it extremely difficult to understand GRBs through observations alone, the numerical approach is crucial to understanding GRBs, and could be the sole approach to investigate some of GRB features.

In the previous chapter, the research plan and how it would be carried-out, in an original study based on the engine duration of collapsars, was described. This chapter is slightly technical as it describes the basics of the numerical code and the equations that it solves. It also explains how the data, from the simulations, is treated to derive the temporal and angular properties of the outflow (§ 4.4.4), for one exemplary model (L700). These properties are discussed in § 5 in detail, for the different engine models. In addition, the procedure followed to derive the probability of observing a given prompt emission

isotropic energy, is explained, and how some reasonable assumptions were used. This last quantity is important as it would allow to discuss the rate of *ll*GRBs over the rate of GRBs, from each engine, and compare it with the observational predictions (Coward 2005; Piran et al. 2006; Soderberg et al. 2006; Cobb et al. 2006; Guetta & Della Valle et al. 2007 & Liang et al. 2007) as followed in § 6.2. Further technical discussions about the code and its robustness follow in the appendices (§ 10).

As the central engine's properties are hardly unknown, and as it is extremely difficult to understand the central engine from observation alone, numerical investigations, like this one, are the privileged way to better understand GRBs phenomenology.

4.2 THE NUMERICAL APPROACH

4.3 NUMERICAL METHOD

I performed numerical simulations with a two-dimensional special relativistic hydrodynamical code, the same code used in (Yoshida et al. 2014 & Okita et al. 2012), with a newly added AMR treatment as described in § 4.4.2. The explosion and jet propagation is assumed to be axisymmetric. The basic equations solved in this code are given as:

$$\frac{\partial U}{\partial t} + \frac{1}{r^2}\frac{\partial(r^2 F^r)}{\partial r} + \frac{1}{r\sin\theta}\frac{\partial(\sin\theta\,F^\theta)}{\partial\theta} = S + G \tag{1}$$

Where *U*, *F^i*, *S* and *G* are conserved vector, *i*-component of numerical flux, source term and gravitational source, respectively. Under geometrical unit $G = c = 1$, where *G* and *c* are the gravitational constant and the speed of the light, these vectors are written as follows (e.g. Leismann et al. 2005):

$$U = (\rho\Gamma, \rho h\Gamma v^r, \rho h\Gamma v^\theta, \rho h\Gamma^2 - p - \rho\Gamma) \tag{2}$$

$$F^i = (\rho\Gamma v^i, \rho h\Gamma^2 v^i v^r + \delta_r^i, \rho h\Gamma^2 v^i v^\theta + p\delta_\theta^i, \rho h\Gamma^2 v^i - \rho\Gamma v^i) \tag{3}$$

$$S = \frac{1}{r}\left(0, \rho h \Gamma^2 v^\theta v^\theta + p, -\rho h \Gamma^2 v^r v^\theta, 0\right) \tag{4}$$

$$G = (0, \rho h \Gamma \partial_r \Phi, 0, \rho h \Gamma \partial_r \Phi) \tag{5}$$

Here, ρ, v and p are the rest mass density, velocity and pressure. h and Γ are specific enthalpy and Lorentz factor, respectively, defined as $h = 1 + \varepsilon + p/\rho$, where ε is specific energy density, and $\Gamma = \sqrt{1/1 - v^2}$. Gravitational potential Φ includes the contributions of self-gravity and the central remnant. The integration form of the Poisson equation approximated in Newtonian mechanics (Hachisu 1986) is applied for self-gravity. Time integration is calculated using the second-order Runge-Kutta Method developed by Shu & Osher (1988). I use a simple equation of state (EOS), the so-called gamma law EOS $p = (\gamma - 1)\rho\varepsilon$, with an adiabatic index $\gamma = 4/3$, which accounts for both the gas and radiation components. The choice of a simple EOS is due to the focus on the jet general properties, which a simple EOS would not overlook.

As long as only penetration through the stellar mantle and propagation in the CSM is considered, the incoming jet can be characterized by several parameters, regardless of the detailed mechanism of central engine. Here, I follow the method proposed in Tominaga (2009) to determine the boundary condition of (ρ_0, v_{r0}, p_0), where the index "$_0$" indicates that the quantity is calculated at the inner boundary of the computational domain. Thus, characterizing a jet comes down to defining the following 6 parameters: T_{inj}, E_{tot}, R_{in}, θ_{op}, f_{th} and Γ_0. The key parameter of this study is T_{inj}, the duration of the energy injection in the simulation, which reflects the engine duration. E_{tot} is the total energy injected, up to *time* = T_{inj}, in other words, it is the supposed total energy released by the central engine in the form of two relativistic polar jets (assumed as 10^{52} erg). Thus, I can get the energy deposition rate $\dot{E} = E_{tot}/T_{inj}$. R_{in} and θ_{op} are parameters to determine the geometric property of outflow: the inner boundary where the injecting nozzle is placed and the opening angle of the jet cone, respectively. With these two parameters, I can get the intersection area of the inner boundary and jet cone as $A_0 = 4\pi R_{in}^2 (1 - cos\theta_{op})$. Finally, f_{th} is the ratio of the thermal to total injected energy and Γ_0 is the Lorentz factor of the outflow at the inner boundary. Once these parameters are set, the boundary condition is obtained as:

$$v_{r0} = \sqrt{1 - 1/\Gamma_0^2} \tag{6}$$

$$p_0 = \frac{f_{th}\dot{E}}{v_{r0}A_0(\frac{\gamma}{\gamma - 1}\Gamma_0^2 - 1 + f_{th})} \tag{7}$$

$$\rho_0 = \frac{(1 - f_{th})\left(\frac{\dot{E}}{v_{r0}A_0} - p_0\right)}{\Gamma_0(\Gamma_0 - 1)} \tag{8}$$

As mentioned above, I focus on the properties of GRB central engine with various duration times. As Lazzati et al. (2013b) has suggested, central engines, on average, are active over several tens of seconds. Shorter engines would be likely, but very long engines might be rare. Thus, I set T_{inj} from 0.1 to 100 seconds covering a wide range. I note that although the models vary in T_{inj}, but E_{tot} is always the same. Thus, the input energy (or central engine power) $\dot{E} = E_{tot}/T_{inj}$, also varies according to T_{inj}. As the density of the jet material is proportional to $\dot{E}$ from equation (8), long T_{inj} favor low-density jets and short T_{inj} gives denser jets (for more details see: Figure 5.5 & § 5.1.3).

In the context of the collapsar scenario, the energy conversion efficiency η is defined as the ratio of the energy powering the jet, or the input energy, to the rest mass energy accretion rate onto the BH. As I assume these parameters not to vary in time, using an accretion rate $\dot{M}$, η is defined as:

$$\eta = \frac{\dot{E}}{\dot{M}c^2} \tag{9}$$

Since both the time derivative values are considered to be constant in time, total accretion mass M_{acc} can be derived with time integration of equation (9) as:

$$M_{acc} = \frac{E_{tot}}{\eta c^2} \tag{10}$$

The right side is only dependent on E_{tot} and independent of T_{inj}. Therefore, the assumption of taking a constant E_{tot} and various T_{inj} means that I always assume the same total accreted mass but with different accretion rates. Such different accretion rates can be justified by parameters related to the progenitor or the environment (e.g: rotation & metalicity).

4.4 SETUP OF THE SIMULATIONS

4.4.1 STELLAR MODEL

The progenitor model for the simulations presented here is made from a 25 $M_\odot$ initial mass star model as in Umeda & Nomoto (2008). The star loses a fraction of its H envelope by mass-loss wind, down to 20.4 $M_\odot$ at the pre-SN phase. I artificially remove the H envelope to make a 6.1 $M_\odot$ of He Wolf-Rayet star for the GRB progenitor, with a radius of 3.3×10^{10} cm (see the progenitor density profile in Figure 4.1). Initial pressure and density are taken from the progenitor model. Matzner (2003) argued that such a compact progenitor is preferable, as some of the observed GRBs have short durations, about a few seconds and such short durations must be explained by a compact progenitor. The surrounding medium is taken uniform with a density $\rho = 10^{-10}$ g cm^{-3}. A Courant Number (CFL) of 0.3 is used for the simulations presented here.

The rotation is not considered as it would not have a significant effect considering the relatively short timescale of the simulations (100 sec), and thus its effect can be safely ignored. Neutrino pressure and general relativistic effects from the central engine are not considered either, as the inner boundary at 10^8 cm, is at about 10^3 gravitational radii away from the region dominated by this effects, thus both effects could be safely neglected.
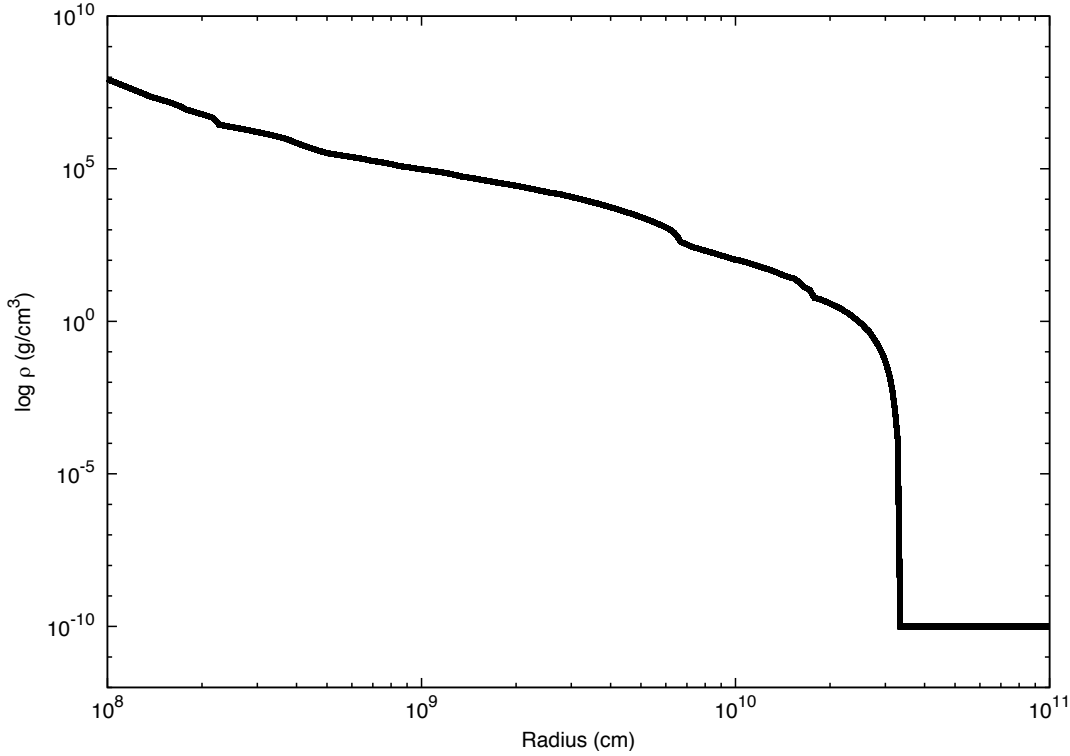
Figure 4.1: Density profile of the progenitor.

4.4.2 GRID

I use a 2D spherical coordinate system (r, θ) with axisymmetry and equatorial plane symmetry. Apart from the injection region, the boundary conditions at the polar axis and equatorial plane of the grid are reflective, as I consider that a symmetric jet is emerging in the opposite direction. Computational domain extends from $R_{in} = 10^8$ to R_{out} = 3.01×10^{12} cm, allowing the relativistic outflow to be followed for about 100 seconds (in $0° \leq \theta \leq 90°$). Radial grid is set to vary in an AMR mode, initially from 2500 up to over some 10 000 for long injection models, following and attributing higher resolutions for the relativistic outflow ($\Gamma > 1$) accordingly. I use 11 levels of refinement, and the corresponding resolutions varies as: $\Delta r_l = \Delta r_0 \times 2^l$, where l corresponds to the level of mesh refinement (from 0 to 10) and Δr_0 is the lowest resolution ($\Delta r_0 = 10^{10}$ cm, 0 level

of refinement). Δr_0 is considered in the exterior of the star, at regions where there is no relativistic outflow (where $\Gamma = 1$). The highest radial resolution is adopted at the stellar surface ($\Delta r = 9.7 \times 10^6$ cm, 10 levels of refinement) in order not to miss any potential precursor structure, inside the progenitor, at the innermost region (10^7 cm $\leq \Delta r \leq 3.9 \times 10^7$ cm, taking resolutions higher than level 8), and at the jet head ($\Delta r = 3.9 \times 10^7$ cm, 8 levels of refinement). Although the radial resolution is still lower than that of ML07 (7.8125×10^6 cm), it is reasonably good considering most previous studies' resolutions (such as Mizuta et al. 2011 with $\Delta r_{min} = 10^7$ cm and Nagakura et al. 2011 with $\Delta r_{min} = 10^8$ cm).

For the polar grid θ, I employ $N_\theta = 256$ uniform logarithmic grids, with angular resolutions varying from $\Delta\theta_0 = 0.088°$, at the jet on-axis, to $\Delta\theta_{max} = 0.896°$ at the equator, such that: $\Delta\theta_n = \Delta\theta_0 \times C^n$, where C = 1.009. This angular resolution is reasonably high in comparison to many previous works (for example 0.25°, for Mizuta et al. 2011 and Zhang et al. 2003) although the resolution in ML07 is still higher (0.0358°).

The inner boundary is placed at a relatively deeper region, 10^8 cm, in comparison to most previous studies, which generally used 10^9 cm (ML07, 2010, Lazzati et al. 2009, 2011, 2013a, Mizuta et al. 2006, 2009, Nagakura et al. 2011 & Lopez-Camara et al. 2014). This deep inner boundary is to better capture the evolution of the jet inside the star, especially for the short engines that this study includes. It is also more realistic as it is closer to the region where the central engine is expected to inject energy, near the BH horizon at $\sim 10^{6-7}$ cm. Although, such deep injection is very consuming in terms of computational power; I believe that I still could afford very good resolutions compared to previous studies that used a similar deep injection, at the cost of increasingly poor resolution at large radii, and limited computation domain (Zhang et al. 2003 injecting at 2×10^8 cm & Aloy et al. 2000 at 2×10^7 cm)

4.4.3 Jet Conditions and Engine Models

The jet energy is inputted at a radius of $R_{in} = 10^8$ cm from the center of the progenitor, at the inner boundary of the computational domain. The maximum Lorentz factor,

defined as the terminal Lorentz factor at infinity when all internal energy will be converted to kinetic energy, is $\Gamma_{max} \sim 160$ (according to Bernoulli relativistic equation: $\Gamma_{max} \sim h\Gamma$). The jet initial opening angle is adopted as 10°, as in major previous studies (ML07, Mizuta et al. 2006, Lazzati et al. 2013a etc.). According to Mizuta et al. (2006) who investigated the preferable conditions for GRB jet, hot and mildly relativistic initial jet is required for successfully launching the highly collimated and ultra-relativistic jet necessary to produce GRB. Thus, thermal energy fraction and initial Lorentz factor of the injected jet are taken as $f_{th} = 0.975$ (hot) and $\Gamma_0 = 5$ (mildly relativistic).

The injection duration is considered from 0.1 to 100 seconds. To easily analyze the different engine models, I separate them into four groups, from the shortest: "*brief*" engines ($T_{inj} < T_{Breakout} \sim 2$ s), "*short*" engines (~ several seconds; 2 s $\leq T_{inj} < 10$ s), "*intermediate*" engines (~ several ten seconds; 10 s $\leq T_{inj} < 40$ s) and finally "*long*" engines (50 s $\leq T_{inj} < 100$ s). This engine notation will be followed, all along this paper. The computed models are summarized in Table 4-1, with their corresponding inputted luminosities per jet (Figure 4.2). As the duration varies over 3 orders of magnitude while the total energy is constant at 10^{52} erg, the luminosity of the inputted jet is also very diverse (from 5×10^{52} to 5×10^{49} erg s^{-1}), covering intense-short to long-mild engines.
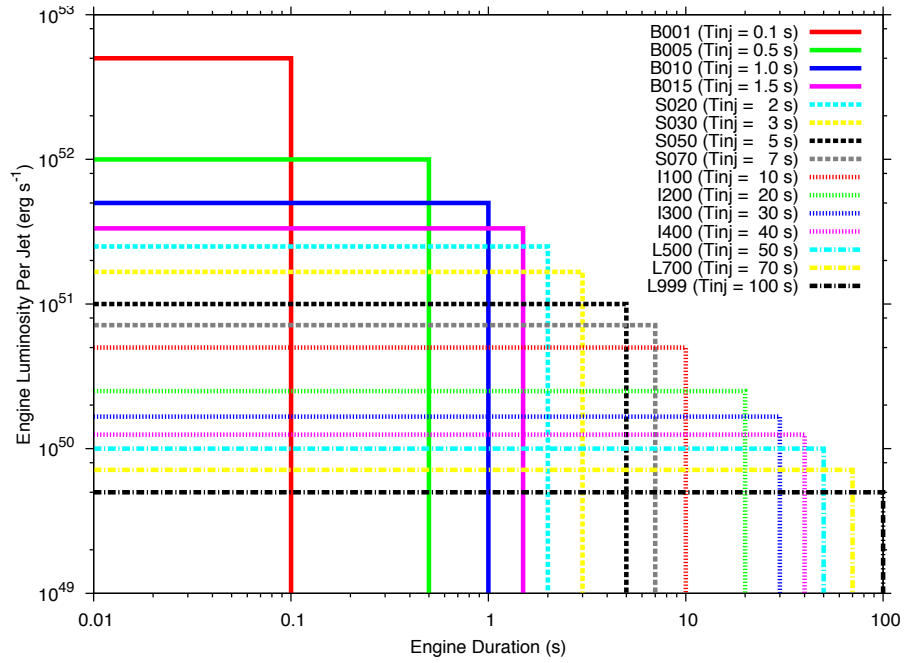
Figure 4.2: Engine durations and the corresponding luminosities, per jet.

Table 4-1: Parameters of the computed models.

Model	Injection Time (s)	Black Hole Luminosity Per Jet (erg s^{-1})	Engine Type
B001	0.1	5.0×10^{52}	*Brief*
B005	0.5	1.0×10^{52}	*Brief*
B010	1.0	5.0×10^{51}	*Brief*
B015	1.5	3.3×10^{51}	*Brief*
S020	2.0	2.5×10^{51}	*Short*
S030	3.0	1.6×10^{51}	*Short*
S050	5.0	1.0×10^{51}	*Short*
S070	7.0	7.1×10^{50}	*Short*
I100	10.0	5.0×10^{50}	*Intermediate*
I200	20.0	2.5×10^{50}	*Intermediate*
I300	30.0	1.6×10^{50}	*Intermediate*
I400	40.0	1.2×10^{50}	*Intermediate*
L500	50.0	1×10^{50}	*Long*
L700	70.0	7.1×10^{49}	*Long*
L999	100.0	5×10^{49}	*Long*
16TIg5-like (ML07)*	50.0	5.32×10^{50}	*Long*

* The calculation 16TIg5-like, as in ML07, was carried assuming an outer injection nozzle at 10^9 cm, and an engine total energy of 5.32×10^{52} ergs, while for all the other calculations the injection is at 10^8 cm, and the engine energy is 10^{52} ergs.

4.4.4 Procedure to Derive Temporal and Angular Properties

In this section, I explain how the temporal and angular properties were derived from the data, using the engine model L700 as an example. I adopt the same method as in ML07 (see ML07 § 4.1) to derive the synthetic light curves and angular properties of the relativistic jets. A snapshot of the simulation data is saved every 1/10th seconds of simulation time (1/15th seconds for ML07). As in ML07, the energy flux is determined as a function of angle and time by finding all the points that will cross a given fixed radius within the next 0.1 seconds. I use the same approximation for sideways expansion as in ML07, by spreading every point's energy equally over an angle of ±1/Γ from the direction of motion of the fluid at that point. As argued in ML07, this accounts for hydrodynamic spreading and the relativistic beaming of the eventually emitted radiation. The energy is then placed into the same system of angular bins as in ML07, where the total energy in each angular bin is calculated considering contribution from all points of the same radius. Finally, only outflow energy above a specified minimum Lorentz factor is considered, excluding any fluid energy with a lower Lorentz factor. In this way, the simulation data from each snapshot file can be added over time, to estimate the total energy seen at a fixed radius for different angles. I consider the same minimum Lorentz factor and radius in ML07, Γ_{min} = 10, to derive each model's synthetic light curve (see ML07's Fig. 12). Both the light curve and the energy angular distribution are calculated for the same minimum Lorentz factor, and at the same radius (R = 1.2×10^{11} cm). I use 45 angular bins, identical to those considered in ML07, consisting of (from small to large angles, with 0° at the on-axis region of the jet): 14 bins with an angular width of 0.25° (ranging from 0.125° to 3.375°), 17 bins with a width of 1.0° (from 4.0° to 20.0°), and finally 14 bins spaced every 5.0° (23.0° to 88.0°). Figure 4.3 shows the derived results for the model L700, (T_{inj} = 70 s). The top panel shows the synthetic light curve for this model, and the resulting angular distribution is shown on the bottom panel. The light curves and angular distributions of

the different models are presented in § 5, and the astrophysical implications are discussed in § 6.

Hamid Hamidani - February 2016
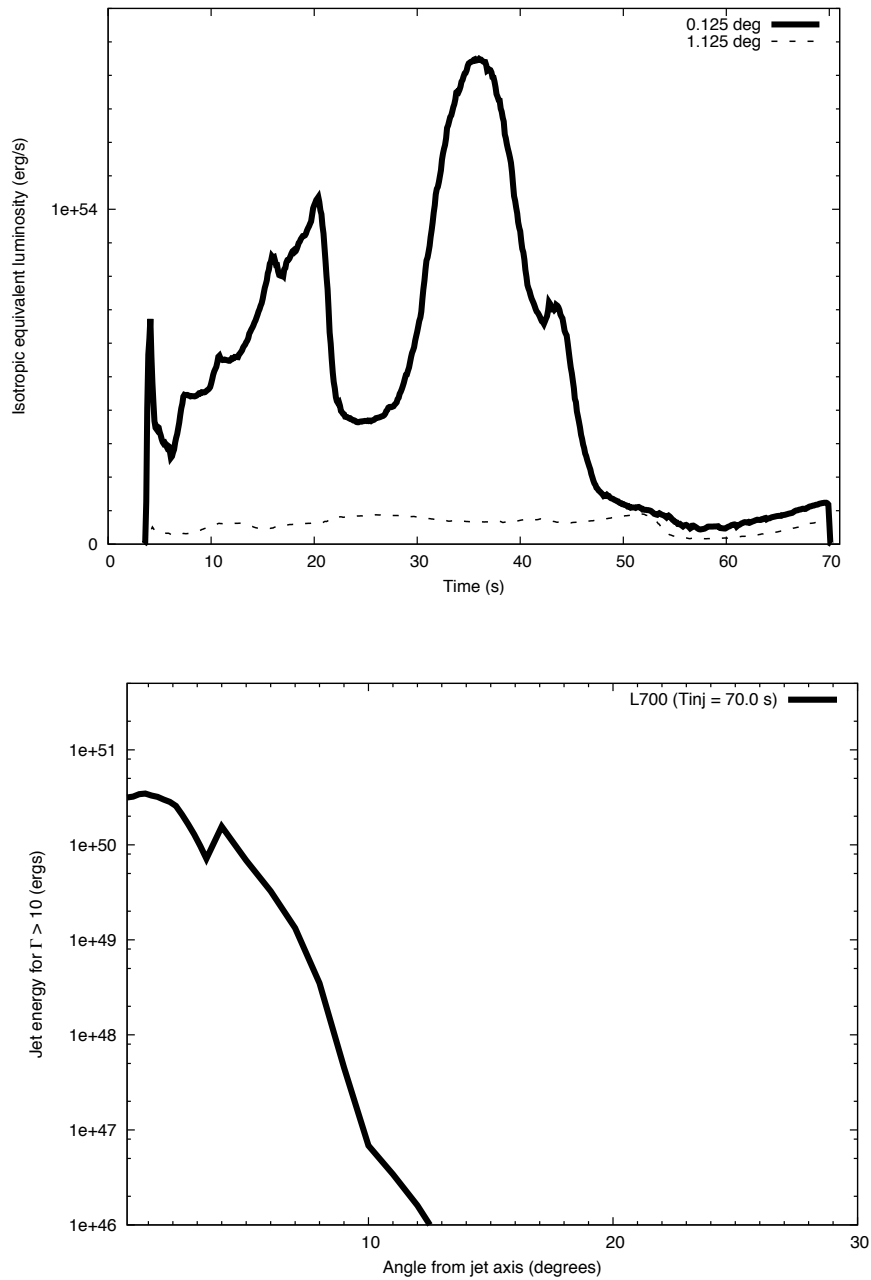
Figure 4.3: On the top panel, isotropic equivalent luminosity of the jet over time – synthetic light curve – with the solid line for an observer in the jet on-axis region (the innermost bin, centered at 0.125°), and the dashed line for an observer at 1.125° from the jet axis. On the bottom panel, the angular distribution of the relativistic outflow energy. Both figures are for the engine model L700 ($T_{inj} = 70$ s), calculated at a radius 1.2×10^{11} cm from the star center, and with a minimum Lorentz factor of 10.

In order to carry out with the discussion further, from a "jet" to a "GRB" context, the prompt emission energy has to be estimated. As in ML07, I assume that only relativistic outflow can contribute in the GRB prompt emission. Thus, considering relativistic outflow with $\Gamma > 10$, I estimate the energy contributing in the prompt emission from the total jet energy. Still, it is obvious that regardless of the emission process (non thermal synchrotron or thermal) not all the energy carried by the relativistic outflow would be converted to gamma and X-ray photons. There is a certain conversion efficiency factor. Thus, in order to estimate the energy that will contribute to the prompt emission, I consider a conversion efficiency of the jet energy to gamma photons, known as: Radiative efficiency. This parameter (η_γ) has been intensively investigated. As in Zhang et al. (2007b), it is defined as:

$$\eta_\gamma = \frac{E_\gamma}{E_\gamma + E_K} \tag{11}$$

Where E_γ is the energy carried by gamma-photons (total energy of the prompt emission), and E_K is the kinetic energy of the outflow just after the prompt emission. E_γ is generally estimated from the prompt emission and E_K from the afterglow. In one major work Zhang et al. (2007b) estimated this parameter for 31 Swift GRBs. The radiative efficiencies $\eta_\gamma(t_b)$ were found to be < 10% in general (Zhang et al. 2007b, table 3 & 4). In this work considering Zhang et al. (2007b) findings, I assume a symbolic $\eta_\gamma = 1\%$ to roughly derive the energy of the prompt emission for the engine models, regardless of the true emission mechanism. This, assumption allows us to carry an angular and energetic comparison for the prompt emission of different engines.

Figure 4.4 shows the angular distribution of the isotropic equivalent energy estimated for the prompt emission of L700 (on the top). I consider the lower limit of the observed isotropic energy at 10^{47} erg (in the order of the least energetic observed *ll*GRBs). On the bottom panel I show the same energy as a function of the probability of observation considering a randomly located observer in the sky again for the same model L700. The probability of observation was calculated considering minimum energies ranging from 10^{47} to 10^{53} erg. It was calculated simply by dividing the solid angle inside which

prompt emission above the minimum energy was observed over the total solid angle of the sky in one pole (2π) as in the following equation:

$$P(E \geq x) = \frac{2\pi(1 - \cos(\theta_{E \geq x}))}{2\pi} \times 100 \qquad (\%) \qquad (12)$$

Where P is the probability of observing an event with an isotropic equivalent energy above x, and $\theta_{E \geq x}$ is the angle inside which the isotropic energy is above the minimum x. The same results for the other engine models are shown and discussed in § 6.
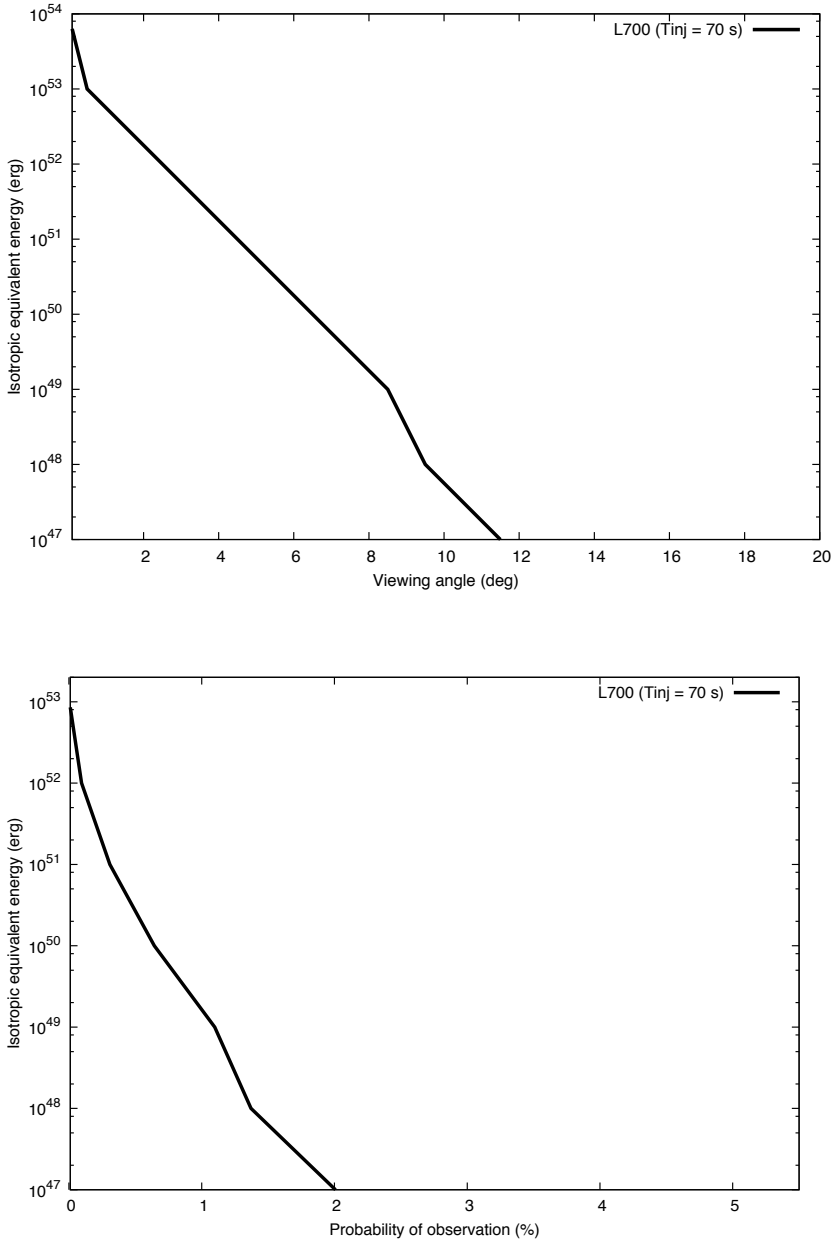
Figure 4.4: On the top panel, the estimated isotropic equivalent energy of the prompt emission as a function of different observers viewing angle (relative to the jet axis). On the bottom panel, the estimated isotropic energy of the prompt emission as a function of the probability of observation, considering randomly positioned observers in the sky. Both panels are for the engine model L700 (T_{inj} = 70 s).

4.5 SUMMARY

I follow a classic numerical approach: I carry out numerical simulations of the collapsar of a typical Wolf-Rayet star (Umeda et al. 2005), using a newly developed AMR special relativistic hydrodynamic code. Using the code I consider engines deploying the same total energy but in a different timescale over three orders of magnitude (from $0.1 - 100$ seconds). I have explained how I derive the hydrodynamical properties of the collapsar jet, properties that are deeply discussed in the next chapter (§ 5). In addition, I explained how the probability of observation could be calculated, considering some assumptions. This last quantity has never been derived before, and thus its importance. I considered this probability of observation to discuss *ll*GRBs rate for all the engine models in § 6.2, a critical discussion (in this thesis), as it enables interesting results on *ll*GRBs origin and on the collapsar engine duration distribution (§ 6.2.3).

5 HYDRODYNAMICAL RESULTS

"An experiment is a question which science poses to Nature and a measurement is the recording of Nature's answer." — Max Planck, Scientific Autobiography.

5.1 OUTLINE

A crucial question will be addressed and answered in this chapter: "*How does the engine duration influence the properties of the jet?*" As overviewed in the § 1, GRB are very diverse, occasionally questioning the collapsar model. With the numerical approach presented in § 3, artificial collapsar engines, diverse in terms of the engine duration, are created and their jets will be analyzed in this chapter. This diversity in the engine duration is meant to trace the diversity of engine durations – related to the accretion time – that must be considerably diverse in nature.

This chapter explores how the engine duration has a dramatic influence on the jet propagation inside the star (the confined phase), and on the three radiative phases. Many important quantities – for the prompt emission – are found to strongly affect by difference in the engine duration, although the deployed total energy is the same. Such

results have been described in Lazzati et al. (2012), but here I investigate more properties, and on a much wider and deeper level.

This chapter is limited to discuss difference in hydrodynamical properties for the different engines. The implications of differences found in this chapter are discussed in the next chapter (§ 6).
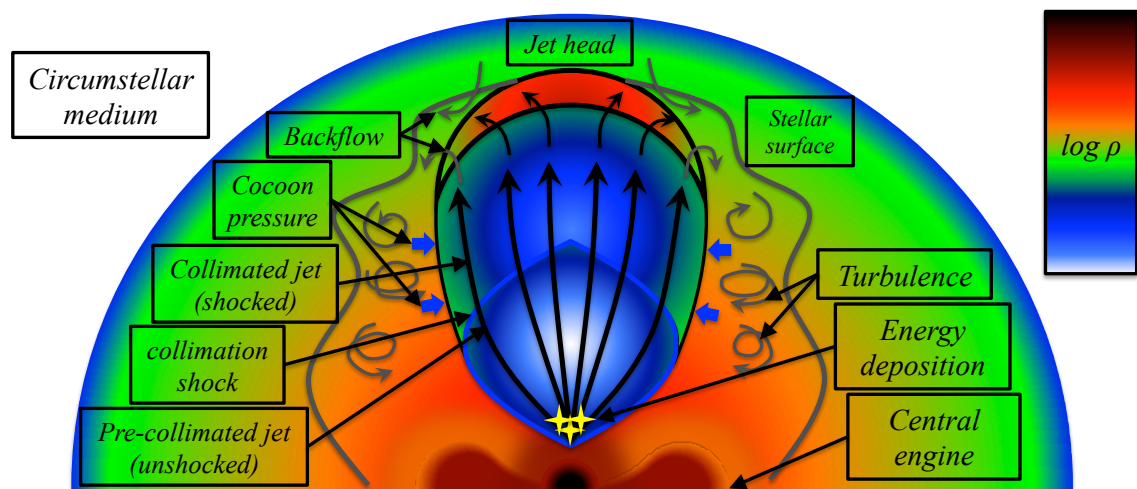
Figure 5.1: Illustration of a collapsar jet, confined in the stellar envelope, before the breakout out, showing its key elements (central engine, cocoon, shocked outflow, unshocked outflow, collimation shocks, and the jet head).

5.1.1 THE CONFINED PHASE

Before breaking out of the progenitor and proceeding into the CSM, the jet's propagation through the progenitor was noted in Lazzati et al. (2007) as the "confined" phase. It is a non-radiative phase where a supersonic shock, the jet head, progresses between the injection nozzle, and the stellar surface, collimated by the cocoon pressure. In this phase the premature jet is formed and shaped, which would strongly influence the next radiative phases. ML07 & Lazzati et al. (2007) findings demonstrate that the speed of the jet head is independent of the stellar properties. ML07 & Lazzati et al. (2007), also demonstrated that the energy stored in the cocoon is proportional to the

engine luminosity (Lazzati et al. 2007). Thus, the different engine duration models, with their different engine luminosities, are expected produce diverse jet structures.

Figure 5.2 shows the propagation of the jet head for different jet models, from the *briefest* B001, to the *longest* L999, all with *short* and *intermediate* engine models S050 and I100. An engine similar to that studied by ML07 (16TIg5), with the same initial Lorentz factor, opening angle, total energy (5.32×10^{52} erg), and nozzle position (10^9 cm) is also shown. At small radii, less than ~10% of the stellar radius, the *brief* engine is ahead at a relativistic speed, with a slope close to that of the speed of light *c*. Both the *short* and the *intermediate* engines' speeds are sub-relativistic, with slopes close to that of Lorentz factor of 1.01. Soon after, at larger radii, the *brief* engine is inactive, and the behaviors are inversed: the jet head in S050 and I100 gradually accelerate and increase in speed, becoming significantly relativistic and converging to *c*; the jet head speed in B001 decreases to a roughly constant sub-relativistic speed, until the break-out. As a consequence, *short* and *intermediate* engines' jets have the shortest breakout times, ~2 seconds, and the highest Lorentz factors at the moment of the breakout, whereas *brief* engines' simulations have the longest breakout times, up to 7.0 seconds, and some of the lowest Lorentz factors (see Table 5-1, second column & § Breakout Times and Properties5.1.3). In the L999 simulation, the jet head evolution is similar to that of S050 and I100, however it takes a considerably longer time (~3 seconds) for the jet head to be significantly launched in the inner region. This delay is explained by the significantly lower energy deposition of this engine (5×10^{49} erg/s). Once the jet head is effectively launched, it shows an evolution similar to that of S050 and I100 jets, with an initially sub-relativistic speed in the inner radii, and then gradually increasing speed at larger radii until the jet head breaks out relativistically. Affected by the initial delay, L999 calculation shows a significantly longer breakout time than that of S050 and I100, of 5.6 seconds. Thus, engine duration appears to have a significant influence on the jet head propagation inside the progenitor. This is most apparent when comparing with *brief* engines' behavior to that of longer engines (for more details see § 5.1.3).

The simulation similar to that of ML07 and Morsony et al. (2010), starting at an injection nozzle of 10^9 cm instead of 10^8 cm, shows similar results to that of ML07 and Morsony et al. (2010). Although the calculations are still not identical, including some differences such as: ratio of internal over rest mass energy, progenitor, EOS, resolution, etc. The 16TIg5-like simulation has a breakout time of 6.8 seconds, in ML07's 16TIg5

it is 7.53 seconds, and in Morsony et al. (2010) 6.2 seconds. The jet head evolution inside the progenitor is clearly similar, starting as sub-relativistic and gradually becoming relativistic. For a comparison of this figure, see Morsony et al. (2010) Fig. 4, and Aloy et al. 2000 Fig 3.
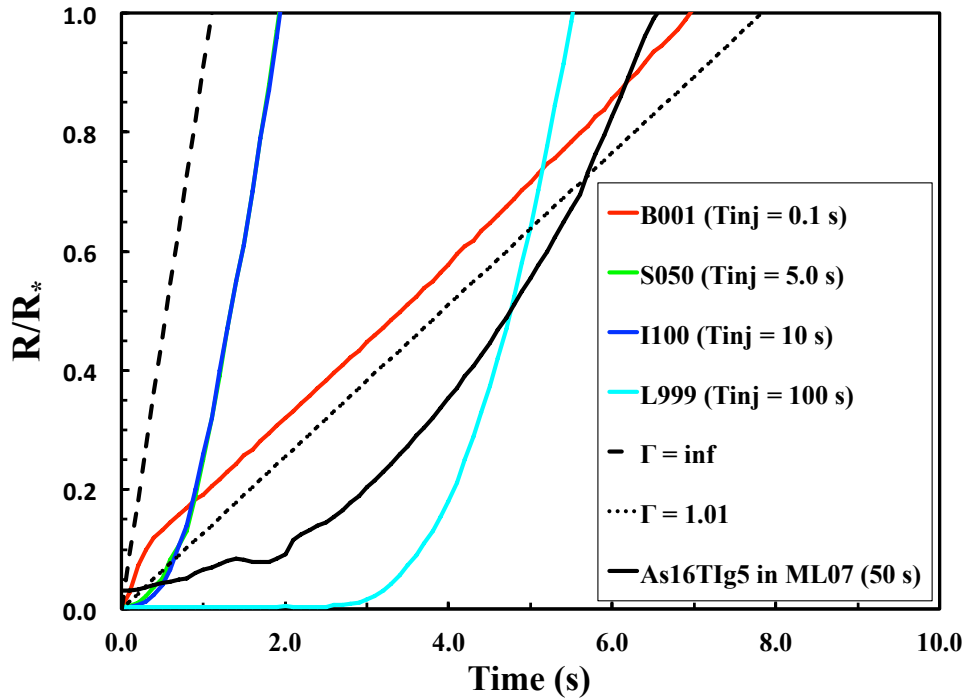
Figure 5.2: Jet head propagation inside the progenitor before the breakout, for the Briefest computed engine model (B001), a *short* engine model (S050), an *intermediate* engine model (I100) and the longest engine model considered (L999). An engine model similar to 16TIg5 used in ML07 is also plotted. For a comparison, dashed lines shows the maximum allowed speed (c), dotted lines shows a sub-relativistic speed's slope of a Lorentz factor of 1.01.

5.1.2 THE THREE RADIATIVE PHASES

As shown by many previous works, collapsar jets show distinct phases, three of which are radiative (Aloy et al. 2000, Zhang et al. 2003, Lazzati et al. 2007, ML07, Bromberg et al. 2011b etc.). The first radiative phase is the "breakout", or the "precursor" phase, as referred to in ML07. It is the phase where the cocoon hot material breaks through the stellar surface, forming a quasi-spherical fireball. It is the shortest and the least relativistic phase. Furthermore, as it is quasi-isotropically spread, this phase is the only that can be observed at large angles (ML07 & Lazzati et al. 2007). The second phase is the "shocked" jet phase. It is a phase where the jet is collimated by the cocoon's pressure, through multiple tangential shocks inside the star, called recollimated shocks. Consequently, the shocked phase material is highly variable. It is also a phase where the jet is the most collimated due to the many transversal recollimation shocks (Lazzati et al. 2007). The third and last phase is the "unshocked" phase, where after several tens of seconds the jet gradually develops into a stable structure (Lazzati et al. 2007). The core of the jet consists of a free-streaming outflow that accelerates according to the adiabatic expansion, and is limited by a strong recollimation shock. The propagation of the free-streaming inner core is mostly unperturbed from the inner engine, and thus the "unshocked" phase name. This phase develops between the injection nozzle position up to the first recollimation shock, which marks the limit between the outer shocked phase and the inner unshocked phase (Lazzati et al. 2007, ML07, Bromberg et al. 2011b). Right behind this first collimation shock, the Lorentz factor is significantly high and the pressure is significantly low, which helps identify the limit between the two phases, and the breakout time of the unshocked phase (Mizuta et al. 2009 & ML07). In terms of energy, the transition between the first precursor phase and the shocked phase is defined as the moment at which the energy flow becomes continuous, although variable. Transition from the shocked to the unshocked phase is the time at which the on-axis energy drops and becomes steady reflecting the engine constant injection (ML07). In this calculation, different from most pervious studies, a relatively deeper injection nozzle is considered, at 10^8 cm. This deep nozzle adds a dense region to the computation domain, where the star-jet interaction is significantly strong. This affects the development of the unshocked phase's free-streaming core, as the jet is more affected by recollimation shocks deeper in the progenitor, delaying the deployment and breakout of the unperturbed unshocked phase.

Table 5-1 summarizes the breakout times for the different phases of the jet, with the corresponding breakout Lorentz factors. As in previous studies (ML07 in particular), relativistic jets of the collapsar model confirm the existence and nature of the three main phases. However, since I consider a lower energy injection and a jet birthplace at a relatively deeper place, the structure is a little more complex, mainly in the shocked phase that displays a first highly variable part followed by a second smoother part. This smoother part comes at a time where the recollimation shock frequency is gradually reduced, shortly before the breakout of the unshocked phase. In other words, transition between shocked and unshocked regimes in my calculations is less brusque, but it is still clearly identifiable.

Figure 5.3 shows the main phases as a function of radius, in the top, and time, in the bottom. In the top panel, the first sharp peak, in the outer region, is the "precursor" phase. Next, is the "shocked" phase, which can be separated into two parts, the first of which is "highly" shocked/variable and the second is "less" shocked/variable. Then comes the third and last "unshocked" phase. A strong shock separating the shocked phase from the unshocked phase can be identified as a sharp increase in the Lorentz factor, and a sharp drop in the pressure, as a function of radius, on the top panel of Figure 5.3 (for T_{inj} = 70 s model). For a comparison of this figure with previous studies see: Aloy et al. (2000) Fig. 2, Zhang et al. (2003) Figs. 4, 5, and 6, Mizuta et al. (2006) Figs. 6 and 7, and Fig. 10 in ML07. The bottom panel of Figure 5.3 shows the energy flow along the jet on-axis region, calculated at 1.2×10^{11} cm, in the CSM. The three phases can be clearly identified. The unshocked phase, however, shows some variability although it remains significantly smooth and steady. This is also most likely due to the deep injection nozzle considered at 10^8 cm. A comparison of the unshocked phase here with that of an engine similar to that of 16TIg5 in ML07 with an injection nozzle at 10^9 cm, confirms that the small variability in the unshocked phase of L700 is indeed due to the deep injection nozzle at 10^8 cm (see the Appendix § 10). For a comparison of this figure with a previous study see: ML07 Fig. 4.
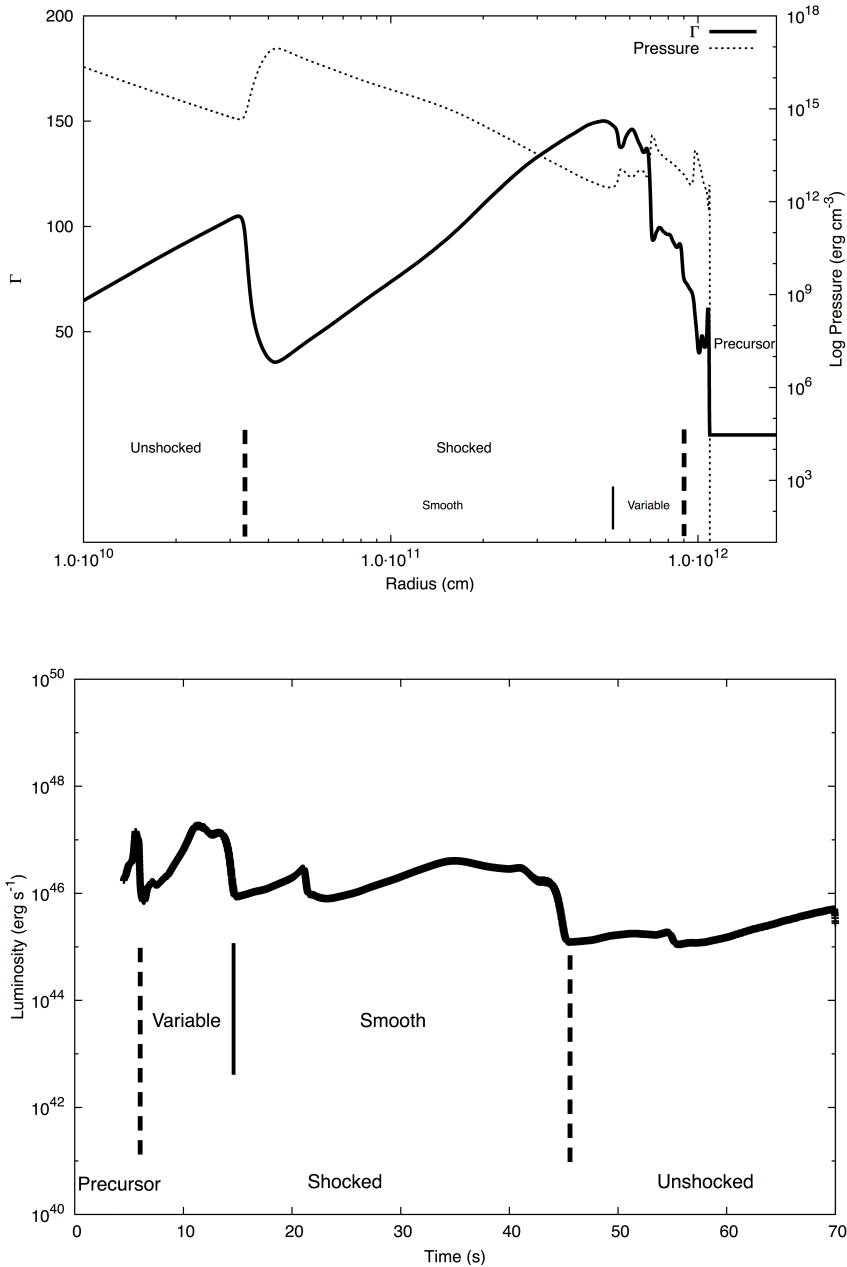
Figure 5.3: On the top, Lorentz factor (solid line) and the pressure (dotted line) along the jet axis as a function of the radius, for L700 model (T_{inj} = 70 s), at the moment of the unshocked phase breakout, t = 40 s. Dashed lines mark dramatic changes in pressure and Γ, due to the presence of strong shocks. In the bottom panel, the energy flux of the jet after the breakout, at 1.2×10^{11} cm, again with the dashed lines to separate the three phases.

5.1.3 BREAKOUT TIMES AND PROPERTIES

Following the discussion on the confined phase in § 5.1.1, Figure 5.4, shows the time of breakout of the radiative phases, for each model. The first group, *brief* engines, consists of only the precursor phase with a relatively low Lorentz factor. In *brief* engines, the cocoon, or precursor, is relatively slow at breaking out despite the engine high luminosity for this group of engine models. This is due to their jet head tendency to get denser and heavier (equation 8). As it can be seen in Figure 5.5, the *brief* engine jet head at the breakout (B010), is about two orders of magnitude denser than jet heads of other engines (B010). Such a jet head would not efficiently accelerate, loosing a large fraction of its power on the periphery. It is important to mention that only in the case of *brief* engines, the cocoon breaks out at a time when the engine is no longer working, making this group of engine models very different and peculiar. For all other longer engines, the engine is still running during, and after, the cocoon's breakout (see the dotted line in Figure 5.4). This element will have profound consequences on *brief* engines' jets behavior. *Short* and *intermediate* engines' cocoon is the fastest at breaking out, about ~2 seconds after the start of the injection. In addition, these two groups jets are the more relativistic. In terms of phases, both, *short* and *intermediate* engines produce a jet consisting of a precursor followed by the variable shocked phase. The shocked phase is quite variable, but it becomes progressively smooth as it makes its way through the star. Only *intermediate* (and *long*) engines are long enough to display this smooth part of the shocked phase. After the shocked phase, comes the steady unshocked phase, with a drop in the jet's luminosity (Figure 5.3, right panel & Figure 5.5, bottom right panel). As the injection nozzle is relatively deep (at 10^8 cm), the star-jet interaction is relatively stronger, than in ML07, and thus it takes longer for the unshocked phase to be launched and to eventually breakout. Only *long* engines run long enough to display this phase. The breakout times for the phases are relatively later for this group of *long* engines. This is due to the *long* engines low energy deposition rate $\dot{E} = E_{tot}/T_{inj}$, inversely proportional to the engine duration (as discussed in § 5.1.1). Thus, *long* engines' jets need some time to accumulate energy, enough to buildup a relativistic shock. This also explains why they have lower Lorentz factors at the breakout (Table 5-1). For a comparison of Figure 5.4, see figure 4 in Lazzati et al. (2012).
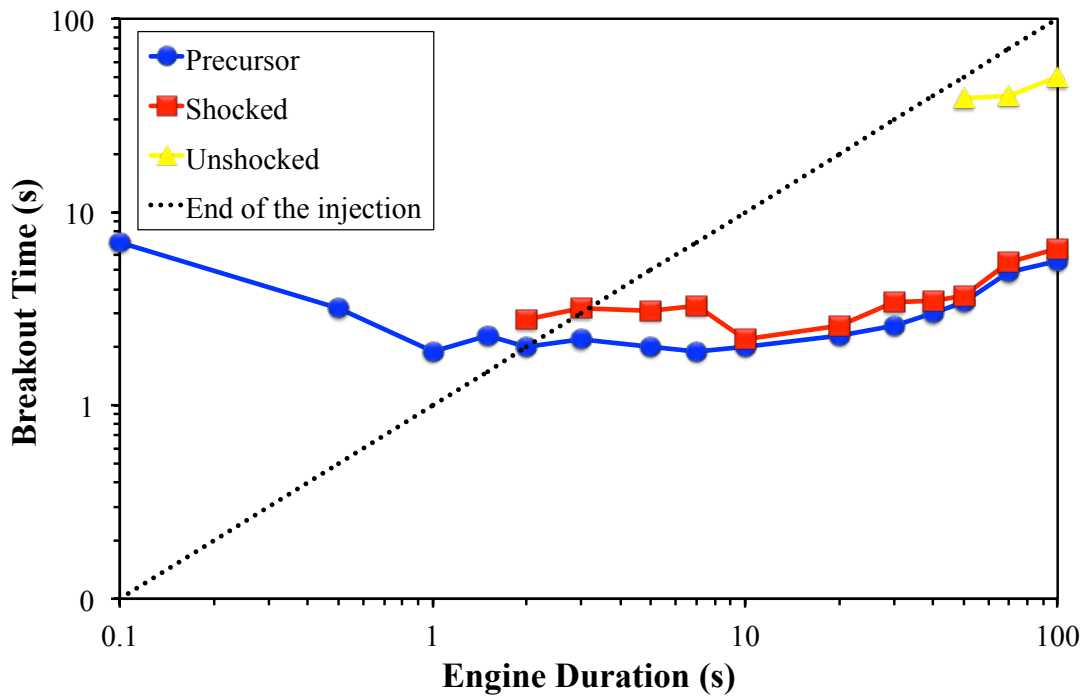
Figure 5.4: Breakout times for the three radiative phases of the computed models: precursor in blue, shocked in red, and unshocked in yellow. The dotted line shows the time when the injection stops for each model.

Figure 5.5 shows the density and Lorentz factor at, and after the breakout, in the top two and bottom two panels, respectively, for *brief, intermediate* and *long* engines (from left to right). A clear correlation is that the longer the engine duration is, the more well-collimated the jet seems to be. The *brief* engines' outflow is relatively denser and widely spread, with a significantly dense jet head, and dense materials blown in a short timescale in the off-axis region. The other longer engines' outflow structure contrasts, in terms of collimation and density, with power focused on-axis, in a jet like structure. This explains why *long* engines have been favored to reproduce GRBs in the relativistic/collimated jet scenario, and confirms that fact. (Hence the relatively numerous and deep studies dedicated to such *long* engine models.)
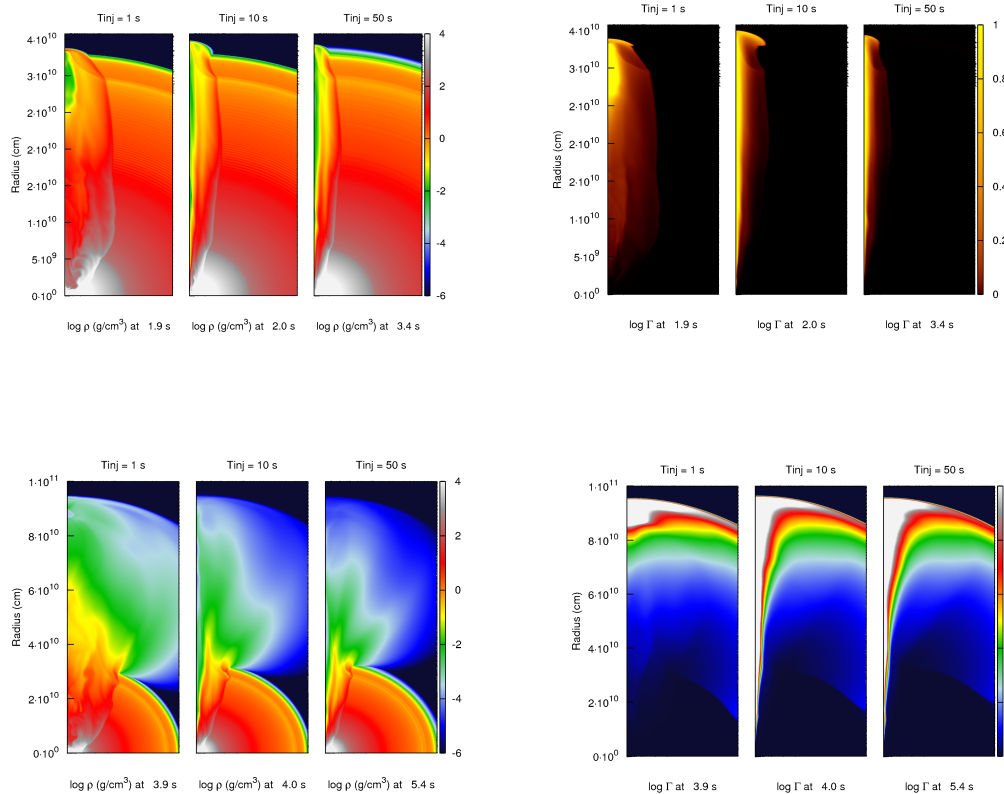
Figure 5.5: Density (at the left) and Lorentz factor (at the right), at the breakout time (in the top) and 2 seconds after the jet head breaks out (bottom). Breakout density and Lorentz factor (top panels) shows a wider jet for the *brief* engine (1 s) and a well-collimated jet for *long* engine (50 s). After the breakout (bottom panels), short injection models produce a poorly collimated jet, with the breakout shock relatively dense even at large angles. While longer engines (50 s injection model in particular), give a well-collimated jet structure.

Table 5-1: Breakout times of the main phases at the star surface (in the on-axis region)

Model	Cocoon Breakout Time (Lorentz Factor)	Shocked Breakout(s) (Lorentz Factor) Variable	Smooth	Unshocked Breakout(s) (Lorentz Factor)
B001	7.0 (1.02)	-	-	-
B005	3.2 (1.1)	-	-	-
B010	1.9 (33)	-	-	-
B015	2.3 (37)	-	-	-
S020	2.0 (34)	2.8 (52)	-	-
S030	2.2 (43)	3.2 (70)	-	-
S050	2.0 (40)	3.1 (55)	-	-
S070	1.9 (34)	3.3 (65)	5.7 (68)[1]	-
I100	2.0 (37)	2.2 (42)	8.2 (77)	-
I200	2.3 (25)	2.6 (23)	8.0 (75)	-
I300	2.6 (29)	3.4 (36)	7.3 (62)	-
I400	3.0 (17)	3.5 (30)	6.4 (59)	-
L500	3.4 (15)	3.7 (26)	7.0 (55)	38.9 (77)[1]
L700	4.9 (14)	5.5 (22)	9.0 (44)	40.1 (104)
L999	5.6 (14)	6.5 (32)	10.2 (31)	50.1 (109)
16TIg5-like[2]	6.8 (20)	7.8 (40)	-	25.0 (71)

[1] Not powered long enough to take part in the breaking out jet or influence it significantly.

[2] A model computed using the same injection nozzle as in ML07, 10^9 cm, instead of the 10^8 cm used for all the above models. The same total energy used in ML07 (5.32×10^{52} erg), and engine luminosity is also considered.
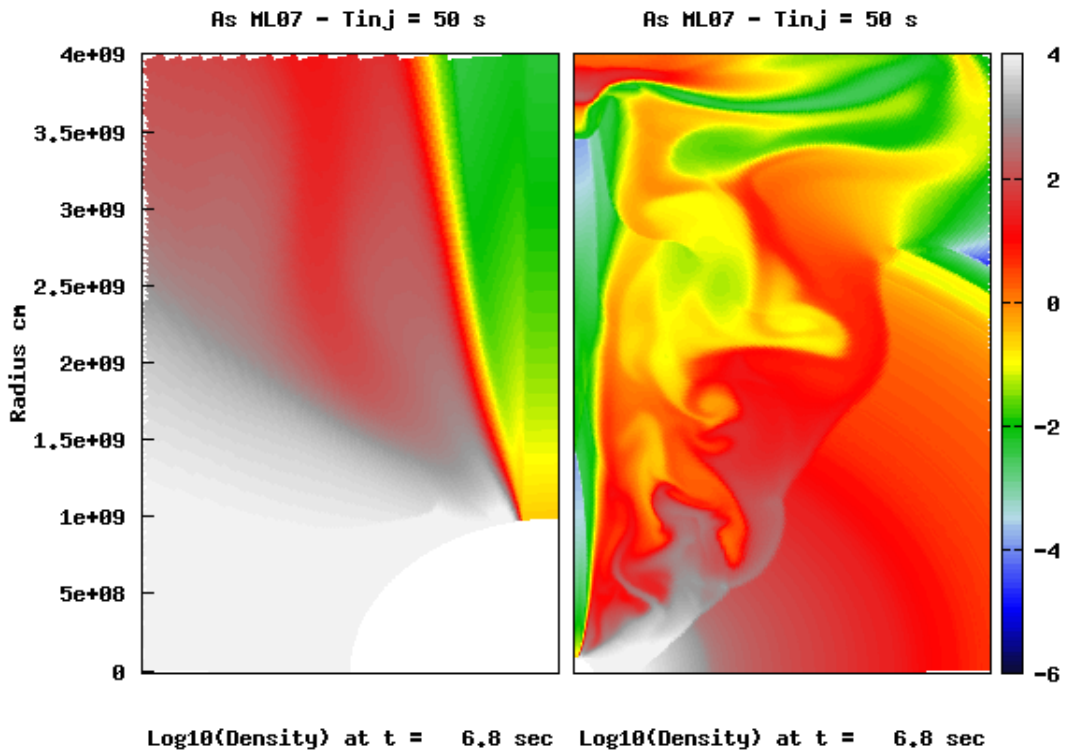
Figure 5.6: Snapshot of one jet (16TIg5 as in ML07). The relativistic jet (low density), is collimated by the lateral collimation shocks, and the hot cocoon's pressure (higher pressure). The figure on the right is a zoom out (x10).

5.1.4 SYNTHETIC LIGHT CURVES

Table 5-2 shows the phases contributing to each jet, and the structure of the resulting light curve. Figure 5.7 shows light curves representing each of the four types of engines, all estimated as in ML07 (Fig. 12 & § 4.1 of ML07 for details), at the same location $(1.2 \times 10^{11}$ cm), with the same outflow conditions ($\Gamma > 10$), and with the same angular bins (as explained in § 4.4.4). *Brief* engines produce a sharply single peaked light curve; it is the signature of the precursor phase. *Short* engines produce a wider single peak structure, showing high variability. This is due to the contribution of the shocked phase effectively launched by *short* engines, and dominating their jet. *Intermediate* engines are long enough to display a second bulk (I200 in Figure 5.7, from ~10 to 20 s),

showing a double peaked structure. Only *long* engines are long enough to display the unshocked phase contribution in the light curve, with luminosity decreasing sharply and showing a steady structure that reflects the constancy of the injected jet (L700 in Figure 5.7, from ~47 to 70 s). With this last phase, the structure of such *long* engines is the more complex, resulting from the contribution of all the three different phases.

Isotropic equivalent luminosities in the light curves of Figure 5.7 are very high. This is because I consider an observer line of sight in the on-axis region, at 0.125˚, which gives an isotropic factor of ~10^5. As discussed in § 4.4.4, it is clear that only a small fraction of the jet luminosity would contribute to the prompt emission. Roughly considering a radiative efficiency of 1% would bring the prompt emission luminosities to the observed domain for LGRBs 10^{48-54} ergs/s (Levan et al. 2014). In this study I considered a total engine energy of only 10^{52} erg, which reasonable and not very extreme. Nevertheless, with such an ordinary engine, extremely energetic GRBs might be explained if I assume an observer line of sight in the jet on-axis region, as has been generally considered.
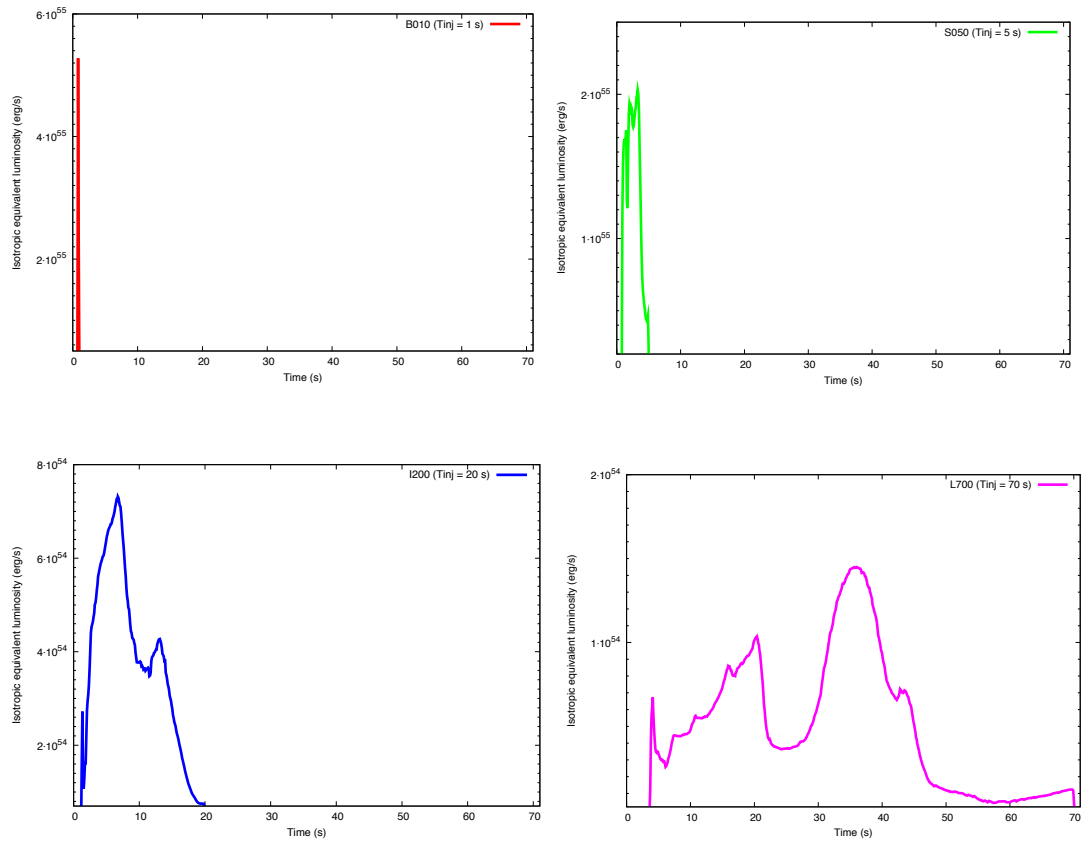
Figure 5.7: Light curve for an on-axis observer of the four different types of engine models. On the top left, *brief* engine jet ($T_{inj} = 1$ s), the light curve is a single sharp peak. On the top right, *short* engine jet ($T_{inj} = 5$ s), the peak is wider and shows high variability. On the bottom left, an *Intermediate* engine ($T_{inj} = 20$ s), the light curve display two bulks structure. Finally, *long* engine jet's light curve ($T_{inj} = 70$ s), showing more that two bulks; a more complex structure. Light curves were estimated as explained in § 4, and after ML07.

Table 5-2: Light curve structure according to the contribution of the jet main phases (considering the energy flux at 1.2×10^{11} cm for an on-axis observer and outflow with $\Gamma > 10$, as in ML07).

Model	Precursor Phase (Quasi-Isotropic)	Shocked Phase (Narrowed & Well-Collimated) Variable	Smooth	Unshocked Phase (Wide & Collimated)	Light curve Structure
B001	Yes	-	-	-	Sharp Narrow Peak
B005	Yes	-	-	-	Sharp Narrow Peak
B010	Yes	-	-	-	Sharp Narrow Peak
B015	Yes	-	-	-	Sharp Narrow Peak
S020	Yes	Yes	-	-	Wide Variable Peak
S030	Yes	Yes	-	-	Wide Variable Peak
S050	Yes	Yes	-	-	Wide Variable Peak
S070	Yes	Yes	-	-	Wide Variable Peak
I100	Yes	Yes	△	-	Wide Variable Peak
I200	Yes	Yes	Yes	-	Two Main Bulks
I300	Yes	Yes	Yes	-	Two Main Bulks
I400	Yes	Yes	Yes	-	Two Main Bulks
L500	Yes	Yes	Yes	△	More than Two Bulks
L700	Yes	Yes	Yes	Yes	More than Two Bulks
L999	Yes	Yes	Yes	Yes	More than Two Bulks

△ : This last phase, or part, is launched, but not long enough to contribute in the light curve.

Hamid Hamidani - February 2016

5.2 ANGULAR PROPERTIES

5.2.1 ANGULAR DISTRIBUTION

In Figure 5.8, the top panel shows the fraction of the jet total energy that is contained inside the polar angle θ. Figure 5.9, shows the angle inside which 50% (in dashed blue, θ_{50}) and 99% (in solid red, θ_{99}) of the total energy carried by the jet is contained. It is clear that the longer the engine duration is, the more well-collimated the jet outflow and energy is. The bottom panel in Figure 5.8 shows the averaged Lorentz factor, with the polar angle θ. The averaged Lorentz factor was calculated as in Duffel et al. (2015), with the ratio of outflow total energy to total mass at the angle θ. The results support those of the top panel; the longer the injection duration is, the more collimated and relativistic the launched jet is. It is noticeable how contrasting *brief* engines with *long* engines are, in terms of relativistic properties. On average, the *brief* engine model ($T_{inj} =$ 1s) poorly accelerates outflow to the relativistic domain ($\Gamma > 10$) in the on axis region, while it shows a tail of sub-relativistic outflow very widely (and isotropically) spread in the off-axis region (that is, a quasi-isotropic structure). For longer engine, the jet outflow is more efficiently accelerated, and concentrated in few degrees around the on-axis region (exhibiting a typical "jet" structure). In summary, the behavior of *brief* engines contrasts with other types of engines by dominating in the off-axis region, while the longer engines dominate in the on-axis region.
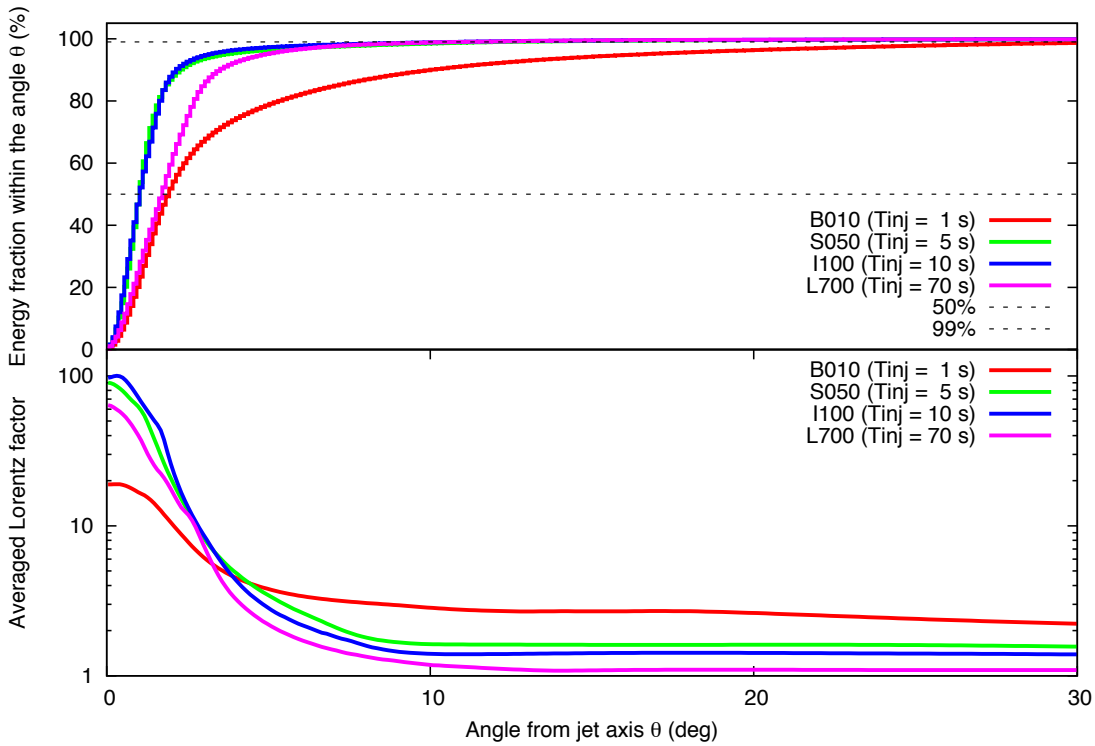
Figure 5.8: On the top panel, we show the cumulative distribution of the jet energy fraction inside the angle θ, with angle (*brief* engine in red, *short* in green, *intermediate* in blue and *long* in cyan). The two dashed lines shows the angles where 50% and 99% of the energy is located, and how these angles differ in the four engine models. The bottom panel shows "the averaged Lorentz factor" as a function of the angle. It is defined as the ratio of energy to mass at the given angle (same definition as in Duffell et al. 2015).
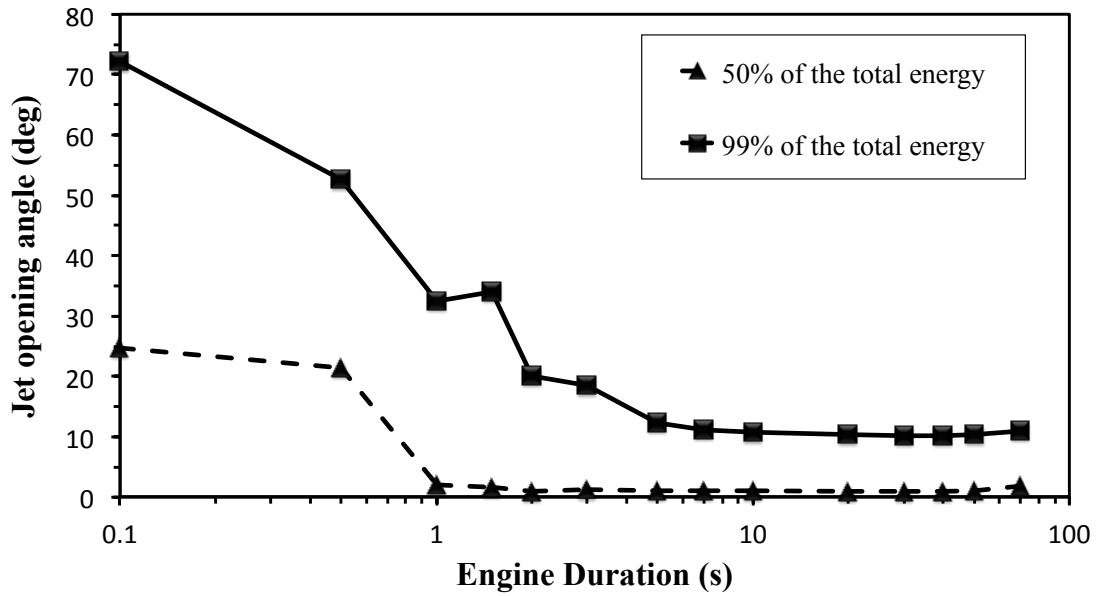
Figure 5.9: The opening angle of outflow containing 50% of the total energy θ_{50}, in triangles with a dashed line, and 99% of the total energy θ_{99}, in squares with a solid line.

5.2.2 COLLIMATION

Next, I carried out a comparison between each engine's on-axis and off-axis energetic and relativistic outflow properties, and compared the results for the different types of engines. I use the same angular bins as explained in § 4.4.4, at the same radius (1.2×10^{11} cm). I take the minimum Lorentz factor as 1, that is, I consider all the outflow energy at both relativistic and non-relativistic velocities. By the on-axis region, I mean the innermost angular bin centered at 0.125º, and for the off-axis region, I consider the 21st angular bin, centered at 10º away for the jet axis. The choice of the off-axis region at 10º is because it is the farthest angle from the on-axis, at which outflow from all the models is effectively present (thus allowing a comparison to be made). I analyzed the averaged Lorentz factor, and the total energy in these two regions. I also analyzed the

ratio of both the energy, and Lorentz factor, at the on-axis region, over the same quantity at the off-axis region, for different engine models.

The results are shown in Figure 5.10. The figure's top panel shows that the relativistic and energetic properties are different for the different engine models. For *brief* engines, on-axis and off-axis quantities are almost of the same order of magnitude. I can deduce that the outflow from the star is indeed spread in a quasi-isotopic angular distribution for such *brief* engines. In a jet context, *brief* models produce a poorly collimated jet. With longer engines, the gap between on-axis and off-axis quantities increase dramatically, where on-axis relativistic and energetic quantities are about 1 to 2 orders of magnitude higher than the same quantity in the off-axis region. This high gap continues for most *short* and especially for *intermediate* engines, indicating that it is for these engine durations where the jet collimation is the best. For *long* engines, the gap is slightly reduced, but the produced outflow is still reasonably well collimated. The general trend is that, the longer the engine duration the more relativistic and energetic the outflow is at the on-axis region, and the less relativistic and energetic the outflow is in the off-axis region. However, for engines, longer than ~ 40 seconds, the tendency is slightly inversed.

Figure 5.10: the bottom panel, show the behavior of the jet (energy and Lorentz factor) in the studied engine duration domain, in particular at the two extreme limits, *brief* and *long*. The collimation behavior implies a "sweet spot" in between the two limits, where the ratio and thus the collimation is the best (optimal for producing an energetic GRB's relativistic jet). *Intermediate*, followed by *short* engines, make the finest jets in terms of collimation. *Long* engines come next, making less collimation as the engine duration is longer. While *brief* engines come last, producing very poorly collimated jets, although the ratio, thus the collimation, improves as the engine duration increases. For the engine luminosities and durations presented here, the "sweet spot" is at $T_{inj} \sim 5 - 30$ seconds, corresponding to engine luminosity per jet in the range: $1.6 - 10 \times 10^{50}$ erg/s. This "sweet spot" would certainly depend on progenitor properties, such as size and density profile, and the considered engine total energy. The choice of the off-axis region here was at 10º. The choice of this off-axis region may influence the domain of the sweet spot, but certainly not the general trend found here.

The poor collimation of jets from *brief* engines can be explained by the quasi-isotropic properties of the unique jet phase launched by these engines, the precursor phase. The excellent collimation of jets from *short* and *intermediate* engines can be related to one main factor: The properties of the shocked phase, which dominates these two groups of engines, and which is the narrowest among the three phases. Finally, the inversed trend in the case of *long* engine jets is likely to be related to two factors. First, the effective launch of the third unshocked phase by such *long* engine durations, which is characterized by wider angular distribution than the shocked phase. The second factor would most likely be the low luminosity of these *long* engines, which might be lower than a certain critical luminosity necessary to effectively accelerate and collimate the jet.
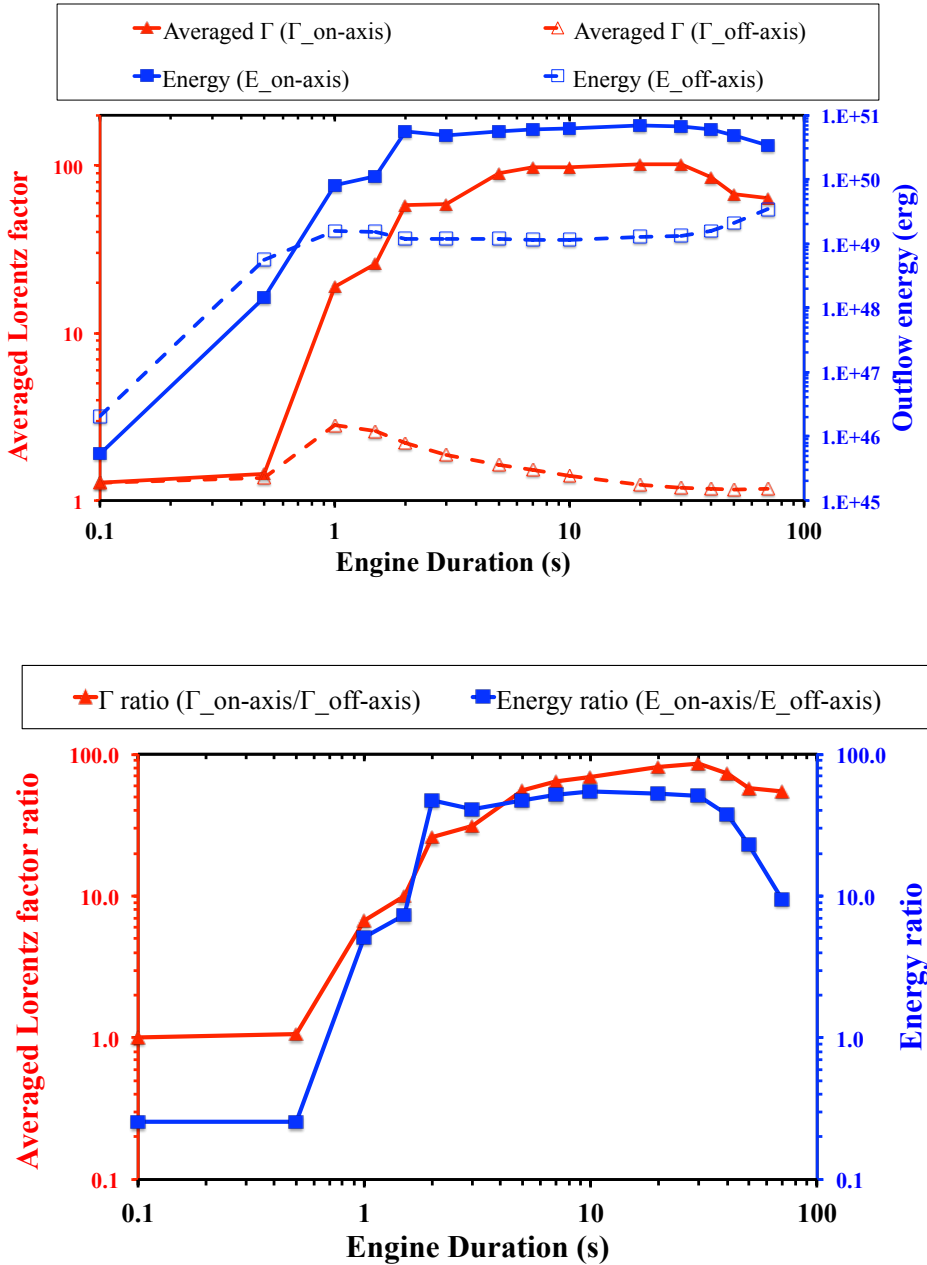
Figure 5.10: On the top, the averaged Lorentz factor, in red, in the on-axis (0.125º) with filled triangles and solid line, and in the off-axis region (10º) with unfilled triangles and dashed line. In blue, the outflow total energy, in the on-axis (0.125º) with filled squares and solid line, and in the off-axis region (10º) with unfilled squares and dashed line. Both measured at 1.2×10^{11} cm, for different engine duration models. In the bottom, the ratio of the averaged Lorentz factor at the on-axis over that at the off-axis, in red line and triangles. The blue line and squares, is the ratio of the total energy at the on-axis over that at the off-axis.

Hamid Hamidani - February 2016

5.3 ENERGY ACCELERATION

In this section, I present how the engine duration affects the relativistic feature of the resulting outflow's energy. Different engine models display different behaviors at transmitting the engine total energy into non-relativistic or relativistic outflow, with different efficiencies. This transmission, or relativistic transformation, of the engine energy, depends on how the jet is able to form and expand. Some key parameters of the engine model may play a role, parameters such as: The engine duration, the cocoon breakout time, and the engine luminosity. In the engine models, the parameters above differ as the engine duration change from an engine to another. I analyze how the engine duration plays a role at this relativistic transformation and at the nature of the energy in the expanding outflow, by comparing the different engine models.

I present the fraction of the total injected energy transformed - and transferred - into the expanding outflow at different relativistic levels: 1) Sub-relativistic domain: Fraction of the injected energy in material moving at more that 10% the speed of light, corresponding to Lorentz factor $\Gamma > 1.005$. 2) Relativistic domain: Fraction of the energy in material with $\Gamma > 10$. 3) Highly-relativistic domain: Fraction of the energy in material with $\Gamma > 100$.

Figure 5.11 shows the effect of the engine duration on the nature of the energy propagating in the CSM. *Brief* engines' resulting energy is poorly accelerated, and is moving the slowest among the engine models presented here. Most of the engine energy moves at non-relativistic speed. For longer *brief* engines, B010 and B015, about 1/4th of the injected energy is successfully accelerated to relativistic domain $\Gamma > 10$. With longer engine durations, the acceleration efficiency is significantly higher for *short* engines, increasing from ~60% up to ~90%, for energy in material moving with $\Gamma > 10$. The efficiency's increasing tendency with longer engine durations continues, up to *intermediate* engines domain, where the efficiency is the highest in the three domains ($\Gamma > 1.005$, $\Gamma > 10$ and $\Gamma > 100$), and roughly constant through *intermediate* engines' duration interval. For *long* engines, the tendency is inversed, with less efficiency for

longer engines, although these engines remain considerably capable of converting - and accelerating – more than 50% of the engine energy into relativistic domain.

Thus, the general tendency of the engine energy acceleration efficiency, at the two extremities of the engine duration domain, shows a "sweet spot" here too with efficiency increases first up to the *intermediate* engines' domain where the efficiency is the highest and constant, then a decreasing efficiency at the *long* engines' duration domain. Generally, apart from *brief* engines, all other engines are efficient at accelerating the engine energy into relativistic domains. Thus, the interesting contrast here is that, for *brief* engines the relativistic nature of the produced jet outflow leaves considerable energy to power a non-relativistic event, a SN explosion, which would be observed along a relatively soft GRB. While for longer engines, most of the energy would be accelerated to contribute to producing a much more powerful GRB, leaving much less energy in the non-realistic domain.
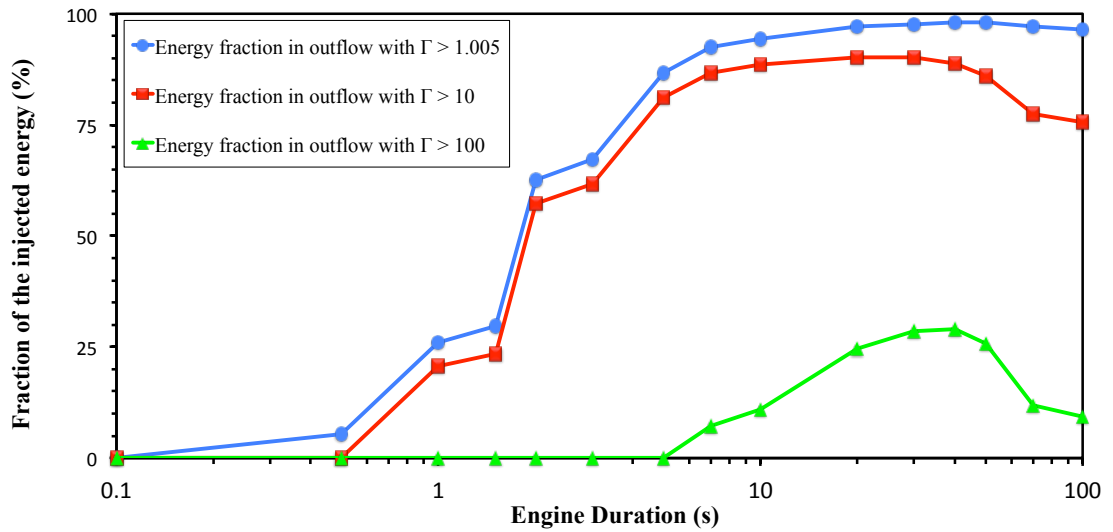
Figure 5.11: Total injected energy converted into different relativistic levels as a function of the engine duration. In blue circles, total injected energy fraction in material with $\Gamma > 1.005$, in red squares, energy fraction in material with $\Gamma > 10$, and in green triangles, energy fraction in material with $\Gamma > 100$. All measured at a radius of 1.2×10^{11} cm.

5.4 PHASE CONTRIBUTION

An important question was addressed in this chapter: *"How the collapsar engine timescale shapes the produced relativistic jet?"* As it was found that the shock progression, in the confined phase, is strongly affected by the engine duration, especially between *brief* engines and the other longer engines, I have obtained diverse breakout times.

As shown in the Figure 5.12 an interesting finding is that, the engine duration is a jet recipe, as different engine durations result in different combinations of the three radiative phases. The consequence of the different phase contributions is different products that are different in several important jet properties it has been shown. Among the different properties that were discussed, two are of profound consequences on the

expected type of event to be seen: 1) the angular distribution, and 2) the energy acceleration efficiency. In the next chapter I will discuss the astronomical implication of these two differences on: 1) the rate of *ll*GRBs over the rate of GRBs, and 2) SN energy, respectively. Here is a first study that discusses the two above properties in the context of *ll*GRBs, thus it is of central importance in this thesis.
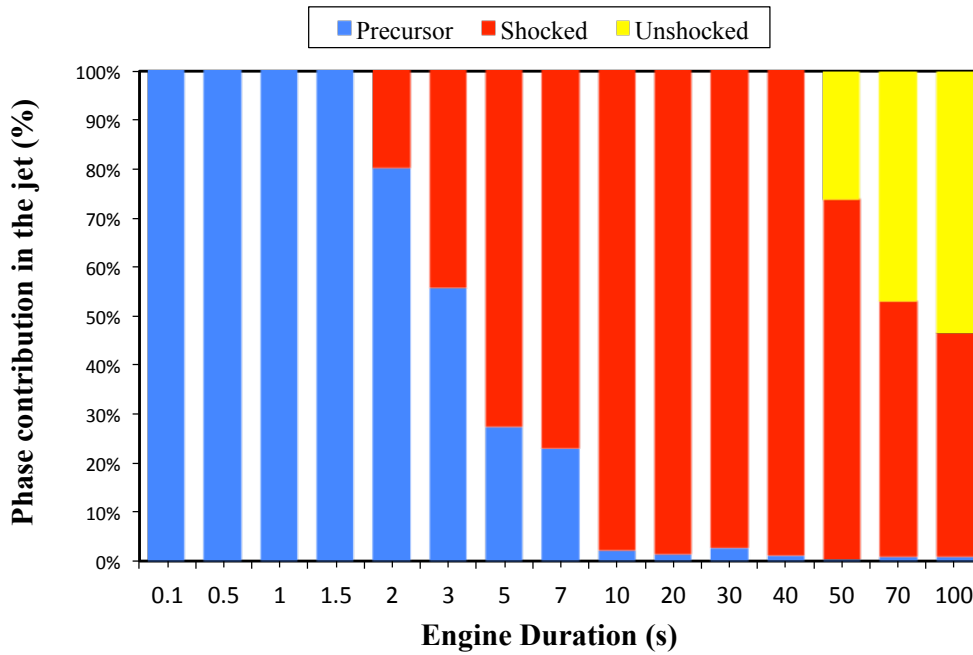
Figure 5.12: Time and energy contribution of each of the three radiative phases in the propagating jet for the different engine models. The observe jet properties are different because of this crucially different recipes of radiative phases.

6 ASTRONOMICAL IMPLICATIONS

"Poets say science takes away from the beauty of the stars - mere globs of gas atoms. I, too, can see the stars on a desert night, and feel them. But do I see less or more?" — Richard Feynman

6.1 OVERVIEW

A varied version of collapsars, in terms of the engine duration, has been explored. The engine duration was found to strongly affect the resulted jet properties. However, *what would be the observational consequences of such different hydrodynamic properties? How would these differences affect the observed prompt emission, the probability of observation and the SN explosion energy?* This chapter discusses the above questions in the context of *ll*GRBs high rates (~ 100 − 1000 times higher that standard GRBs rates), and in the framework of GRB-SN connections.

Finally, at the end of this chapter, one last question is explored; by considering different collapsar engine duration distributions, which attribute different probabilities to the different engines in the duration range 0.1 − 100 seconds; *what is the adequate*

collapsar duration distribution that explains the relative rate of llGRBs to GRBs, at least in the nearby universe?

6.2 LLGRBs Vs. GRBs

6.2.1 Angular Structure

In order to relate the jet outflow to a GRB context, the study should be limited to relativistic outflow, as relativistic Lorentz factors are an essential requirement to produce GRB's prompt emission. Figure 6.1 illustrates the total energy angular distribution, considering only the relativistic outflow, $\Gamma > 10$. The angular distribution was plotted following the same procedure as in Figure 4.3, considering different engine models (at 1.2×10^{11} cm with the same angular bins as in ML07, as explained in § 4.4.4). A quantitative comparison confirms the previously pointed-out general trend, where the shorter the wider (as for B010) and the longer the more narrowly spared the energy, and outflow, are (panel a). Using the phases different angular distributions (Lazzati t al., 2007), panels b, c and d, help understanding the reason behind the diversity of the angular structure for the different models: *Brief* models' jets are dominated by the precursor, and thus show a similar angular structure, widely spread and relatively soft at small angles (panel b). *S*hort and *intermediate* models' jets are dominated by the shocked phase, thus showing a similar structure, hard and sharply decreasing at small angles (panel c). Finally, *long* models, dominated by the unshocked phase at late times show an angular structure gradually converging to that of the unshocked phase, displaying a flat distribution in small angles (< 10º) (panel d). Lazzati et al. (2007), showed how the viewing angles can be behind some of the diversity in the light curve. Here I clearly show how the jet and all of its properties can be diverse and variant, from precursor-like, shocked-like to unshocked-like, just with different engine times.

An interesting contrast is that short engine models energetically dominate in the off-axis region, while *intermediate* and *short*, followed by *long* engines are energetically dominate in the on-axis region. This suggests that for latter engines, this on-axis jet energy, after being partially converted to gamma and X-ray photons, would have the potential to produce extremely luminous and energetic events, assuming an observing

Hamid Hamidani - February 2016

angle close to the jet on-axis region. The isotropic equivalent energies would be brought to the same domain of isotropic energies observationally estimated for GRBs. On the other hand, *brief* engines, with their wide tail of soft energies in the off-axis region might not only explain the recently debated *ll*GRBs energies, but might also explain their huge rates as well.

Due to their significantly low luminosities, *ll*GRBs can be detected only at low redshift, at the opposite of the standard/cosmologic GRBs. Estimates of the *ll*GRB rate, show enormously high rates (Piran et al. 2006: 290 – 90 Gpc^{-3} yr^{-1}, compare to ~1 Gpc^{-3} yr^{-1} for cosmological GRBs; Coward 2005: ~220 Gpc^{-3} yr^{-1}; Soderberg et al. 2006: 230^{+490}_{-190} Gpc^{-3} yr^{-1}). This implies a rate 100-1000 times higher than the rate of standard GRBs (Bromberg et al. 2011a).
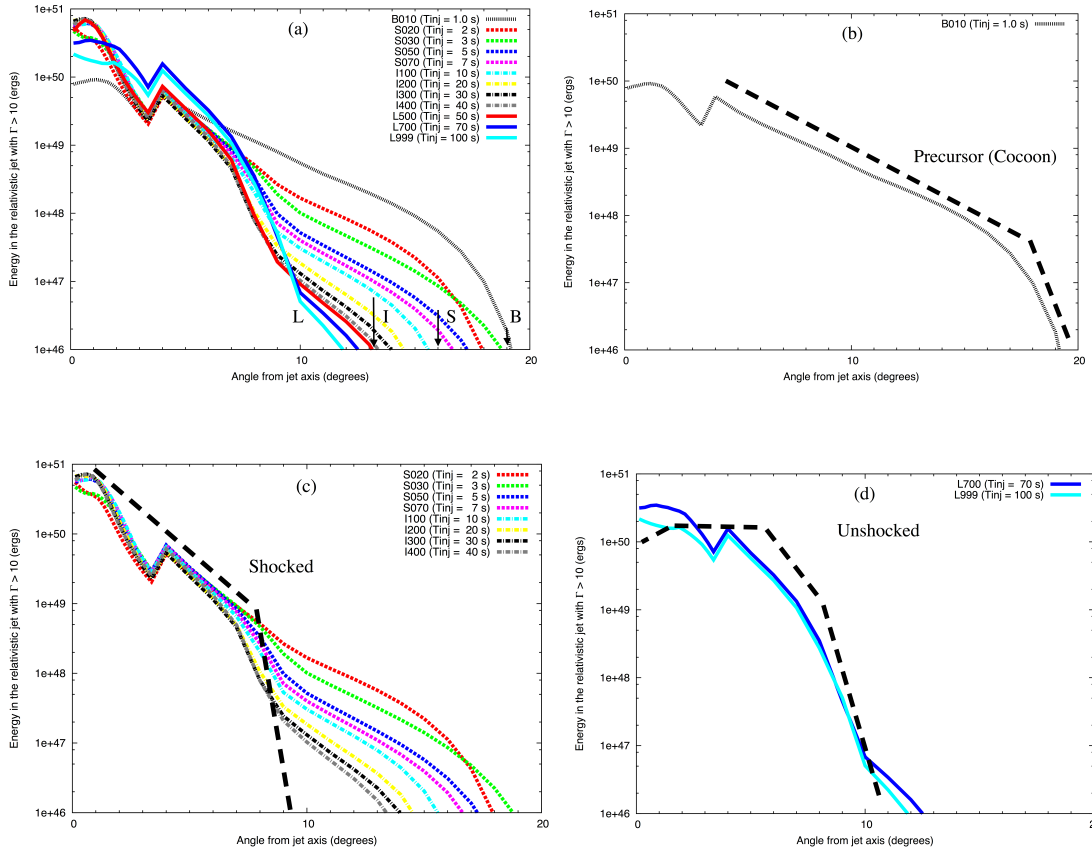
Figure 6.1: Angular distribution of energy for the relativistic outflow $\Gamma > 10$, considering different engine durations from 1 to 100 s. Panel (a): The *brief* engine distribution is the widest, up to large angles, as limited by the short arrow and marked a the capital B. *Short* engines are between the short and medium arrows, marked with a capital S. Between the medium and the long arrows is the *intermediate* engines marked with a capital I. *Long* engines are on the left of the long arrow at the shortest angles, marked with a capital L. Panel (b), (c) and (d) show the angular distributions of different models and how the angular distribution is shaped by the angular structure of the dominating phase (in dashed lines). *Brief* model angular distribution is shaped by the precursor phase (b). *Short* and *intermediate* models' angular distribution is strongly shaped by the shocked phase at small angles, which dominate their outflow (c). *Long* models show angular distribution gradually converging to that of the unshocked phase (d).

6.2.1.1 JET STRUCTURE: UNIFORM JET VS. UNIVERSAL JET

6.2.1.1.1 THE DEBATE ON JET CONFIGURATION

After the launch of HETE-2 mission, XRFs (or *ll*GRBs) started to gain importance. As the measure of some GRB jet's opening angle from the breaks in the light curve gave evidence of a beamed structure (Frail et al. 2001), a debate start on the configuration of GRBs' relativistic jets. In order to explain both XRFs (*ll*GRBs) and GRBs, in a uniform model, two configurations have been proposed by Ramirez-Ruiz & Lloyd-Ronning (2002), as shown in Figure 6.2. Lamb et al. (2003 & 2005) investigated which of the two configuration would explain and unify GRBs and XRFs: a) the power-law universal jet model, where the jet energy is assumed to decrease as the viewing angle θ, in a power-law (the index might be ~2); b) the uniform jet, where different opening angles for a standard energy reservoir of the jet was considered. Lamb et al. (2003 & 2005) aimed to explain GRBs and XRFs detection and rates together in one jet configuration (either a or b). Lamb et al. (2005) finding was that the variable opening angle uniform jet configuration alone would unify and explain both XRFs and GRBs. But this lead to implication difficult to explain, as it implies that GRBs must have very small opening angle (~ 0.5º), which infers extremely high rate for standard GRBs, comparable to the rate of type Ic core-collapse SNe.
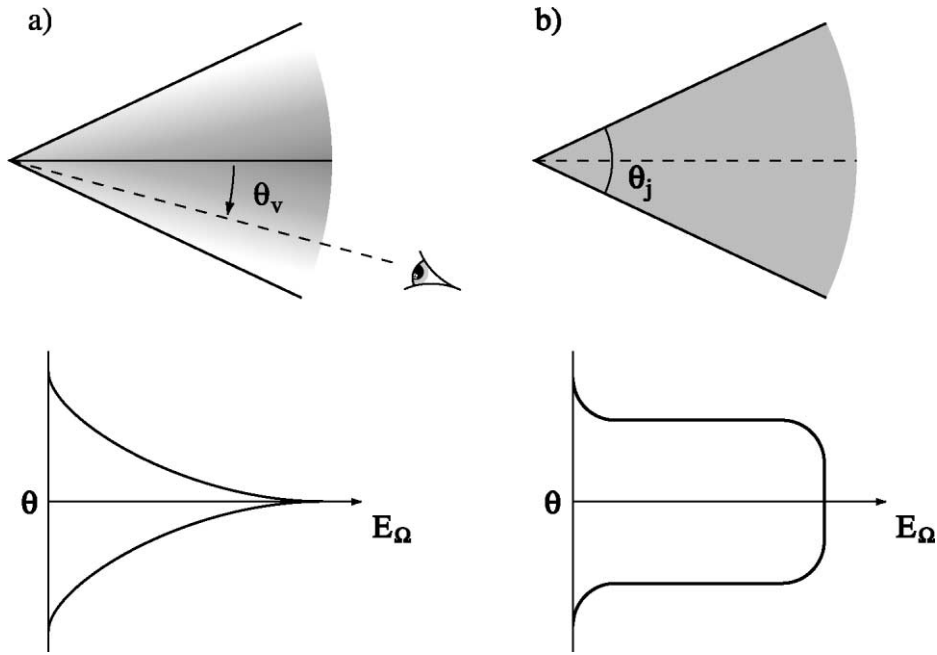
Figure 6.2: Illustration of two configuration to explain GRB beaming: a) is the power-law universal jet model, the jet energy is assumed to decrease as the viewing angle θ: $E(\theta) \propto \theta^{-\beta}$, b) is the variable jet opening angle uniform jet, where different opening angles for a standard energy reservoir are assumed (Credit: Ramirez-Ruiz & Lloyd-Ronning 2002; Lamb et al. 2003; 2005).

6.2.1.1.2 THE EFFECT OF ENGINE DURATION

Analyzing the produced angular distributions of the produced relativistic jets by the different engine duration suggest that: The relativistic jet configuration can, theoretically be either a) or b) (Figure 6.1: panel c) and d) respectively). As the shocked phase represent a configuration close to the universal jet (a), and the unshocked phase has rather a configuration closer to the uniform jet (b), both configuration was reproduced in my models based on whether the jet is a "shocked-phase" dominated jet, or an "unshocked-phase" dominated jet, respectively (Lazzati et al. 2007).

However, as the engine duration must be diverse in nature, both "shocked-phase" dominated jet, and "unshocked-phase" dominated jet, can be launch; and both would account for the observed. Thus, it is very hard to imagine that only one out of the two configurations – a) or b) – to unify GRBs with their diversity; it is even harder to imagine the unification in one pattern for GRBs and *ll*GRBs in nature. The concept of one universal jet configuration that would unify GRBs is very hard to imagine in the framework of huge diversity in GRBs. The contribution to the debate on jet structure, above, based on numerical simulations, is that both a) and b) configurations are accounting for the observed GRBs; neither of a) or b) can explain all GRBs.

Thanks to Swift, Fermi, and other missions, GRBs data has dramatically increased in quality and quantity. In this framework, it is difficult to imagine one universal jet configuration unifying GRBs, and certainly not GRBs with *ll*GRBs. GRBs large and diverse population has to be explained by both configuration, and other particular configurations might be required. As it will be explained in the following section § 6.2.2 and then § 6.3, *ll*GRBs requires different type of jets to explain their peculiar properties: failed jets, or "precursor-phase" dominated jet (Figure 6.1: panel b), which present different angular configuration of energy. Thus, the jet configuration of GRBs and *ll*GRBs must be much rich and diverse than previously thought.

6.2.2 PROBABILITY OF OBSERVATION AND RATES

The jets' angular structure is in agreement with the unification model proposed by Nakamura (2000), Yamazaki et al. (2002, 2004); quantitatively discussed in Zhang et al. (2004). The model attributes the different origins of GRBs and *ll*GRBs (or XRFs) to the observer's different viewing angles, being close to the on-axis, or far in the off-axis region, respectively. However, the new interesting point here is that the different engine durations show contrasting energy angular distributions, thus the different engines would be quantitatively different at favoring GRBs over *ll*GRBs, and vice versa. This would be interesting especially in a context where *ll*GRBs are expected to mysteriously have hugely unexplained rates.

In this section, I discuss the astrophysical implications for the different models. In Figure 6.3 (top), I show the angular distribution of the isotropic equivalent energy estimated for the prompt emission, as explained in § 4.4.4. Results show that: The shorter the engine duration is, the more the isotropic energy is spread at larger angles and thus, the more chances to observe the energy considering a random observer in the sky (Figure 6.3, bottom panel). *Long* engines present narrow jets and thus, are less likely to be observed. *Intermediate* engines are between the two extremities. A comparison between B010 (T_{inj} = 1s) and L700 (T_{inj} = 70 s) shows that B010 collapsar has a ~150% higher chance to be observed. One other interesting difference is that *brief* engines energy distribution falls below the domain of typical GRBs (E_{iso} ~10^{52} erg). This makes such *brief* engines, capable of producing *ll*GRBs with extremely high chances of detection, in the nearby universe, relative to standard GRBs. Indeed, *ll*GRBs have been estimated to have extremely high rates, 100-1000 times those of GRBs: Soderberg et al. (2006) and Bromberg et al. (2011a), since *ll*GRBs have been observed at very low redshifts (z < 0.1) in comparison to GRBs, suggesting a high density of *ll*GRBs, at least in the nearby universe. Such soft and less relativistic jets produced by these *brief* engines, present a possible approach to explain these peculiar *ll*GRBs and their huge rates.

Next, as in Figure 6.4 I calculate the probability of observing the event as a function of its isotropic equivalent energy. Then as shown in Figure 6.5, the ratio of probabilities is shown as a function of the engine duration. It is the probability of observing the engine's emission in *ll*GRB typical energy range (E_{iso} = 10^{47-49} erg, although some *ll*GRBs show slightly higher isotropic equivalent energy, e.g: GRB031203, with E_{iso} ~ 10^{50} erg), over the probability of observing the same engine's emission in GRB typical energy range (E_{iso} ≥ 10^{52} erg, though there are few exceptions with E_{iso} ~ 10^{51} erg). I calculate the probabilities using the estimated prompt emission isotropic equivalent energy's angular distribution for each model (as explained in § 4.4.4). Using the probability formula in (12), and with simple calculation the ratio can be written as in the equation (13):

$$Rate_{llGRB/GRB} = \frac{P(E \geq 10^{47}) - P(E \geq 10^{49})}{P(E_{GRB} \geq 10^{52})}$$

$$= \frac{\cos(\theta_{E \geq 10^{49}}) - \cos(\theta_{E \geq 10^{47}})}{1 - \cos(\theta_{E \geq 10^{52}})} \qquad (13)$$

Where E is the isotropic energy in "*erg*" unit, $\theta_{E \geq x}$ is the opening angle of the region where the prompt emission is above "*x* erg" (as in equation (12)). As for most GRBs with redshift, E_{iso} is generally $\geq 10^{52}$ erg, and for *ll*GRBs, E_{iso} is in the domain 10^{47-49} erg. The results are illustrated in the Figure 6.5: The ratio of probabilities, *ll*GRB/GRB, decreases with the increase of the engine duration. The longer the engine duration is the more efficiently (or chances) GRB events will be produced (or observed). In contrast, with *Long* engines, *brief* engines are *ll*GRB-makers at extreme rates (or probability of observation), relative to GRBs. Only *brief* engines could populate the region of *ll*GRBs rates at 100 - 1000 times the regular GRBs. This clearly indicates that only *brief* engines ($T_{inj} < T_{Breakout}$), are capable of explaining the huge rates of *ll*GRBs in the nearby universe, estimated in Soderberg et al. (2006) and Bromberg et al. (2011a). This is also in an excellent agreement with Bromberg et al. (2011a), implying that:

i) A large fraction of *ll*GRBs have their engine duration shorter than their breakout time, as for the *brief* engines: B010 with $T_{inj} = 1.0 < T_{Breakout} = 1.9$ s, and, B015 with $T_{inj} = 1.5 < T_{Breakout} = 2.3$ s.

ii) For regular GRBs the engine duration has to be significantly longer than the breakout time, in order to successfully power a GRB, which is here satisfied in the case of *long* engines: L500 with $T_{inj} = 50 \gg T_{Breakout} = 3.4$ s, and, L700 with $T_{inj} = 70 \gg T_{Breakout} = 4.9$ s.
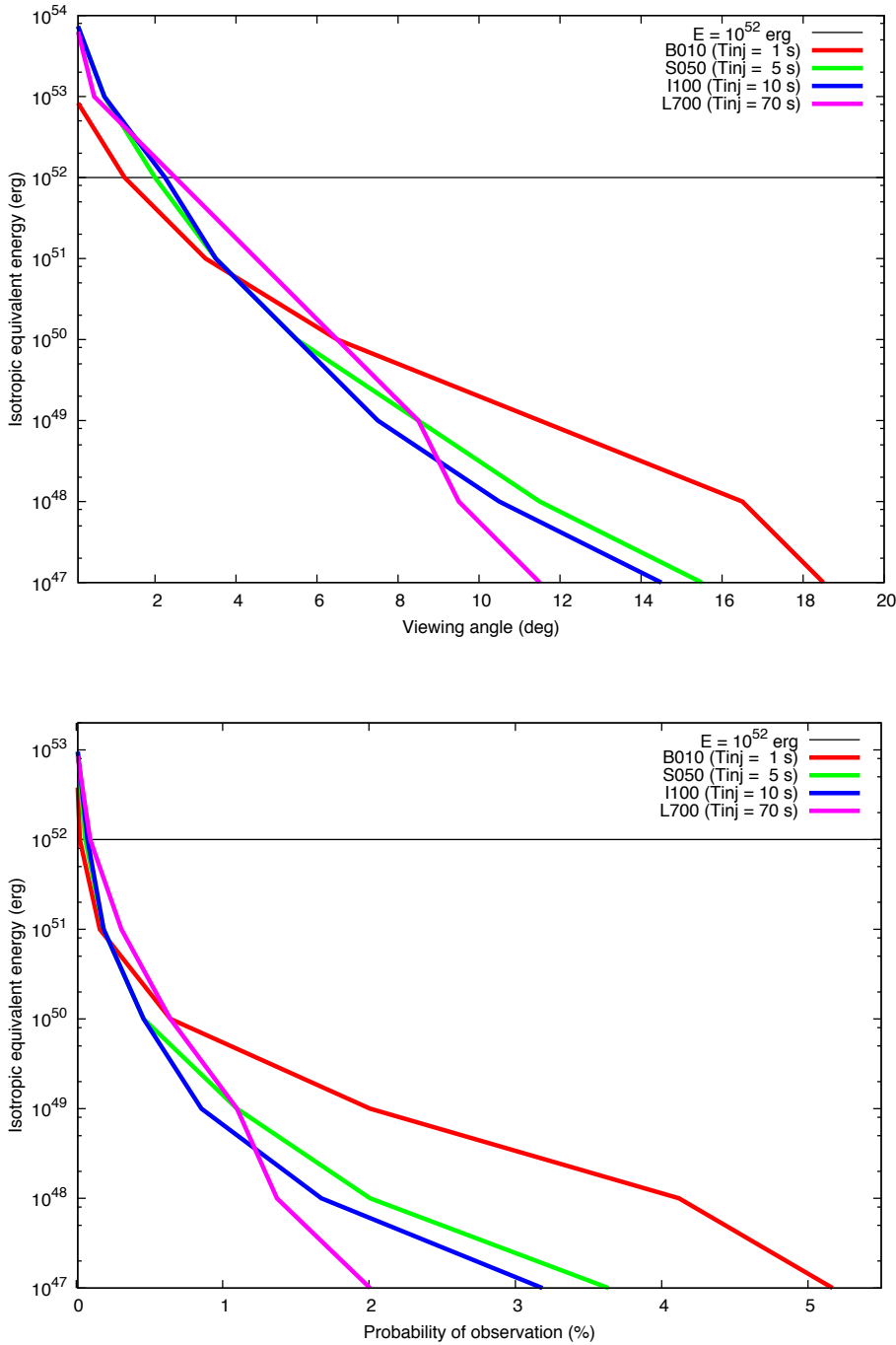
Figure 6.3: *Brief* (red), *short* (green), *intermediate* (blue), *long* engines (cyan) and their angular distribution. On the top panel, the estimated isotropic equivalent energy of the prompt emission as a function of the observer's viewing angle (relative to the jet axis). On the bottom panel the estimated isotropic energy of the prompt emission as a function of the probability of observation.
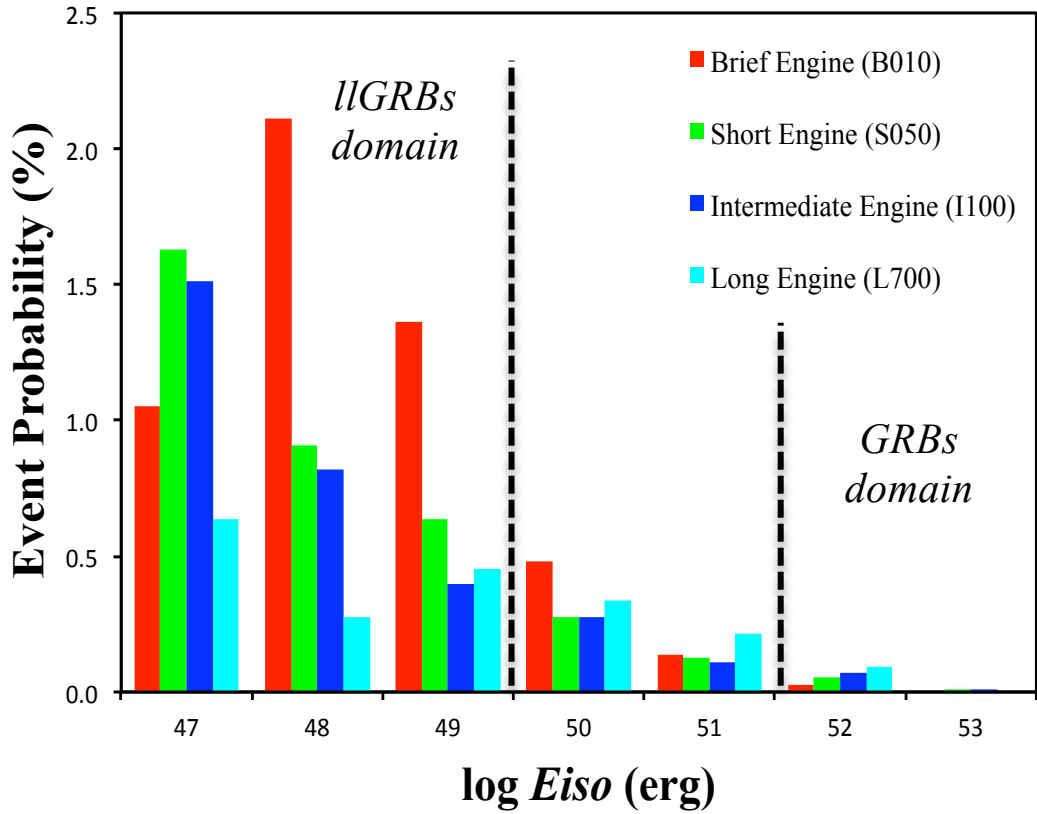
Figure 6.4: The probability to observe the event for a random observer in the sky, as a function of the event isotropic equivalent energy range (for four different engines: *Brief* T_{inj} = 1 s, a *short* T_{inj} = 5 s, an *intermediate* T_{inj} = 10 s and a *long* T_{inj} = 70 s engine). At the difference of the other engines, *brief* engine's jet is very likely to be observed as *ll*GRBs (10^{47-49} erg) while the chances of producing a standard GRBs (> 10^{52} erg) are very low.
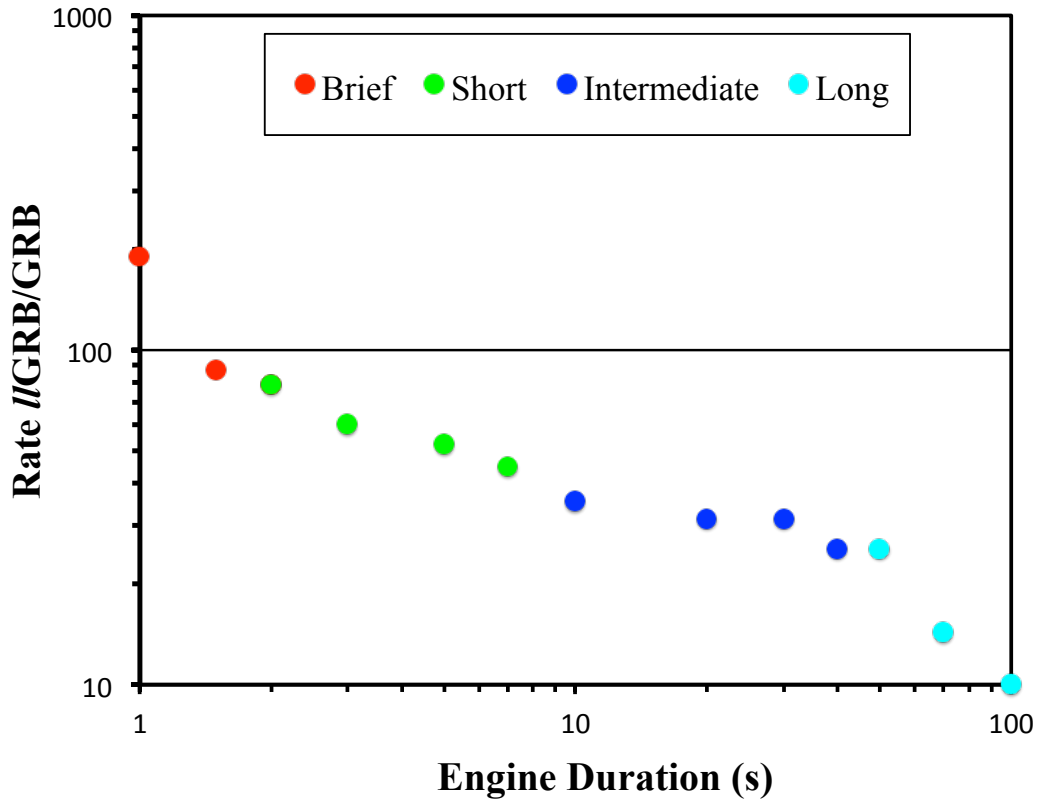
Figure 6.5: The ratio of rates, *ll*GRBs/GRBs, as a function of the engine duration. The ratio of rates was calculated with the ratio of probabilities: The probability of observing *ll*GRB (10^{47-49} erg) over the probability of observing a typical GRB (10^{52-54} erg). The region where *ll*GRB/GRB rates are in the domain 100-1000 times (as estimated in Soderberg et al. 2006; see Bromberg et al. 2011a and the references within) is limited by a dashed horizontal line. Only *brief* engines could reproduce *ll*GRBs at such a huge rate.

6.2.3 COLLAPSARS' DURATION DISTRIBUTION IN THE UNIVERSE

Finally, I show in Figure 6.6, the total rate of *ll*GRBs over that of GRBs, considering the different engine models (I consider engine durations equally spread in a logarithmic scale: 0.1, 0.3, 0.7, 1, 3, 7, 10, 30, 70 & 100 s), assuming different distributions for engine durations (in the universe). First, I consider a flat engine duration distribution, that is, all the engine durations are equiprobable (a distribution with a power law index of 0). I consider also power law distributions with indexes 0.5, 1, 1.5 and 2. The probability of occurrence, for each engine with duration T_{inj}, can be written as: $P(T_{inj}) \propto T_{inj}^{-p}$. Higher indexes favors short engines. For example, an index of 1 stands for assuming that B010 ($T_{inj} = 1$ s) is 10 times more probable (or common in the universe) than I100 ($T_{inj} = 10$ s) and is 10^2 times more probable than L999 ($T_{inj} = 100$ s). An index of 2 means that B010 is 10^2 times more probable than I100 and is 10^4 times more probable than L999 ($T_{inj} = 100$ s).

Although nothing is known about the true distribution of collapsar engine duration in the universe, I would like to investigate in what conditions (distributions) the observed rates can be reproduced. The results shows that the flat distribution gives a total *ll*GRBs/GRBs rate around ~ 50. Considering the many assumptions of this study, and considering the estimation of *ll*GRBs/GRBs rate derived from the observations (*ll*GRBs/GRBs > 100; Piran 2006 & Soderberg et al. 2006), it is reasonably a good number. Furthermore, considering that the engine duration distribution is a power law with an index ≥ 1, the total rate of *ll*GRBs/GRBs is more than 100, in agreement with the observations, in the range of 100-1000 (Bromberg et al. 2011a). Although, relaying on several rough assumptions, I estimate that this research outputs on an interesting result that have an impact on our understanding of the collapsar model, GRBs and *ll*GRBs, at least in the nearby universe.

We not that, the minimum power law index ≥ 1, necessary to reproduce *ll*GRBs rates, is in perfect agreement with Bromberg et al, (2012), which found that long engines

distribution shows a power law index ~3 − 4 (≥ 1). This, our results and those of Bromberg et al. (2011a & 2012), again, are in a good agreement.
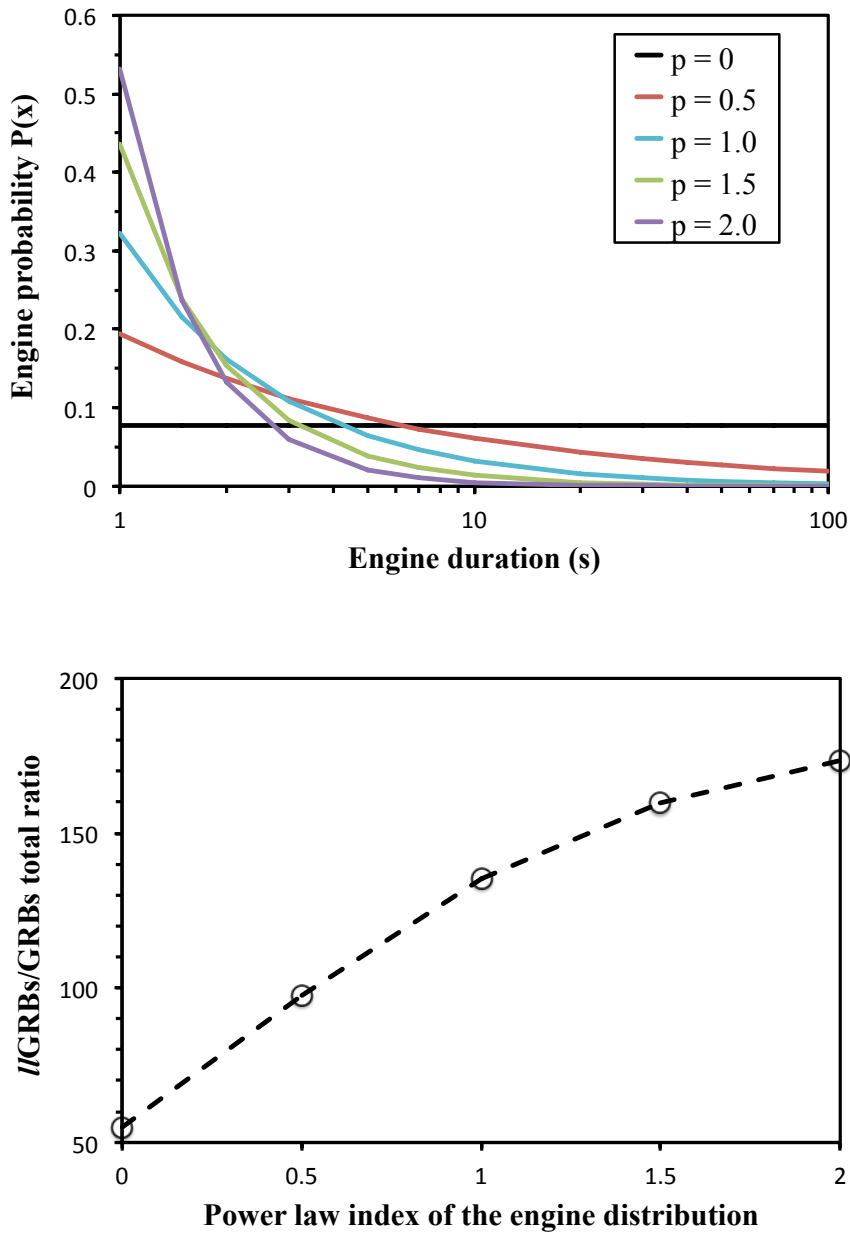
Figure 6.6: The total rate of *ll*GRBs/GRBs considering all the engine models in this study from 0.1 to 100 seconds. I show the total rate of *ll*GRBs/GRBs, computed considering different distributions of the engine duration, with power law indexes: 0 (flat distribution), 0.5, 1, 1.5 and 2. Flat distribution cannot explain the high rate of *ll*GRBs/GRBs, estimated > 100; at least a power law index of 1 is needed to reproduce the estimated *ll*GRBs numbers in the nearby universe.

6.3 GRB Vs. SN

6.3.1 REMINDER OF llGRBs' SNE

As I reviewed in § 6, *ll*GRBs are associated with unusually energetic SNe/HNe (Iwamoto et al. 1998 & Nomoto et al. 2006). *ll*GRBs are often associated with the very rare type of Broad Line SNe, showing highly energetic ejecta. Only ~5% of SNe Ibc are from this Broad Line type (BL) (Soderberg et al. 2006). However the energy released as "prompt emission" seems to be at orders of magnitude much fainter than the SN explosion. This represents one other mysterious feature of *ll*GRBs, especially when compared to the standard GRBs; as GRBs are hardly associated with even typical SNe (save GRB 030329/SN 2003dh). Below, is a table showing four *ll*GRBs, with faint prompt emissions, but in contrast, associated with energetic SNe.

Table 6-1: The first four *ll*GRBs and their energetic SNe

GRB	SN	z	T_{90} (s)	E_{iso} (10^{49} erg)	E_K (10^{52} erg)
980425	1998bw	0.0085	35	9	5
031203	2003lw	0.1055	37	17	6
060218	2006aj	0.0334	2100	4	0.2
100316D	2010bh	0.0591	1300	6	1

6.3.2 GRB Vs. SN

In the context of the contrastive relativistic nature of the expanding material, for the different engines models as examined in § 5.3, I discuss the impact of this difference on SN detection. As in Zhang et al. (2003), I estimate that energy in material moving at less than 10% of the speed of light, $\Gamma < 1.005$, can contribute to supernova event. A second estimate of non-relativistic energy, which would contribute to SN emission, can be made through the estimation of the energy "wasted" in the jet cocoon, most of which is non-relativistic and would end up contributing to SN emission. Engine energy is wasted, deposited in the cocoon, as the jet slowly progress inside the progenitor (Ramirez-Ruiz et al. 2002). This energy transmitted to the cocoon, rather than the collimated jet, can be written as follows (after Ramirez-Ruiz et al. 2002, see figure 1, & Zhang et al. 2003):

$$E_c = \begin{cases} \dfrac{t_b - R_*/c}{T_{inj}} \times E_{tot} & t_b < T_{inj} + R_*/c \\ E_{tot} & t_b \geq T_{inj} + R_*/c \end{cases} \qquad (14)$$

Where E_c is the wasted energy in the cocoon, E_{tot} is the total energy delivered by the engine, R_* is the progenitor's radius, c is the speed of light, t_b is the cocoon breakout time and T_{inj} is the engine duration. Most of this energy would be transmitted to non-relativistic hot material, which can power the SN (Ramirez-Ruiz et al. 2002 & Zhang et al. 2003).

The fraction of this "wasted" energy in the jet cocoon, E_c/E_{tot}, is shown in Figure 6.7, along with the non-relativistic energy, moving at less than 10% of the speed of light. These two energies are roughly the same. This confirms that (indeed) it is the jet cocoon that provides the non-relativistic material, which is would contribute to power the SN non-relativistic explosion (as in Zhang et al. 2003). It is notable how this wasted energy in non-relativistic domain differs in the considered engine models. On one hand, using this estimation of non-relativistic energy as a proxy for the energy contributing to SN explosion, an estimation of how potentially powerful – and thus visible, and clearly identifiable - the SN is can be derived for the different engine models. On the other hand, along with this non-relativistic energy, relativistic energy that would power the

GRB, $\Gamma > 10$, is also shown. Using this relativistic energy as a proxy, for the GRB's energetic scale, would allow an interesting discussion on the GRB's energy and how clearly visible, and potentially identifiable, the SN is expected to be.

For the briefest engines, almost all the energy is in non-relativistic domain; such engine models would (theoretically) power only a SN explosion. Such a SN would be more energetic than the typical SNe, probably similar to "engine-driven" SN 2009bb (Soderberg et al. 2010). For slightly longer *brief* engines (B010 & B015), about 75% of the energy is in non-relativistic domain, with about 25% successfully accelerated into the relativistic domain. Theoretically, such engines would provide some relativistic energy but only for a faint or *ll*GRB, which would be accompanied by a potentially luminous – and thus clearly visible - SN explosion's signature. For the longer *short*, *intermediate*, and *long* engines, almost all the engine energy, up to ~ 90%, is accelerated to relativistic domain, and only about a few percent is left in the non-relativistic domain. It is in these sufficiently *long* engines' durations where the jet is well formed and efficiently accelerated, providing large relativistic energy to explain typical GRBs' energy output. Although low in fraction, the non-relativistic energy could still be able to power some SN emission, in theory. However, the SN explosion, in case that it actually occurs, would be relatively faint, by roughly one order of magnitude than in the case of *brief* engines (although this factor may depend on the viewing angle). Thus the SN signature might not be observationally easy to identify in such longer engines, as in the case of *brief* engines.

To discuss these theoretical predictions, the observational results on GRB-SN connections are summarized in Table 6-2. Table 6-2 shows the sample of GRBs associated with SN, in the order of clear association evidence, decreasing from the highest evident, "gold", to "silver", than the lowest "bronze". Table 6-2 and Figure 6.8, shows that: the gold sample is dominated by *ll*GRBs, with five out of the six clearest GRB-SN connections related to *ll*GRBs. Only one GRB-SN connection is rather related to a typical GRB (GRB030329/SN2003dh). The silver sample is dominated by GRBs, with only one *ll*GRBs. However, the average isotropic energy range of these GRBs is significantly lower than that of typical GRBs, with only two events with ~10^{52} ergs. While in the bronze sample, where the SN is the least evident, the GRBs in question are relatively energetic GRBs. No *ll*GRB is found in this sample, and several events show isotropic energies in the range 10^{53-54} ergs (e.g: GRB991208, GRB000911, GRB020405,

GRB060729, GRB080319B and GRB090618). See Figure 6.8 for a clear energetic comparison.

This contrastive observational trend, of *ll*GRBs showing clear SN signature, while energetic GRBs showing less evident SN associations, can be explained by two main hypotheses: i) Parameter such as the redshift, which is higher in the typical energetic GRBs. At such redshift, the SN becomes fainter and it would be difficult to obtain a sufficient signal to ratio (Hjorth & Bloom 2011). Contamination by the host galaxy and afterglow, at such higher redshift also makes it difficult to clearly identify the SN (Hjorth & Bloom 2011; Hjorth 2013 figure 2). But the serious problem with this argument is the discovery of less SN-GRBs, at low redshift. These less SN-GRBs have no SN observation at deep limits, down to absolute magnitudes around -12 to -14, while the SN-GRBs' SNe show absolute magnitudes around -17 to -19 (Hjorth 2013, §6 & figure 1). This represents a huge gap between SN-GRBs and less SN-GRBs (Hjorth 2013). Two examples are: the low redshift GRB060614 (z = 0.125), with no SN observation at deep limits, and GRB060505 (z = 0.089), with no SN detection down to a limit 100 times fainter than SN1998bw (Hjorth & Bloom 2011; Hjorth 2013). This leads to the second possible hypothesis: ii) SN explosion in GRBs and *ll*GRBs might be fundamentally different, in scale, or in nature, with some GRBs either not successfully producing SNe, or producing relatively fainter SNe (Nomoto et al. 2006b; Tominaga et al. 2007 & Hjorth & Bloom 2011), as in the "failed Ib" scenario (Woosley 1993). My results strongly support ii), although i) is not excluded, and both i) and ii) can be behind this observational trend. As in *long* engines models in my simulations, energetic GRB jets produce weak cocoon and leave small engine energy fraction in non-relativistic domain to power the SN explosion, making the SN signature significantly softer, or absent, at least observationally. While *ll*GRBs leaves a significantly higher fraction of the fresh engine energy in non-relativistic material or cocoon, producing significantly powerful, and thus much clearer and identifiable SN explosions. The detection of the very bright SN2012bz, one of the brightest SNe associated with GRB ever (Hjorth 2013), which is associated with the *ll*GRB, GRB120422A (Zhang et al. 2012), strongly supports my argument.

Table 6-2: The sample of GRB-SN connections

GRB	Event type	SN	Evidence Grade [b]	Redshift	T_{90} (s)	$E_{\gamma,iso}$ (10^{52} erg)	Ref. [c]
Gold (A) [a]							
980425	*ll*GRB	1998bw	A	0.0085	34.9 ± 3.8	9×10^{-5}	1,2
030329	GRB	2003dh	A	0.1685	22.9	1.3	1
031203	*ll*GRB	2003lw	A	0.1055	37.0 ± 1.3	0.017	1,3
060218	*ll*GRB	2006aj	A	0.0334	2100 ±100	0.004	1,2
100316D	*ll*GRB	2010bh	A	0.0591	>1300	0.006	1,4
120422A	*ll*GRB	2012bz	A	0.283	5.35 ± 1.4	0.0045	5,6,14
Silver (B) [a]							
011121	GRB	2001ke	B	0.362	~ 28	2.7	7
020903	*ll*GRB		B	0.251	~ 20	0.0011	8,9
021211	GRB	2002lt	B	1.006	~ 4	0.66	10
050525A	GRB	2005nc	B	0.606	8.8 ± 0.5	2.3	11
081007	GRB	2008hw	B	0.5295	8	0.15	12
101219B	GRB	2010ma	B	0.55	51	0.42	13
Bronze (C, D, E) [a]							
970228	GRB		C	0.695	56	1.6	15
990712	GRB		C	0.433	19	0.67	15
991208	GRB		E	0.706		22.3	15
000911	GRB		E	1.058		67	15
020405	GRB		C	0.691	40	10	15
040924	GRB		C	0.859	2.39	0.95	15
041006	GRB		C	0.716	18	3	15
050416A	GRB		D	0.654		0.1	15
060729	GRB		E	0.543		13.8	15
080319B	GRB		C	0.938	124.86	114	15
090618	GRB		C	0.54	113.34	25.7	15

[a] Gold and silver samples adopted in Hjorth & Bloom (2011), & Zhang et al. (2012), adding bronze sample for GRB events with measured redshift, isotropic equivalent energy evaluation and SN evidence level. The gold sample includes GRBs that have spectroscopically identified SN association, and well-monitored SN emission (A evidence level). The silver sample includes GRBs that have a clear SN bump along with

Hamid Hamidani - February 2016

some spectroscopic evidence (B evidence level). The bronze sample is constituted from [15], including all GRBs with evidence level below B (C, D and E)

[b] Evidence level of a SN associated with the GRB. With A is the highest level and E is the lowest [15].

[c]References: [1] Hjorth & Bloom (2011); [2] Zhang et al. (2008); [3] Sazonov et al. (2004); [4] Sakamoto et al. (2010); [5] Barthelmy et al. (2012); [6] Schulze et al. (2012); [7] Garnavich et al. (2003); [8] Sakamoto et al. (2004); [9] Soderberg et al. (2004); [10] Crew et al. (2003); [11] Blustin et al. (2006); [12] Jin et al. (2012); [13] Sparre et al. (2011); [14] Zhang et al. (2012); [15] Hjorth's Dark Cosmology Center web page: (http://www.dark-cosmology.dk/GRBSN/GRB-SN_Table.html).
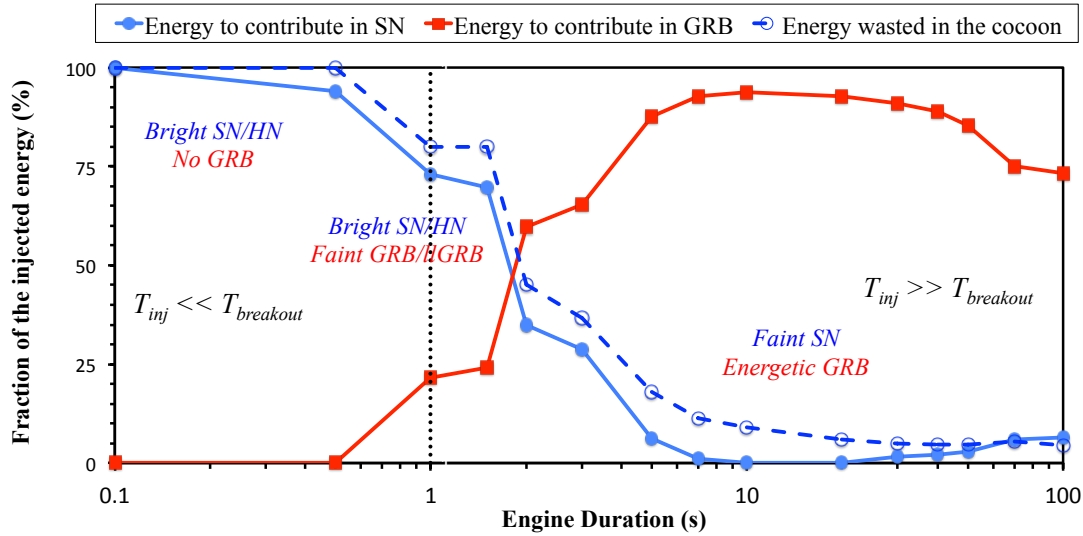
Figure 6.7: The relativistic nature of the injected energy after the explosion, for the different engine duration models. In blue filled circles, fraction of energy propagating in non-relativistic domain with $\Gamma < 1.005$. In red squares, fraction of energy in relativistic domain (in material moving with $\Gamma > 10$), and in blue unfilled circles, the fraction of energy wasted in the jet cocoon before the breakout, which would contribute in the SN (Zhang et al. 2003). All measured at a radius of 1.2×10^{11} cm.

Hamid Hamidani - February 2016
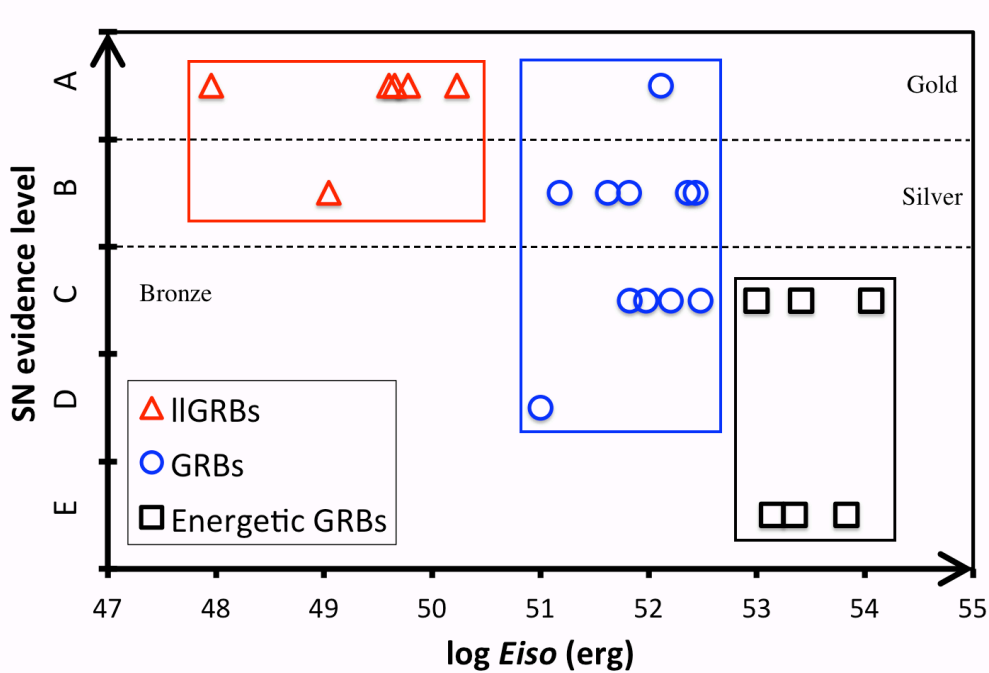
Figure 6.8: SN evidence level as a function of the GRBs' isotropic equivalent energy. *ll*GRBs are plotted in triangles, GRBs in circles, and exceptionally energetic GRBs in squares. The two dashed lines separate the gold, silver and bronze samples (see Table 6-2 and the references within).

6.4 LLGRBS: SUCCESSFUL OR FAILED JETS?

In this section, the above results (Figure 6.5 & Figure 6.7) are expressed as a function of the ratio of the engine duration over the breakout time ($T_{inj}/T_{breakout}$), rather than as a function of the engine duration alone (T_{inj}). As the success or fail of the jet is determined by the ratio $T_{inj}/T_{breakout}$, it is a more universal parameter to describe the jet

nature, and the expected type of event. The nature of the resulted jet can be classified as follows (Bromberg et al. 2011b):

- Failed jet, which results in a breakout shock (weak GRB/*ll*GRB) for $T_{inj}/T_{breakout} < 1$ (Bromberg et al. 2011a; 2011b & 2012)

- Successful jet, which breaks out highly relativistic and collimated (and would power a classical GRB) for $T_{inj}/T_{breakout} \gg 1$ (the collapsar model; MW99)

The Figure 6.9 shows the rate ratio of *ll*GRBs over GRBs (top panel), and SN and GRB energy reservoirs (bottom panel) a function of the ratio $T_{inj}/T_{breakout}$. Until now, most numerical studies focused on the right extremity duration domain of this figure ($T_{inj}/T_{breakout} \gg 1$). Here I illustrate a more global picture of collapsar jets, covering both failed and successful jets with $T_{inj}/T_{breakout}$ covering a large domain: from ~0.01 to ~20. In this large domain, three distinct types of jets with different corresponding events can be distinguished:

a. $T_{inj}/T_{breakout} < 0.1$: Failed jet resulting in a non-relativistic cocoon. A SN/HN explosion might be expected/observed. Most likely an engine driven SN (as SN 2009bb; Soderberg et al. 2010)

b. $0.1 < T_{inj}/T_{breakout} < 1$: Failed jet resulting in a mildly relativistic breakout shock. A *ll*GRB-SN; rather than a standard GRB (< 1%); would be very likely observed (> 99 %).

c. $T_{inj}/T_{breakout} > 1$: Successful jets producing a highly relativistic and collimated jet, as in the classical scenario of the collapsar model. A typical GRB, probably SN-less GRB, might be expected/observed, although some *ll*GRB might also be observed with off-axis viewing angles

With this result, and from the above a. and b (c doesn't produce GRBs), a contribution to the debate on the origin of *ll*GRBs (explained in § 2.1), can be made: "*What is the origin of llGRBs, Successful jets viewed by off-axis observers as proposed by the unification model (Yamazaki et al. 2004 & Lamb et al. 2005)? Or, failed jets as*

Hamid Hamidani - February 2016

suggested by Bromberg et al. (2011a & 2012) and Nakar et al. (2012)?" My results strongly recommend the latter option: Considering the high rates of *ll*GRBs, and the trend of *ll*GRBs showing the clearest SN connections, a failed jet; as suggested by Bromberg et al. (2011a & 2012), is the most appropriate scheme to explain *ll*GRBs and their peculiar features. This is an agreement with observations suggesting that XRFs (*ll*GRBs) are the result of failed jets breakout shock (Campana et al. 2006 & Mazzali et al. 2008).
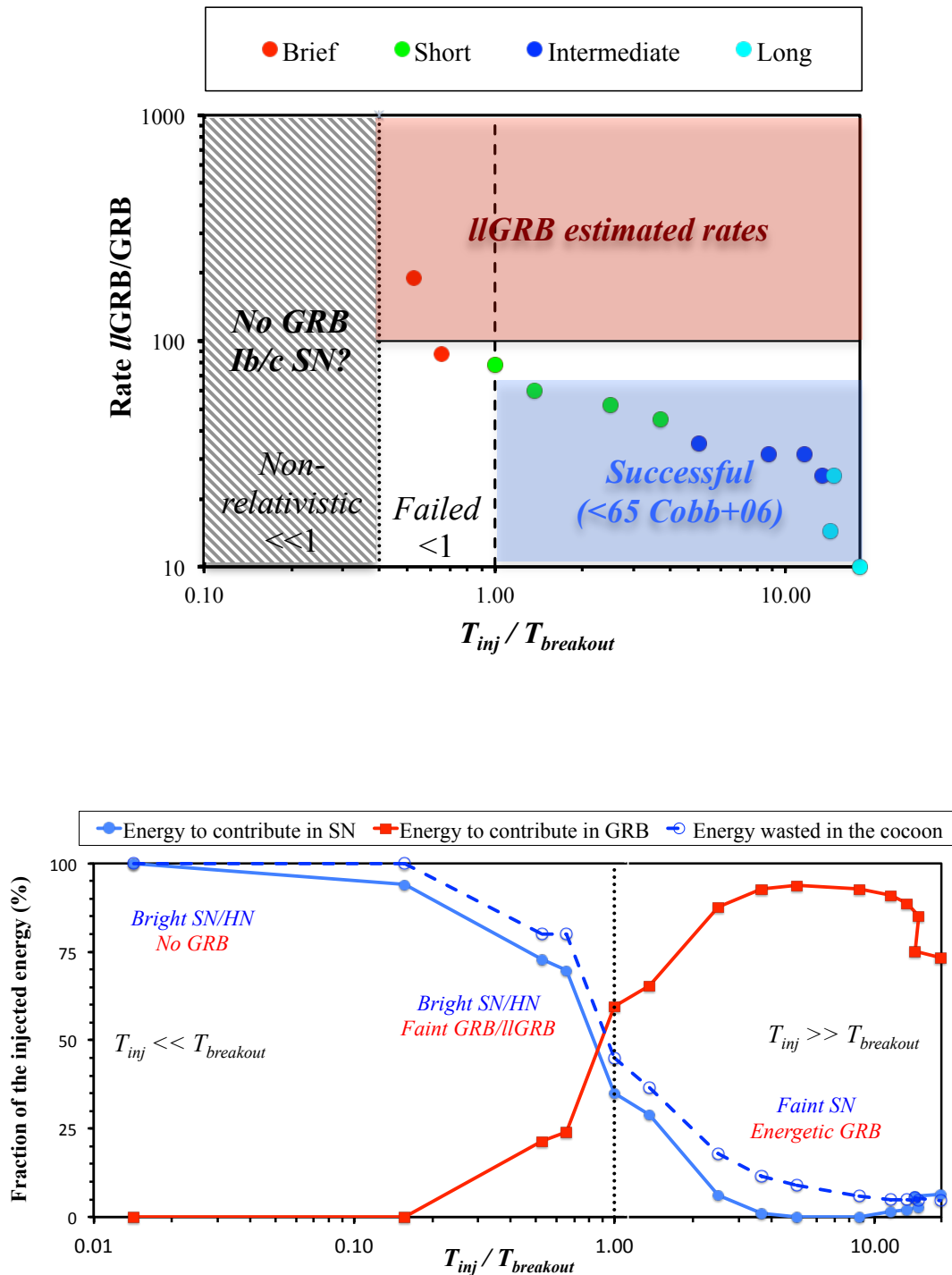
Figure 6.9: Same as results as shown in Figure 6.5 (for the top panel) and Figure 6.7 (in the bottom panel) expressed as a function of $T_{inj}/T_{breakout}$. This summarize my findings: *Brief* engines ($0.1 < T_{inj}/T_{breakout} < 1$) reproduce very well the features of *ll*GRBs: i) a high rate (~100 times that of GRBs) & implies a potentially clear SN, ii) longer engines (with $T_{inj}/T_{breakout} >> 1$) reproduce standard GRBs properties: A strong/relativistic jet, but does not intend a powerful/clear SN as in the case of *brief* engines (which would produce *ll*GRBs).

Hamid Hamidani - February 2016

6.5 DISCUSSION

In this chapter the impact of the different angular distributions and energy acceleration efficiencies, found for the different computed engines, was explored from the perspective of observers on different viewing angles. Table 6-4 presents a general summary for different engine durations and the different events which would be observed.

For the shortest engines ($T_{inj}/T_{breakout} << 1$) no relativistic jet is produced, and all the engine energy is transmitted into non-relativistically expanding cocoon, moving at less than 10% the speed of light c. Thus, a luminous SN emission could be expected (Ramirez-Ruiz et al. 2002 & Zhang et al. 2003). The energy output of such explosion can be high and comparable to that of a HN explosion; as HN is in the order of $\sim 10^{52}$ erg (Nomoto et al. 2006). As it would be a non-relativistic SNe, it can be observed only if in the nearby universe. Such short engine duration, and the produced eject, might be a reproduction of the recently discovered "engine driven SN", SN 2009bb (Soderberg et al. 2010).

For slightly longer engines ($0.5 < T_{inj}/T_{breakout} < 1$), the result is different; a failed jet is produced, which powers a mildly relativistic shock breakout. As a result, a small fraction of the energy is accelerated to relativistic domain ($\Gamma > 10$). This small fraction would power "*ll*GRB prompt emission". Since the discovery of XRFs (or *ll*GRBs) there have been evidences pointing toward breakout shocks, both observational (e.g: Campana et al. 2006 & Mazzali et al. 2008;) and theoretical (Nakar & Sari 2012; Nakar 2015). The energy output, spectrum and timescale of the observed *ll*GRBs can be explained by mildly relativistic breakout shocks (Nakar & Sari 2012; Nakar 2015). The results of this thesis support this "shock breakout" scheme, numerically, as the observational peculiar features of *ll*GRBs – of high rates and a clear SN emission – are found, for the first time, to be very well reproduced by such shock breakout of failed jets. Such an event (*ll*GRB-SN) can be observed further, compared to SNe, thanks to

*ll*GRBs' relatively high luminosity. However, such an event is certainly too faint to be observed if occurring at high redshift.

Finally, engines longer that the necessary time for the jet to breakout of the stellar surface ($T_{inj}/T_{breakout} \gg 1$), can produce extremely relativistic and collimated outflow. This was the main requirement of the collapsar model; long engine activity is essential for a relativistic jet to be successfully launched from the progenitor (MW99), although only possible in extreme conditions, and thus in rare cases (MW99). Accordingly, as in the concept of the fireball model, the highly relativistic jet can explain the GRB prompt emission and its huge isotropic equivalent energy (Piran 2004), consequently classical GRBs are expected from such engine duration domain; engines with $T_{inj}/T_{breakout} \gg 1$. The extreme luminosity of such GRBs, allows them to be observed, up to very high redshifts.

The SN non-relativistic energy reservoir is about one order of magnitude weaker than GRB energy reservoir, in the case of successful jets ($T_{inj}/T_{breakout} \gg 1$). Although it is problematic whether such engines would power an observable SN emission, it is not a question of concern or interest to this thesis. The right question to be asked here is: *will the SN emission (in case it exists) be observed?* That is, *will this GRB be observed as GRB-SN or SN-less GRB?* From a rough energy prospect, in contrast with the GRBs' prompt emission, the SNe, in case it occurs, it would be orders of magnitude fainter. This might explain the general picture of cosmologically GRBs, generally lacking of SN (SN-less GRBs) (Hjorth & Bloom 2011). Furthermore, some GRBs, although at redshifts as low as those of *ll*GRBs, were found SN-less (e.g: GRB 060614 & GRB 060505; Hjorth & Bloom 2011; Hjorth 2013). These SN-less GRBs indicates a huge gap in the brightness of the SNe (in case the SNe exist) relative to *ll*GRBs' SNe; since no SN detection was found even with upper limits on absolute magnitudes about -12 to -14; while the absolute magnitude of *ll*GRBs' SNe is in the range of -17 to -19, which is in some cases ~100 times brighter (Hjorth 2013). **My result here is that the jet failure (*ll*GRBs), or success (GRB), might justify the strength (and thus the clear presence), or the faintness (and thus the absence), of the SN.**

The main result found in this chapter is that the longer the engine duration; and thus the higher the ratio $T_{inj}/T_{breakout}$ than 1; the higher the chances of observing a GRB, instead of a *ll*GRB. As a result, such types of engines must account for the cosmological GRBs,

while *brief* engines ($T_{inj}/T_{breakout}$ < 1) must account for *ll*GRBs at low redshifts and their high rates. **By considering different duration distributions for collapsar engines in Wolf-Rayet stars, a power law distribution with an index of ~1 might solve the mystery of *ll*GRBs and their high rates.**

Note that my restriction on the collapsar engine duration distribution (power law index ≥ 1), so that *ll*GRBs rate would be reproduced and explained, is in excellent agreement with Bromberg et al. (2012) (index 3 − 4). Furthermore, as *ll*GRBs present a theoretically rich source of neutrinos, their detection is theoretically possible and not limited by redshift. Such neutrino detections would present a revolutionary frame in astronomy, if achived. However, such neutrinos energy flux is still much fainter than the available detectors sensitivity (Murase et al. 2006 & 2013). My restriction on the duration distribution index so that observational features are explained (index ≥ 1), is also in agreement with IceCube non-detections (as it gives energy flux ~ 10^{-10} << 10^{-8} GeV cm^{-2} s^{-1} str^{-1}; Murase et al. 2006, fall between "LL-GRB" and "LL-GRB modest" models). I stress however, that the next generation of neutrino detectors, may be able to detect *ll*GRBs' neutrino light for the first time. Such detection would allow a major breakthrough in astronomy and GRB physics, as collapsars would be understood on a large scale (including their distribution), based on observations. It would also allow discussing my above results: *ll*GRB rates and the predicted distribution index, as found ≥ 1 here.

Below, I present a comparison of my research outlines with that of several other different studies aimed to explain some of *ll*GRBs' properties (mainly temporal): Toma et al. (2007), Nakar (2015) & Irwin & Chevalier (2015). The mechanism and engine differ. My study may overlook the physical process of *ll*GRBs; but considering Nakar et al. (2012 & 2015) model, I assume that the shock breakout scenario would explain the temporal and energetic properties of *ll*GRBs. I note that this research (as highlighted in red), is the only one that explains both the SN connection trend, and the high rates of *ll*GRBs.

Table 6-3: The outlines of this research in comparison with previous studies aimed at *ll*GRBs

	Toma+07	Nakar 15	Irwin & Chevalier 15	Hamidani+16
Engine energy (erg)	10^{51} (Magnetar)	10^{51} (BH)	10^{51} (?)	10^{52} (& 10^{51}) (BH)
Engine duration (s)	10^6	20	3000	$0.1 - 100$
Progenitor (Solar radius)	~1	~1	~1	~1
Envelope (Solar radius)	~100	~100	~100	No
Mechanism	Synchrotron	Breakout (BB)	Synchrotron Compton BB	Breakout (?)
Results				
X-ray afterglow of GRB 060218	O	✖	✖	?
Shallow slope of the light curve	?	O	Δ	?
*ll*GRB & GRB rates	?	?	?	O
SN connection	O	O	O	O

Hamid Hamidani - February 2016

The table below may summarize the general picture of the three different events, contributing at different redshifts with different energy fractions, with *ll*GRBs as intermediate events. In the next chapter I will show how the results found in this chapter, considering one opening angle of 10°, would be affected considering different opening angles.

Table 6-4: Engine duration models and the predicted events

$T_{inj}/T_{breakout}$	Product	Energy in SN ($\Gamma < 1.005$)	Energy in GRB ($\Gamma > 10$)	Observed event GRB/SN	Detected up to z
($\ll 1$)	Cocoon	High (> 90%)	No energy (0%)	No GRB, luminous SN/HN	Very low
($0.5 \sim 1$)	Failed jet/BS	High (> 50%)	Low (< 50%)	*ll*GRB-SN (e.g: GRB 980425/SN1998bw)	Low
($\gg 1$)	Successful jet	Low (< 10%)	High (90 - 70%)	SN-less GRB (GRB 060505 & GRB 060614)	High

7 EFFECT OF THE OPENING ANGLE

"The best that most of us can hope to achieve in physics is to misunderstand at a deeper level." – Wolfgang Pauli

7.1 OVERVIEW

The astronomical implications found in the previous chapter, stressing the role of the engine duration, are the first of their genre. However, the diversity in the nature is much more complex. For instance, I assumed one jet initial opening angle typical of collapsar simulations ($\theta_0 = 10°$), which is certainly not always the case in nature (Harikae et al. 2009). Here, the previous results will be generalized, including the effect of the opening angle as well, considering a diversity of opening angles (from 1 to 90°).

7.2 THE MODELS

In this chapter I present 21 additional models, along with the previous engine duration models. I calculated collapsar events for three engine durations (1, 5 & 10 seconds),

considering 7 additional different opening angles in addition to the previously considered θ_0 = 10° (1, 5, 15, 30, 45, 60 & 90°). I then estimate the ratio of rates (*ll*GRB/GRB), and the energy reservoirs (SN & GRB).

7.3 JET STRUCTURE & BREAKOUT

The different opening angle, for the different engine durations, lead to a very interesting result: Not all short engines (~1s) produce failed jets, and not all long engines (~10 s) produce successful jets.

In fact, different parameters may play their role along the engine duration, and change the nature of the jet/explosion. In this case, opening angles lead to different kinds of explosions, and most importantly lead to different breakout times. As I showed in the previous chapter $T_{inj}/T_{breakout}$ is the very decisive parameter for the nature (success/failure) of any collapsar jet. Therefore, different opening angles, leading to different breakout times, stands for different $T_{inj}/T_{breakout}$ ratios, and thus to completely different jets.

In particular, the role of the initial opening angle is as follows:

- Small opening angles lead to more collimation, and thus give faster and more efficiently breaking out jets.

    o *The ratio $T_{inj}/T_{breakout}$*: Gets larger as the opening angle (and $T_{breakout}$) gets smaller, thus producing to standard highly relativistic GRB-like events.

- Large opening angles lead to less collimated jets, waste of the engine energy in the sides. The explosion becomes more and more spherical, and the breakout time is gradually increased.

    o *The ratio $T_{inj}/T_{breakout}$*: Gets smaller as the opening angle is larger (as well as the $T_{breakout}$), thus leading to events related to failed jets (for $T_{inj}/T_{breakout}$ < 1), or non-relativistic events ($T_{inj}/T_{breakout}$ < 1)

$\theta_0 = 1'$ $\theta_0 = 10'$ $\theta_0 = 45'$

$\log \rho$ (g/cm^3) at   1.5 s $\log \rho$ (g/cm^3) at   2.0 s $\log \rho$ (g/cm^3) at 22.5 s

$\theta_0 = 1'$ $\theta_0 = 10'$ $\theta_0 = 45'$

$\log \rho$ (g/cm^3) at   1.4 s $\log \rho$ (g/cm^3) at   2.0 s $\log \rho$ (g/cm^3) at 18.0 s

Hamid Hamidani - February 2016
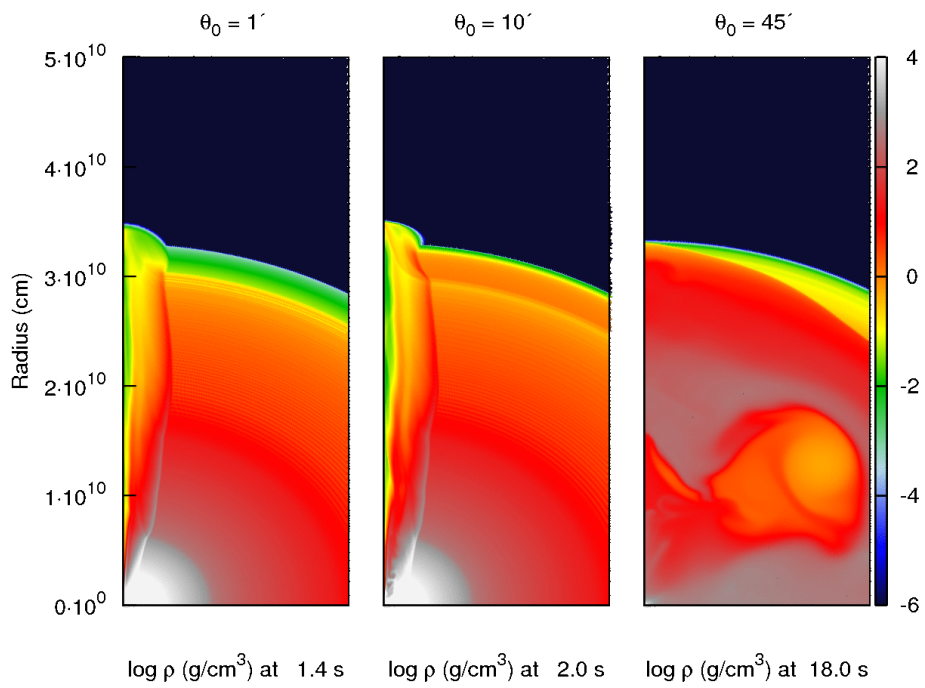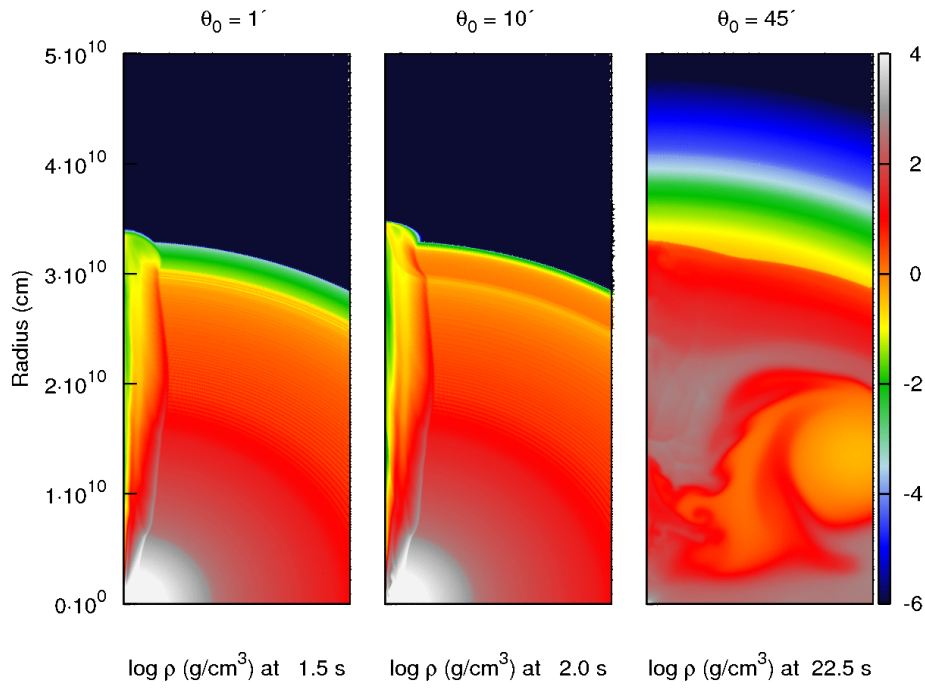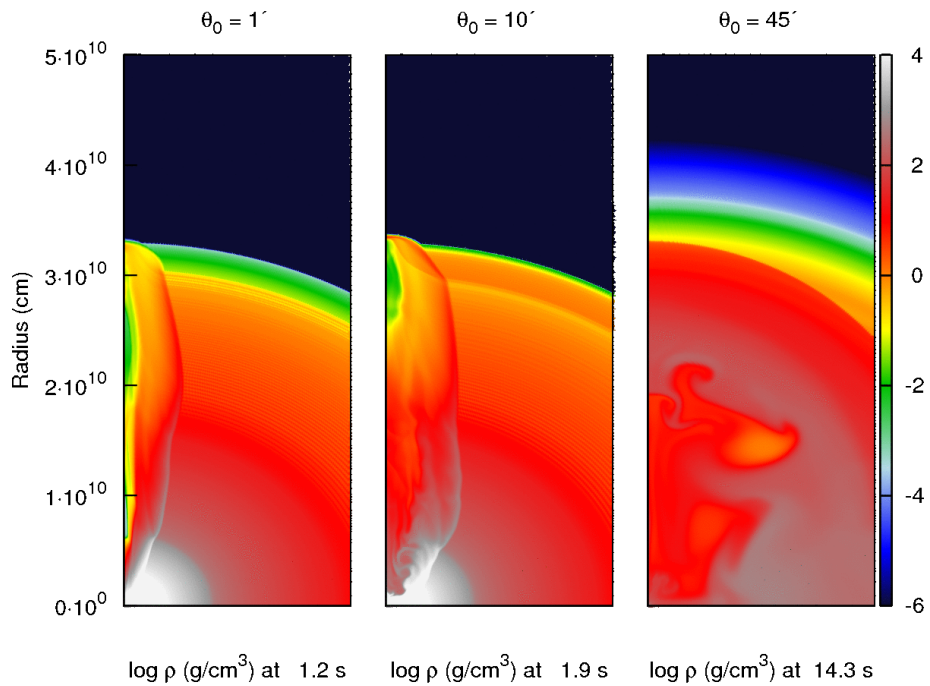
Figure 7.1: The density (logarithmic scale) in different collapsar explosions, from long to short engine durations (top: 10s; center: 5s & bottom: 1s), for small to large opening angles (from the left: 1, 10 & 45 degrees)
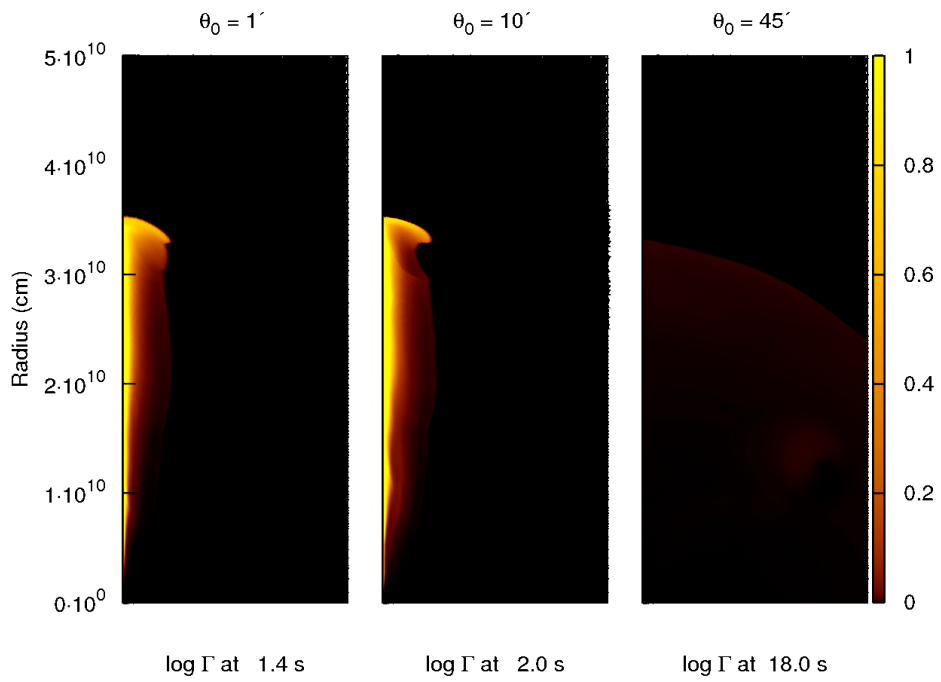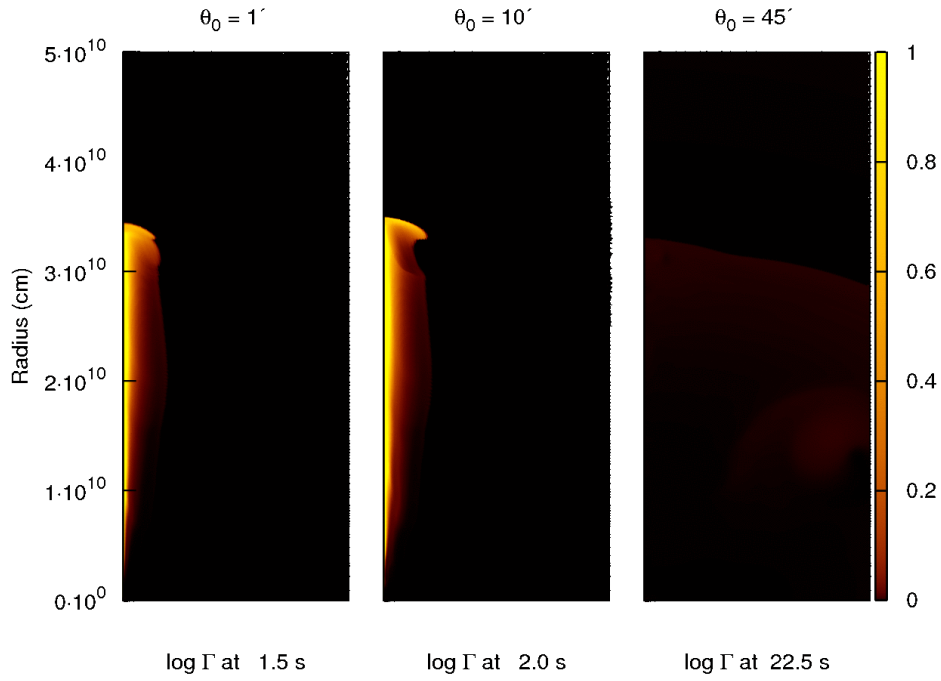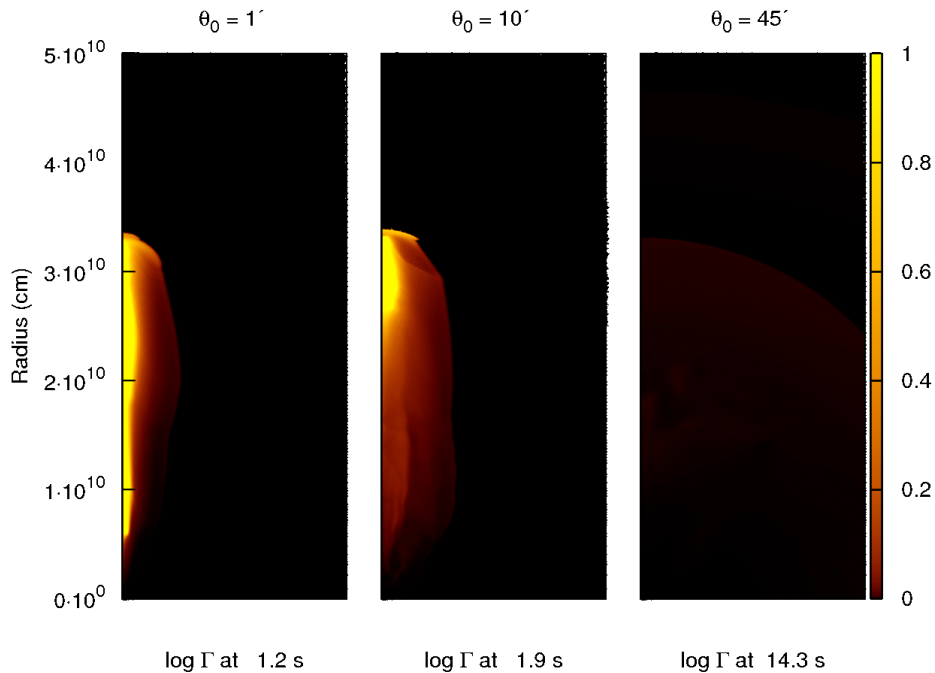
Figure 7.2: The Lorentz factor (logarithmic scale) in different collapsar explosions, considering long to short engine durations (top: 10s; center: 5s & bottom: 1s), for small to large opening angles (from the left: 1, 10 & 45 degrees)

7.4 THE RATES RATIOS

In Figure 7.3, the rates ratio extended for different opening angles, is shown along the previous ratios, found for different engine durations (in black). Two important trends can be identified: 1. The longer the engine duration, the lower the rate ratio (as stressed in the previous chapter), 2. Larger opening angles (>10°), leads to higher rate ratios. Thus, there would be two theoretical ways to reproduce *ll*GRBs rates: short engine duration or large initial opening angle. For instance, we have two events reproducing rate ratios over 100, one due to short engine duration and the second is due to a larger opening angle (although the engine duration is long).
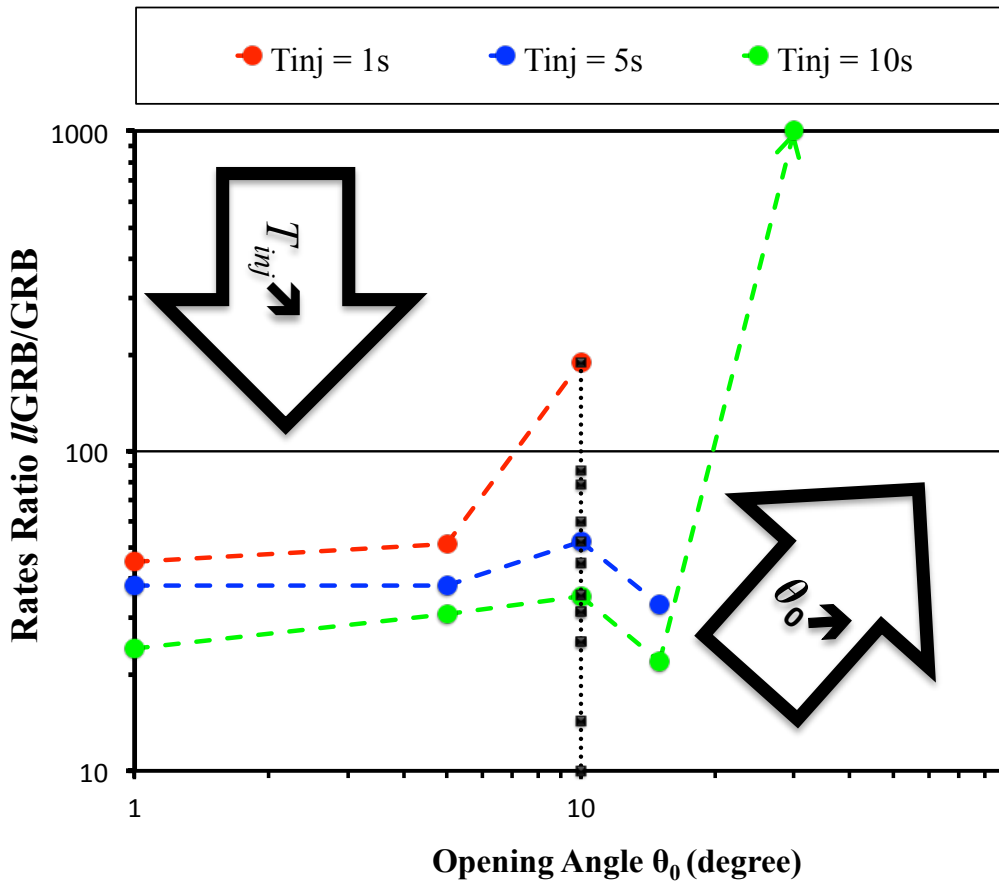
Figure 7.3: The ratio of the probability of observing *ll*GRB and GRB (must be > 100; Piran et al. 2006 & Soderberg et al. 2006), for different jet initial opening angles. Longer engine durations (1s in red, 5s in blue & 10s in green) lead to lower ratios (at the same angle). Larger opening angles, leads to the opposite trend of larger ratios. Black squares show the ratios found in the previous chapter (10°).

7.5 SN & GRB ENERGIES

I calculated SN and GRB energy reservoirs as in § 7, for the additional 21 engine models. As shown in the Figure 7.4, the same trend found previously for increasing T_{inj}, is found by reducing the opening angle: non-relativistic event (SN/HN like), *ll*GRB-SN

like, and SN-less GRB like events: Small opening angles give energetic GRBs, but SN-less. Intermediate opening angles give both weak GRB energies and considerably energetic SNe. And, large opening angles give only SN energy reservoirs, with much larger angles fail at even giving a stellar explosion (energy lost into the black hole).

Thus, *ll*GRBs with both the high rate and strong SN connection could be reproduced and explained, with slightly larger opening angles than the previously assumed 10°. However, too larger opening angles (more than ~30°) could not produce *ll*GRBs, as they would lead to rather non-relativistic events. In the global picture, *ll*GRBs are found as an intermediate type of events, between highly relativistic GRBs and non-relativistic SN explosion.
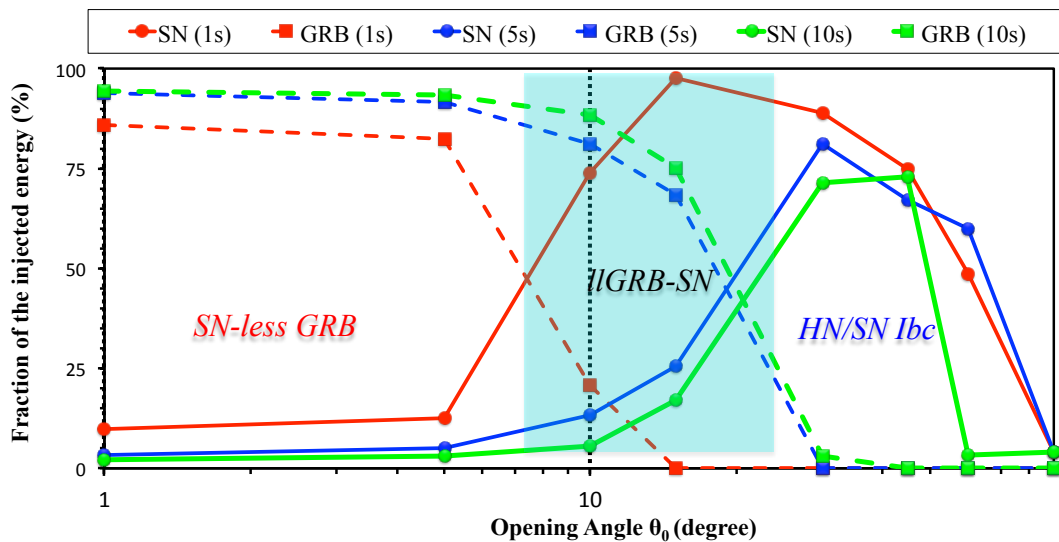
Figure 7.4: SN energy reservoirs (solid) and GRB energy reservoirs (dashed), calculated as in § 7, for different opening angles and engine durations. The regions where SN-less GRBs, llGRB associated with powerful SNe and non-relativistic events (SN/HN) are stressed.

7.6 THE GENERAL PICTURE: θ_0 COMBINED WITH T_{inj}

Finally, I will show the general picture summarizing all the previously calculated engine models, in terms of T_{inj} and θ_0, and the resulted events (in terms of rates). Figure 7.5 shows the combination of the results of this thesis, which include the results of over 44 simulations (~ 100 000 core-hour computing time in total). Four regions can be distinguished, as follows:

No Stellar explosions: At large angles, the engine energy is not able to produce a collimated structure that would breakout the stellar envelope. Therefore, the engine energy is lost to the black hole, and no stellar explosion will occur.

Non-relativistic events: At short ratios of $T_{inj}/T_{Breakout}$ the energy is entirely lost into the cocoon, and no prompt emission can be produce. A powerful SN/HN explosion is then expected.

Intermediate events: At both intermediate angles and $T_{inj}/T_{Breakout}$ ratios, both the cocoon and the jet survives, although the jet is mildly relativistic, and the cocoon caries most of the engine energy. This, combination is the only that can explain llGRBs, and there high rates (as opening angles are significantly large) and the SN connection (thanks to the cocoon).

Extremely relativistic events: At small angles and large $T_{inj}/T_{Breakout}$ ratios, SN-less GRBs can be produce with a relatively higher rate (> 1%). A highly relativistic and collimated jet breakout out of the stellar envelope, and the engine continues to run and powers the jet to high Lorentz factors. Only a small fraction of the engine total energy is then wasted in the cocoon, making such events SN-less. Note that this region is the most extreme in terms of engine duration and opening angle, and thus the less likely.
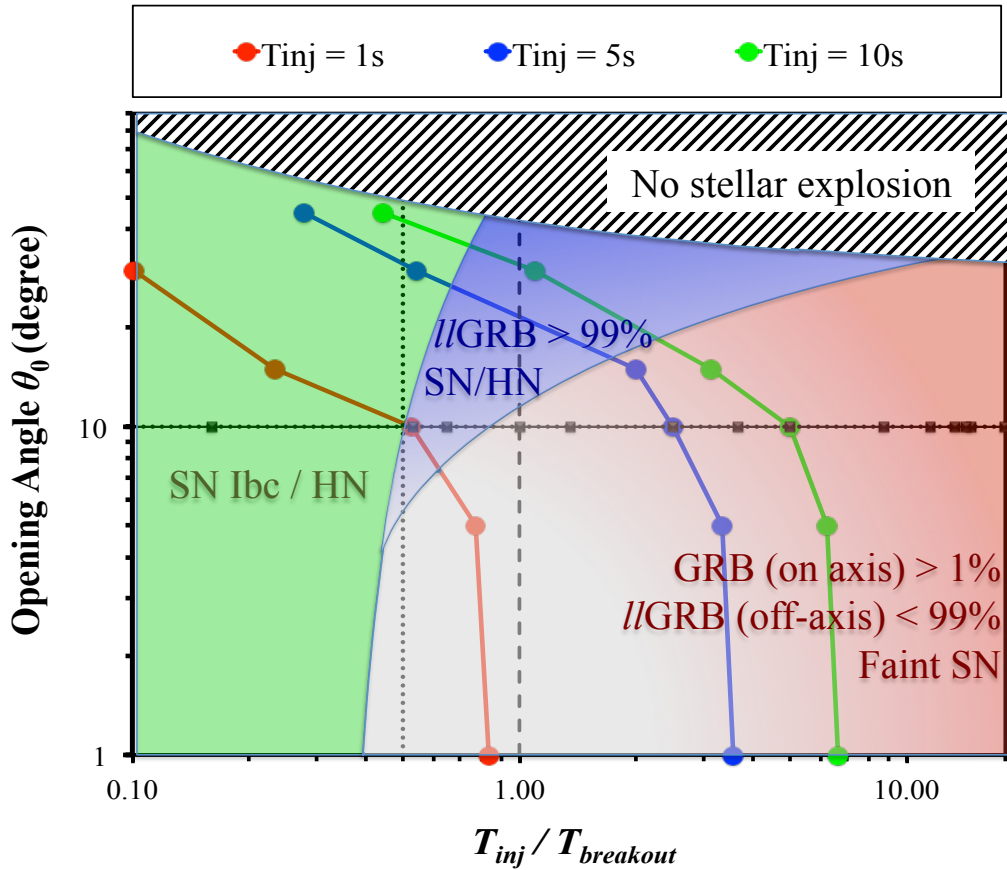
Figure 7.5: The ratio of the engine duration over the breakout time ($T_{inj}/T_{Breakout}$) combined with the jet initial opening angle, and the corresponding events. The simulations show that there are four regions. At large angles, no stellar explosion. At very short $T_{inj}/T_{Breakout}$ non-relativistic stellar explosions. At large $T_{inj}/T_{Breakout}$ highly relativistic & SN-less events. Finally, the intermediate region (in both $T_{inj}/T_{Breakout}$ & the opening angle) where *ll*GRBs can be explained.

7.7 LLGRBs EXPLAINED BY θ_0 & T_{inj}

I showed how the results, found for a diversity of engine durations, were even extended, deeper, by combining with a variety of initial opening angles, which can, as well, be related to the progenitor inner region and its dynamical complexity in nature. The extended results indicate that jets can fail in two ways: either due to a short engine activity, or to a large initial opening angle. Both of these two ways represent intermediate conditions, producing intermediate structures (failed jets), making *ll*GRBs intermediate events (between the non-relativistic SNe and the highly relativistic GRBs). I stress that collapsar engines behind these failed jets, alone, could fully reproduce and explain the peculiar features of *ll*GRBs. In the next chapter a short summary is presented, followed by a discussion and then the conclusion, in the context of previous works. Then, I mention some future attractive perspectives related to *ll*GRBs and to this work.

8 SUMMARY & CONCLUSION

"If I have seen further it is by standing on the shoulders of Giants." —
Isaac Newton, The Correspondence Of Isaac Newton

8.1 SUMMARY

Using a 2D hydrodynamical relativistic code, I performed numerical simulations of a relativistic jet launched in the pole of an accreting BH in a typical Wolf-Rayet star, as proposed by the collapsar model. I presented different models varying in the engine injection duration, which I separated into four groups. My numerical simulations results show that the engine duration; a parameter still not deeply studied so far, both numerically and theoretically; provides considerable diversity to GRBs, and can answer some crucial on *ll*GRBs. The engine duration was found to dramatically affect almost all the jet properties. In summary, the engine duration was found to influences the following:

1- The breakout time: The evolution of jets inside the progenitor was different, for the different engine timescales. In the injection duration two limits, *brief* and *long*, engines' jets were slow at progressing and breaking out, while *short* and *intermediate* engines' jets were the fastest. The breakout time is a very crucial parameter for the relativistic jet evolution and for GRBs (Ramirez-Ruiz et al.

2002; Bromberg et al. 2011b & Nakar et al. 2012). Most of the crucial differences found in this thesis were influenced by the difference in the breakout time.

2- Jet phases and light curve: 1) *Brief* engines' outflow: consists of only the precursor phase, displaying a "cocoon-like" quasi-isotropic properties. The light curve displays a sharp peak structure resulting from the breakout shock. 2) *Short* engines' jet: consists of the precursor and the shocked phase, it shows a variable, one-bulk structure light curve, as it is dominated by the very variable "shocked" phase. 3) *Intermediate* engines' jet: similar to that of a *short* engine, but with a smoother part at the end, making the light curves different, including a second bulk. 4) *Long* engines' jet: long enough to include the unshocked phase at its end, and thus the light curve is a combination of all the three phases and thus, the more complex.

3- Collimation: *Brief* engines produce poorly collimated outflow, in the form of a quasi-isotropically expanding material at mildly relativistic, to sub-relativistic, speeds. However, the longer the engine duration is the better collimated and the narrower the produced jet outflow, and energy, is distributed. However, for *long* engines this trend is slightly inversed, although the jet remains significantly collimated. The result is a "sweet spot" for engine durations were the collimation is the best, in the domain of *short* and *intermediate* engines: $\sim 5 - 30$ seconds.

4- Lorentz factor: *Brief* engines were found incapable of accelerating the outflow efficiently to relativistic velocities, necessary to explain the typical GRBs' prompt emission, instead most of the engine energy is transmitted to non-relativistic expanding outflow. With longer engine durations, the acceleration efficiency increases, and reaches its maximum for *intermediate* engines, in a "sweet spot", making the most relativistic and energetic jets of my sample. For *long* engines, the trend is inversed and the acceleration efficiency gradually decreases, though the relativistic outflow is still considerably accelerated and energetic.

5- *ll*GRBs vs. GRBs: I demonstrated that the shorter the engine duration is, the higher the probability of observing the produced jet. Such that, the collapsar event of *brief* engines possesses the higher probability of observation. Furthermore, with the reasonable assumption of a radiative efficiency of 1% and considering only the outflow with $\Gamma > 10$ to take part in the prompt emission, I showed that *brief* engines alone ($T_{inj} < T_{Breakout}$), can produce *ll*GRBs at huge rates, in the range of 100-1000 times GRBs. This is in agreement with the estimated rates of *ll*GRBs (Soderberg et al. 2006 and Bromberg et al. 2011a and the references within). Thus, my conclusion is that *brief* engines (like B010), are excellent candidates for *ll*GRBs, capable of explaining most *ll*GRBs properties including their high rates in the nearby universe. By considering several duration distributions for the Wolf-Rayet star collapsar, I found that a power-law distribution with an index of about 1, would explain the rates of both *ll*GRBs and GRBs.

6- GRB vs. SN: By taking the assumption that non-relativistic outflow from the jet cocoon, would contribute in the SN explosion, and its detection (as in Zhang et al. 2003), I showed that SN energy reservoir is about one order of magnitude higher – and thus the SN must be clearer – in the case of *brief* engines (which have already been linked to *ll*GRBs). Thus, I gave a possible explanation of the observational trend in GRB-SN connections, clear association for all *ll*GRBs, while the SN signature is not as clear for the standard GRBs.

Next, the effect of the initial opening angle (θ_0), was found to be crucial, as it influence the jet breakout time, and thus the failure or success of any jet. As a consequence, the rate of the events, and the GRB/SN energy reservoirs was dramatically affected. The opening angle combined with the engine duration allows to make some theoretical predictions on some observed particular events: a) *ll*GRBs (as GRB 980425/SN 1998bw) could be failed jets due to either short engine durations (Woosley et al 1999), or a new possibility is a large initial opening angle ($> 10°$ which might be related to some physical properties of the progenitor); while for b) the SN-less LGRBs (e.g: GRB 060505 & GRB 060614), the new possibility is that they can be reproduced and explained with typically long collapsars, but deposing the engine energy in the form of narrow jets ($< 10°$).

8.2 CONCLUSION AND IMPACT

Considering the scheme of the "unification model" (Nakamura 2000, Yamazaki et al. 2002 & 2004), *brief* ($T_{inj} < T_{Breakout}$) and *long* engines ($T_{inj} >> T_{Breakout}$) present an interesting contrast. On one hand, off-axis observations of *brief* (failed) jets, would explain *ll*GRBs with their high rates, soft properties and SN signatures. Such events would be expected to generally dominate at very low redshifts (as their low energies make them extremely faint at high redshift). On the other hand, on-axis observations of *long* engines jets, could explain GRBs' energetic properties and the less frequent SN connections. Such events would dominate at high redshift, as their energetic emission allows them to shine even at cosmological distances. In other words, although the different collapsar's engine durations are expected to follow the unification model, my results show that the different collapsar jets follow the unification model differently: with short engine durations favoring *ll*GRBs over GRB, and explaining low redshift events, while longer engine models favor the classical GRBs (although producing *ll*GRBs as well), and explain high redshift events.

In Figure 8.1, I illustrate the main two findings of this thesis. By varying the engine duration (or the initial opening angle of the jet), I obtained varied ratios of $T_{inj}/T_{breakout}$. I confirmed Bromberg et al. (2011a & 2012) argument, that *ll*GRBs are different from the standard GRBs (successful jets: $T_{inj}/T_{breakout} >> 1$); as *ll*GRBs are well explained with engine durations shorter than the breakout time (failed jets: $T_{inj}/T_{breakout} < 1$). I showed that successful jets alone would not unify *ll*GRBs with GRBs, as the produced rate of *ll*GRBs/GRBs following this scenario would be lower than what the observations suggest. Hence I confirmed Cobb et al. (2006) argument that *ll*GRB rates cannot be explained with a typical GRB jet alone (the ration of rates *ll*GRBs/GRBs cannot exceed ~65 < 100). The second finding is that failed jets make powerful cocoons and thus potentially luminous SNe, while successful jets show much weaker cocoons. As *ll*GRBs are strongly connected to SN explosions (Hjorth 2013), the numerical confirmation of this observational fact shown here is an additional argument in favor of the failed jet origin for *ll*GRBs (of Bromberg et al. 2011a & 2012).

In this study, I considered a central engine delivering a total energy of 10^{52} ergs, in the order of theoretical prediction of the collapsar model (MW99) and of the energy of *ll*GRBs' SNe. However, it is clear that collapsar engines and their progenitors are very diverse in terms of explosion and central engine energy (Nomoto et al. 2006a). Thus, GRBs in the universe are expected to have a distribution of engine energies, with different engine energies associated with different probabilities of occurrence (not necessarily a flat distribution). By considering only one central engine energy, 10^{52} erg, I did not include this element. Nevertheless, I do not expect this to change the main results. In addition, the same idea applies to the engine durations; it is expected that engine durations have different chances of occurrence in the universe. Since it is related to the torus around the central BH, which would have different lifetime scales influenced by key parameters such as progenitor mass, angular momentum, metalicity, magnetic field, etc. Thus, the considered engine durations in the range $0.1 - 100$ s would not be equally probable in nature, and thus would not necessarily have a flat distribution, and neither necessarily the considered power law distributions would represent the true distributions, as such distribution might be related to complicated physical parameters. Still, I do not expect this to change this study main finding, which is that only the *brief* engines are capable of explaining *ll*GRBs huge rates and the clear SN explosions associated with them, all in contrast with longer engine duration that relatively favor standard GRBs, and produce fainter SN explosions.

Note that *ll*GRBs are not necessarily associated with very short engine durations. It would be possible to produce similar *ll*GRBs, with longer engine durations, however this would imply different parameters or environments (Hjorth 2013). Environments that reduces the jet penetration power inside the progenitor, due to a weak engine as it is powered by, e.g: a small collapsing mass Mazzali et al. (2008); or surrounded by a low mass envelope – such as a He layer – that dumps the jet and slows its breakout (Mazzali et al. 2008 & Nakar 2015), hence giving long breakout times even when the engine duration is long, and satisfying $T_{inj} \lesssim T_{Breakout}$. In the case of my calculations, it is the large initial opening angle, which significantly weakened the jet penetration and delayed its breakout, even when the considered engine duration was long.
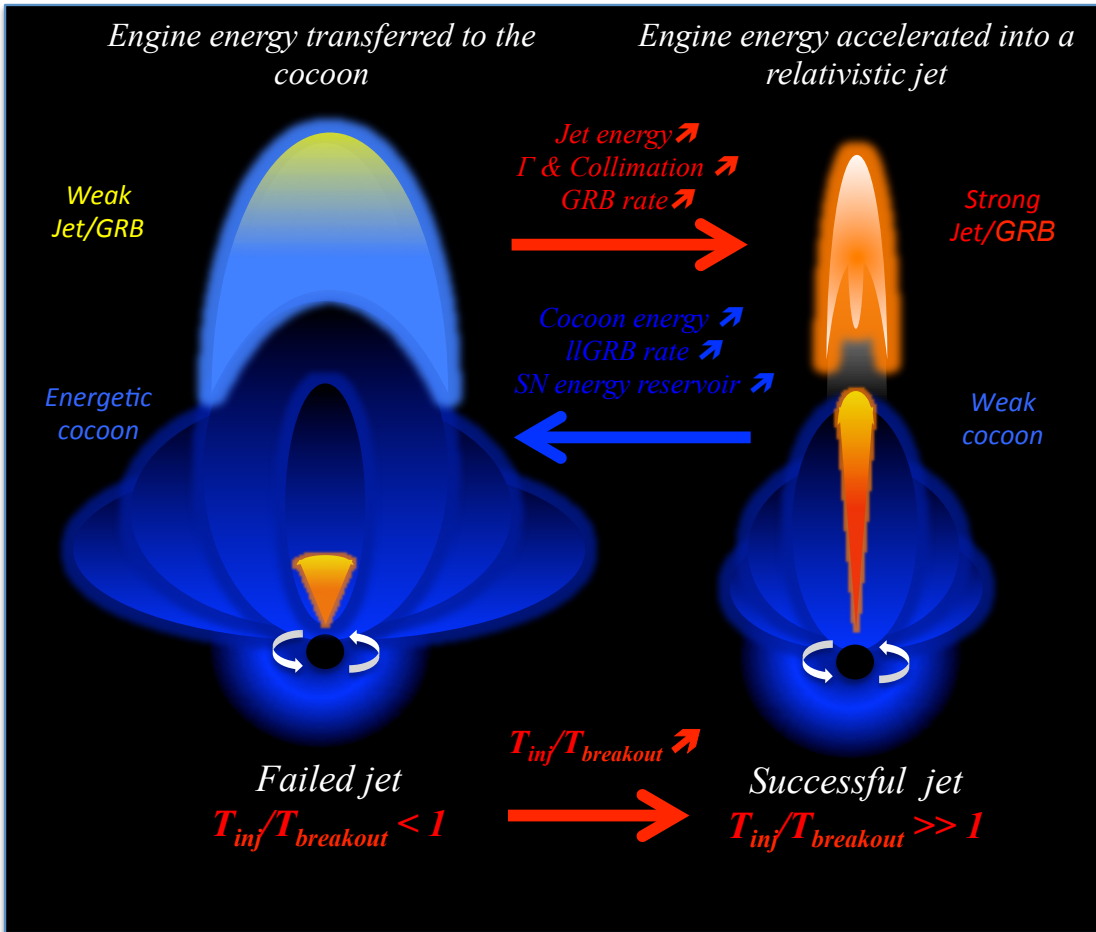
Figure 8.1: The main finding of this thesis summarized in an illustration.

8.3 FUTURE DIRECTIONS

The work presented here is a first attempt to explain *ll*GRB features numerically with different engine durations. To this end, some rough assumptions were made and not all of the relevant physics incorporated. This leaves plenty of room for further improvement regarding a more accurate jet structure (and thus more accurate rates). I

considered that a Lorentz factor of at least 10 is necessary for the outflow to contribute to *ll*GRB and GRB prompt emissions. However, this might not be the case, and might lead to some qualitative differences (especially in the case of *ll*GRBs as the emission process is different: Nakar et al. (2012 & 2015). Thus, different minimum Lorentz factors should be considered for *ll*GRB and GRB prompt emissions. I estimate that the general results and tendencies might not change, but such a treatment would give more accurate estimations. One other assumption is the radiative efficiency, which was assumed for the relativistic outflow. It is not always ~1%, and might differ from an event to another (Zhang et al. 2007b). Especially for *ll*GRBs, as the emission process is different (Nakar et al. 2012). A more rigorous treatment of the radiated energy, as prompt emission, would be an interesting project. I plan to use the photospheric model (for both *ll*GRBs and GRBs) to derive the energy of the prompt emission and avoided this assumption, although this would require a larger computational domain and a longer computational time.

The results of this study can be improved and deepened further by considering more diverse engines, progenitors and progenitor environments. For instance, one very interesting project to consider in the near future is to test Nakar (2015) unification model. Nakar (2015) proposed a unification of *ll*GRBs and GRBs by considering different extended masses around the progenitor: in the case of an extended mass a *ll*GRBs would be favored as the jet breakout will be delayed, while no extended mass model favor a standard GRB. This is an interesting scheme to examine. Using the code previously explained in this thesis, I plan to simulate both models and analyzed the hydrodynamical properties of the produced jets.

Finally, it is notable that this work doesn't include some complex physics that would affect the stellar explosion and the jet propagation (and thus *ll*GRB and GRB rates). Below are of these limitations that would be improved in the future:

- The injection position, which is about 1 to 2 orders of magnitude larger than the BH horizon, which affects the jet evolution (under work).

- The magnetic field, not included in the simulations.

- The neglected rotation.

- The simple equation of state (the gamma law)

- The small computational domain ($\sim 10^{12}$ cm)

9 BIBLIOGRAPHY

"What you learn from others you can use to follow. What you learn for yourself you can use to lead." ― *Richard Hamming, The Art of Doing Science and Engineering: Learning to Learn*

Aloy, M. A., Muller, E., Ibanez, J. M., Marti, J. M., & MacFadyen, A. 2000, ApJ, 531, L119

Amati L., 2010, Proceedings of "The Shocking Universe - Gamma-Ray Bursts and High Energy Shock phenomena", (arXiv:1002.2232v1 [astro-ph.HE)

Amati, L., Frontera, F., Guidorzi, C. 2009, A&A, 508, 173

Amati, L., Frontera, F., Tavani, M., et al. 2002, A&A, 390, 81

Amati, L., Guidorzi, C., Frontera, F., et al. 2008, MNRAS, 391, 577

Antonucci, R., 1993, ARA&A, 31, 473

Band, D., et al. 1993, ApJ, 413, 281

Barish, B., Huchra, J., et al. Neutrinos and Beyond: New Windows in Nature, National Academic Press, Washington, D.C., 2003, p. 20.

Barraud C., Etude de l'émission prompte des sursauts gamma : Expérience HETE-2, PhD thesis, University of Paris VII (2004), 12-24

Barthelmy, S. D., Baumgartner, W. H., Cummings, J. R., et al. 2012, GCN. Circ. 13246

Begelman, M. C., & Cioffi, D. F. 1989, ApJ, 345, L21

Berger, E., et al. 2007, ApJ, 660, 504

Bietenholz, M. F., Soderberg, A. M., Bartel, N., et al. 2010, ApJ, 725, 4

Blustin, A. J., Band, D., Barthelmy, S., et al. 2006, ApJ, 637, 901

Bromberg, O., Nakar E., Piran T., 2011a, ApJ, 739, L55

Bromberg, O., Nakar, E., Piran, T., Sari, R. 2011b, ApJ, 740, 100

Bromberg, O., Nakar, E., Piran, T., Sari, R. 2012, ApJ, 749, 110

Campana, S., Mangano, V., Blustin, A. J., et al. 2006, Nature, 442, 1008

Cano, Z., de Ugarte Postigo, et al. 2014, A&A, 568, 16

Chevalier, R. A., & Fransson, C. 2006, ApJ, 651, 381

Cobb, B. E., Bailyn, C. D., van Dokkum, P. G., & Natarajan, P. 2006, ApJ, 645, L113

Coward, D. M. 2005, MNRAS, 360, L77

Crew, G. B., Lamb, D. Q., Ricker, G. R., et al. 2003, ApJ, 599, 387

Crowther P. A., 2007, ARA&A, 45, 177

Cuesta-Martínez C., et al. 2015, MNRAS, 446, 1737

Del Zanna, L. & Bucciantini, N. 2002, A&A, 390, 1177

Hamid Hamidani - February 2016

Duffell P. C., et al. 2015 (arXiv:1505.05538v1)

Duffell P. C., et al. 2015, ApJ, 813, 64

Frail, D.A. et al. 2001, ApJ, 562, L55

Galama, T. J., Vreeswijk, P. M., van Paradijs, J., et al. 1998, Nature, 395,670

Garnavich, P. M., Stanek, K. Z., Wyrzykowski, L., et al. 2003, ApJ, 582, 924

Gomboc, A., (2012), ConPh. 53 339 arXiv:1206.3127 [astro-ph.HE]

Guetta, D., & Della Valle, M. 2007, ApJ, 657, L73

Hachisu, I.,1986, ApJS, 62, 461

Harikae S., Takiwaki T., & Kotake K., 2009, ApJ, 704, 354

Harikae S., et al. 2010, ApJ, 720, 614

Harikae S., Takiwaki T., & Kotake K., 2010, ApJ, 713, 304

Hjorth, J. 2013, Phil. Trans. R. Soc. A 371, 20120275

Hjorth, J., & Bloom, J. S. 2011, arXiv:1104.2274

Hjorth, J., et al. 2005, Nature, 437, 859

Hjorth, J., Sollerman, J., Møller, P., et al. 2003, Nature, 423, 847

Irwin & Chevalier 2015, arXiv: 1511.00336

Iwamoto, R., 1998, Nature 395, 672

Jin, Z. P. et al. 2013, ApJ, 774, 9

Kaneko, Y., Preece, R. D., Briggs, M. S., et al. 2006, ApJS, 166, 298

Kaneko. Y., Spectral studies of gamma-ray burst prompt emission. PhD thesis, The University of Alabama in Huntsville, United States Alabama, 2005.

Kawai N, et al. 2006, Nature. 440, 184

Klebesadel, W., et al. 1973, ApJ, 182, L85

Kouleviotou, C. 1993, ApJ, 413, L101

Kouveliotou, C., Meegan, C. A., Fishman, G. J., et al. 1983, ApJ, 413, L101

Kulkarni, S. R., Frail, D. A., Wieringa, M. H., et al. 1998, Nature, 395, 663 Lazzati, D., & Begelman, M. C. 2005, ApJ, 629, 903

Lamb, D. Q., Donaghy, T. Q. & Graziani, C., 2005, ApJ, 620, 355

Lazzati, D., 2005, MNRAS357, 722

Lazzati, D., et al. 2013a, ApJ, 765,103

Lazzati, D., et al. 2013b, MNRAS, 436, 1867

Lazzati, D., Morsony, B. J et al. 2012, 750, 68

Lazzati, D., Morsony, B. J., & Begelman, M. C. 2007, RSPTA, 365, 1141

Lazzati, D., Morsony, B. J., & Begelman, M. C. 2009, ApJ, 700, L47

Lazzati, D., Morsony, B. J., & Begelman, M. C. 2010, ApJ, 717, 239

Leismann, T. et al. 2005, A&A, 436, 503

Levan A. J., et al. 2014, ApJ, 781, 13

Liang, E., Zhang, B., Virgili, F., & Dai, Z. G. 2007, ApJ, 662, 1111

Lopez-Camara, D., et al. 2013, ApJ, 767, 11

Lopez-Camara, D., et al. 2014, (arXiv:1404.5319)

MacFadyen, A. I., & Woosley, S. E. 1999, ApJ, 524, 262 (MW99)

MacFadyen A. & Woosley S., Collapsars – Gamma-Ray Bursts and asymmetric supernovae. PhD thesis, the university of California Santa Cruz, 2000

MacFadyen, A. I.; Woosley, S. E.; Heger, A. 2001, ApJ, 550, 410

Matzner, C. D. 2003, MNRAS, 345, 575

Mazzali, P. A., Valenti, S., Della Valle, M., et al. 2008, Science, 321, 1185

McKinney, J.C. 2005, ApJ, 630, L5

Meszaros, P. 2006 Reports on Progress in Physics, 69, 2259

Metzger et al. 1997, Nature 387, 878

Mizuta, A. , Yamasaki, T., Nagakura, S., & Mineshige, S. 2006, ApJ, 651,960

Mizuta, A. & Aloy, M.A. 2009, ApJ, 699, 1261

Mizuta, A., Nagataki, S., & Aoi, J. 2011, ApJ, 732, 26

Morsony, B.J. , Lazzati, D. & Begelman, C. 2007, ApJ, 665, 569 (ML07)

Morsony, B.J. , Lazzati, D. & Begelman, C. 2010, ApJ, 723, 267

Murase et al. 2006, ApJ, 651, L5

Murase & Ioka 2013. PRL, 111, 121102

Nagakura, H., Ito, H., Kiuchu, K. & Yamada, S. 2011, ApJ, 731, 80

Nagakura H., et al. 2012, ApJ, 754, 85

Nagakura H., et al. 2014, ApJ, 784, 28

Nagataki, S. 2010, arXiv:1010.4964

Nagataki S., Mizuta A., Sato K., 2006, ApJ, 647, 1255

Nakamura K., et al. 2015, A&A, 582, A34

Nakamura, T. 2000, ApJ, 534, L159

Nakar, E., & Sari, R. 2012, ApJ, 747, 88

Nakar, E., 2015 arXiv:1503.00441v1

Nakauchi D., et al. 2013, ApJ, 778, 67

Nomoto, K. et al. 2006a, Nuclear Physics A, 777, 424

Nomoto, K., Tominaga, N., Tanaka, M., Maeda, K., Suzuki, T., Deng, J. S., & Mazzali, P. A. 2006b, Nuovo Cimento B Serie, 121, 1207

Nousek, J. A., et al. 2006, ApJ., 642, 389

Okita, S., Umeda, H., Yoshida, T., 2012, Origin of Matter and Evolution of Galaxies 2011, Eds. S. Kubono et al. AIP Conf. Proc. 1484, 418

Pe'er. A., et al. 2008, AIP, Conference Series, 1065, 183

Perlmutter, S., et al. 1999, ApJ, 517, 565

Pian, E., et al. 2006, Nature, 442, 1011

Piran, T. 1999, Phys. Rep., 314, 575

Piran, T. 2004, Rev. Mod. Phys., 76, 1143, astro-ph/0405503.

Piran, T., 2000, Phys. Rep. 333, 529

Hamid Hamidani - February 2016

Racusin, J. L., Liang, E. W., Burrows, D. N., Falcone, A., Sakamoto, T., Zhang, B. B., Zhang, B., Evans, P., and Osborne, J.: 2009, ApJ 698, 43

Ramirez-Ruiz, E. & Lloyd-Ronning, N. 2002b, New Astronomy, 7, 197

Ramirez-Ruiz, E., Celotti, A., & Rees, M. J. 2002a, MNRAS, 337, 1349

Ryde. F., 2004, ApJ, 614, 827

Sakamoto, T. et al. 2006, AIP, 836, 43

Sakamoto, T., Barthelmy, S. D., Baumgartner, W. H., et al. 2010, GCN. Circ. 10511

Sakamoto, T., Lamb, D. Q., Graziani, C., et al. 2004, ApJ, 602, 875

Sari, R. Piran, T., and Narayan. R., 1998, ApJL, 497, L17

Savaglio, S., et al. (2009), ApJ, 691, 182

Sazonov, S. Y., Lutovinov, A. A., & Sunyaev, R. A. 2004, Nature, 430, 646

Schonfelder V., et al. The Universe in Gamma Rays, Springer, New York, (2001).

Schulze, S., Levan, A. J., Malesani, D., et al. 2012, GCN. Circ. 13257

Schulze S., et al. 2014, A&A, 566, A102

Shu, C.W. , & Osher, S.J. 1988, J. Comp. Phys., 77, 439

Soderberg A., et al. 2004b, Nature, 430, 648

Soderberg, A. M., Berger, E., Page, K. L., et al. 2008, Nature, 453, 469

Soderberg, A. M., Chakraborti, S., Pignata, G., et al. 2010, Nature, 463, 513

Soderberg, A. M., et al. 2006, Nature, Volume 442, Issue 7106, pp. 1014-1017

Soderberg, A. M., Kulkarni, S. R., Berger, E., et al. 2004a, ApJ, 606, 994

Sparre, M., Sollerman, J., Fynbo, J. P. U., et al. 2011, ApJ, 735, L24

Suwa, Y. & Ioka, K. 2011, ApJ, 726,107

Svensson, M., K., On the nature of γ-ray burst hosting galaxies, PhD thesis, University of Warwick, 2011, P24 & P28

Toma et al. 2007, ApJ, 659, 1420

Tominaga, N. 2009, ApJ, 690, 526

Tominaga, N., et al. 2007, ApJ, 657, L77

Totani, T., et al. 2014, PASJ, 66, 6313

Umeda, H. & Nomoto, K. 2008, ApJ, 673, 1014

Umeda, H., Tominaga, N., Maeda, K., & Nomoto, K. 2005, ApJ, 633, L17

Virgili F. et al. 2009, MNRAS 392, 91

Willingale, R., et al. 2007, ApJ, 662, 1093

Woosley, S. E., & Bloom, J. S. 2006, ARA&A, 44, 507

Woosley, S. E., & Heger, A. 2006, ApJ, 637, 914

Woosley S.E. & MacFadyen A.I., 1999, Astron. Astrophys. Suppl. 138, 499

Woosley, S. E., & Weaver, T. A. 1986, ARA&A, 24, 205

Woosley, S., E., 1993, ApJ, 405, 273

Woosley, S., E., et al. 2007, RSPTA, 365, 1129

Yamazaki, R., Ioka, K., & Nakamura, T. 2002, ApJ, 571, L31

Yamazaki, R., Ioka, K., & Nakamura, T. 2004, ApJ, 607, L103

Yoshida, T., Okita, S., & Umeda, H., 2014, MNRAS, 438, 3119

Zhang B. B. et al. 2012, ApJ, 756, 6

Zhang, B., et al. 2009, ApJ, 703, 1696

Zhang, B., et al. 2007b, ApJ, 655, Issue 2, pp. 989-1001

Zhang, B., Zhang, B.-B., Liang, E.-W., Gehrels, N., Burrows, D. N., & Meszaros, P. 2007a, ApJ, 655, L25

Zhang, F.-W. 2008, ApJ, 685, 1052

Zhang, W., Woosley, S. E., & Heger, A. 2004, ApJ, 608, 365

Zhang, W., Woosley, S.E., & MacFandyen, A.I. 2003, ApJ, 586, 356

Zhang, Z., Xie, G. Z., Deng, J. G., and Jin, W.: 2006, MNRAS 373, 729

10 Appendices

"science requires of an individual the price of his life. And had you two lives, they would not have been enough" – Ivan Pavlov

Hamid Hamidani - February 2016

APPENDIX 1: CODE TESTING

In order to estimate the accuracy of the newly developed numerical code, I carried out several calculation tests. Here I present a test of the code by solving Riemann problem. I calculated the propagation of a blast wave, generated by left and right phases initially detached by diaphragm, the so-called shock-tube problem. Since it is difficult to get analytical solution in the spherical case, I reproduced the 1D Riemann problem as in Del Zanna & Bucciantini (2002) who proposed the computational convergence by comparing between a solution with coarse grid and with well-resolved fine grid.

Numerical grids are set as $0 \leq r \leq 1$, and the speed of light c is set to 1. All the physical quantities are dimensionless. I divided the numerical domain in r direction by $N_r = 200$ zones and by $N_r = 800$ zones for the "coarse" and "fine" grid cases, respectively. In θ direction $N_\theta = 16$ zones ranging in $0° < \theta < 90°$ for both cases. The initial condition is given as follows:

$$(\rho, v_r, p) = \begin{cases} (1, 0, 1000) & r \leq 0.4 \\ (1, 0, 1) & r \geq 0.4 \end{cases} \qquad \text{(A1)}$$

Explosion generates outgoing and incoming shocks. Figure 10.1 shows the coincidence of those solutions. This proves the robustness of the numerical code for the propagation of a blast wave. For a comparison, see Mizuta et al. (2006) Fig. 21.
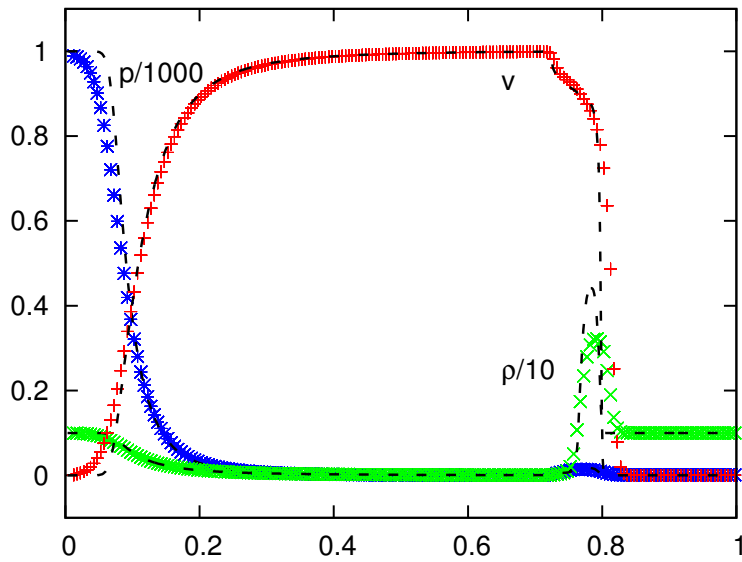
Figure 10.1: Numerical solutions of one-dimensional spherical Riemann problem corresponding to the physical quantities $\rho/10$, v_r, $p/1000$, as marked. Black dashed line is the well-resolved numerical solution where the computational domain is divided by $Nr = 800$ zones. Coarser solution, corresponding to a domain divided by $Nr = 200$ zones, is plotted with marks.

APPENDIX 2: EFFECT OF RESOLUTION

I also tested different angular resolutions. Since, the jet has a collimated structure, it is needed to check whether angular grids can resolve the collimated narrow structure. The test is on whether the considered angular resolution in the study is appropriate. I compared the same calculation in three different grid resolutions: "higher resolution" N_θ = 512 angular meshes, the "used resolution" in the study N_θ = 256, and "lower resolution" N_θ = 512. The "used resolution" is comparable to, or finer than, some previous studies (e.g. Mizuta et al. 2009). Jet initial parameters are all the same, as in B010. Comparison of the three is showed in Figure 10.2. There is a dramatic difference in the jet structure between the "lower resolution" and the two higher resolutions. The calculation with N_θ = 128, seems to lead to some lose of fine structure in the jet, a structure that 256 and especially 512 are displaying. 512 and 256 resolutions are very similar; almost converging, suggesting that 256 grids are reasonably good enough, and the use of 512 is not strongly needed, and would not significantly change the jet structure, and hence the results.
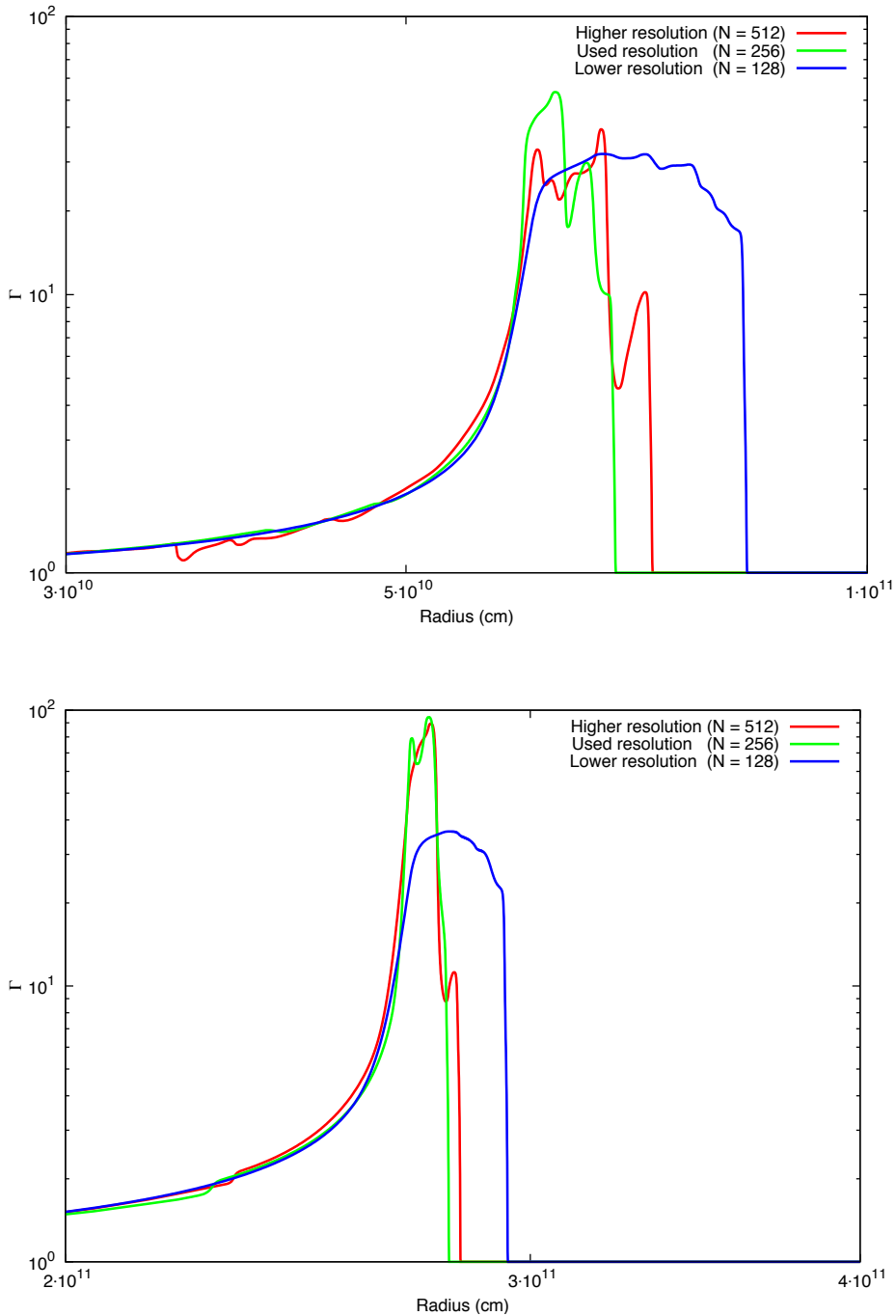
Figure 10.2: Comparison of calculations with different angular resolutions, at different times (On the top at 3.0 s just after the breakout, on the bottom at 10.0 s, a few seconds after the breakout). "Higher resolution" calculation uses 512 grids in θ direction, the "used resolution" in the calculations of this study uses 256, and the "lower resolution" has an angular grid of 128. The used resolution (256) and the higher one (512) show similar profiles, and thus the "256" calculation is good enough.

APPENDIX 3: COMPARISON WITH FLASH CODE (ML07)

The calculation I present here is to compare the output from the calculation to that of ML07's main models, 16TIg5 and t10g5. ML07 used an engine duration of $T_{inj} = 50$ seconds, delivering a total energy of $E_{tot} = 5.32 \times 10^{52}$ ergs, with the injection nozzle situated at $R_{in} = 10^9$ cm. I carried out a simulation with the same above*: R_{in}, T_{inj} and E_{tot},* as in ML07. The aim of this comparison is to test the code output and make sure that the code does not show any deficiencies, and thus is as correct as the FLASH code used in ML07. Thus, I carried a simulation with identical engine properties to that of ML07's 16TIg5 and t10g5 models, with engine luminosity per jet, of 5.32×10^{50} ergs (Table 4-1). I have to mention that the simulation still presents some minor differences in comparison to ML07 and that the two simulations are not fully identical. There are some differences such us ratio of internal over rest mass energy, progenitor, EOS, resolution, etc. Nevertheless, that did not prevent the results from being in an excellent agreement with those of ML07. Table 5-1 last line represents the breakout times of the three phases, small differences in the breakout times exist more likely due to difference in the progenitor, but the difference is minor and the breakout times are in the same order (for a comparison see 16TIg5 model in ML07's table 2).

Next, in Figure 10.4, top panel, I present the properties of the unshocked material at the moment of the breakout, 25.0 seconds after the start of the calculation. The core of the unshocked jet is, indeed, in agreement with the theoretical prediction of a free-streaming jet (Lazzati et al. 2007 and the references within). It is also in excellent agreement with ML07's 16TIg5 model results (see ML07 figure 10). With Lorentz factor proportional to the radius, and the pressure proportional to r^{-4}, the unshocked jet in the calculation is well in agreement with the both theoretical predictions and the previous work presented in ML07 and Lazzati et al. (2007). I have to mention that, as in ML07, with Lorentz factor getting closer to ~100, derivation from the theoretical prediction increases, this is due to, as explained in ML07, the statement that at such highly relativistic speed, the approximation of the flow being pressure-dominated, no longer holds. For a comparison of this figure with previous works see: Aloy et al. (2000) Fig. 2, Zhang et al. (2003) Figs. 4, 5, and 6, Mizuta et al. (2006) Figs. 6 and 7, and Fig. 10 in ML07.

Figure 10.3 (bottom panel) shows the outflow energy flux along the jet axis over time for the calculation. The three phases are clearly identifiable. Here again, the temporal and energetic properties suggest that the calculation is in excellent agreement with that of ML07, despite the few minor differences in the calculation setting. Considering an isotropic equivalent luminosity, would add a factor of $\sim 8 \times 10^5$ bringing the energy to the same order as in ML07 (for a comparison, see ML07 figure 4).

Finally, Figure 10.4, presents light curves calculated as explained in § 4, following ML07 method. Apart from the light curve at 1.125º showing some difference although it remain similar in general, the light curves are at excellent agreement with those presented in ML07 for t10g5 model (see ML07's figure 12 for a comparison). The difference in light curves at 1.125º is most likely due to ML07's considerably higher angular resolution at that region, near the jet axis. One other difference is in the precursor's Lorentz factor, which is lower than 10 in this calculation, at the difference of that of ML07's t10g5. This is most likely due to difference in the progenitor, which is expected to strongly affect this phase, rather than difference in the numerical method or in the physics. In this study, the stellar model is realistic (Umeda et al. 2005), where in ML07's t10g5 it is a power-law stellar model. Nevertheless, apart from these two minor differences, the energy range, dead times, temporal properties, are at excellent agreement, allowing us to conclude that the code is robust and as safe as that of ML07, and confirming ML07 results.

From the above tests and calculations, I can safely conclude that the simulations do not suffer from numerical problems. I can also confirm that the simulation setting, such as the choice of resolution, does not miss the jet structure, and thus is appropriate. Finally, the comparison with ML07's 16TIg5 and t10g5 models shows that the code's output and numerical treatment is at excellent agreement with that of ML07. Thus, I can conclude that the numerical code is robust enough and fully appropriate for the kind of study presented here.
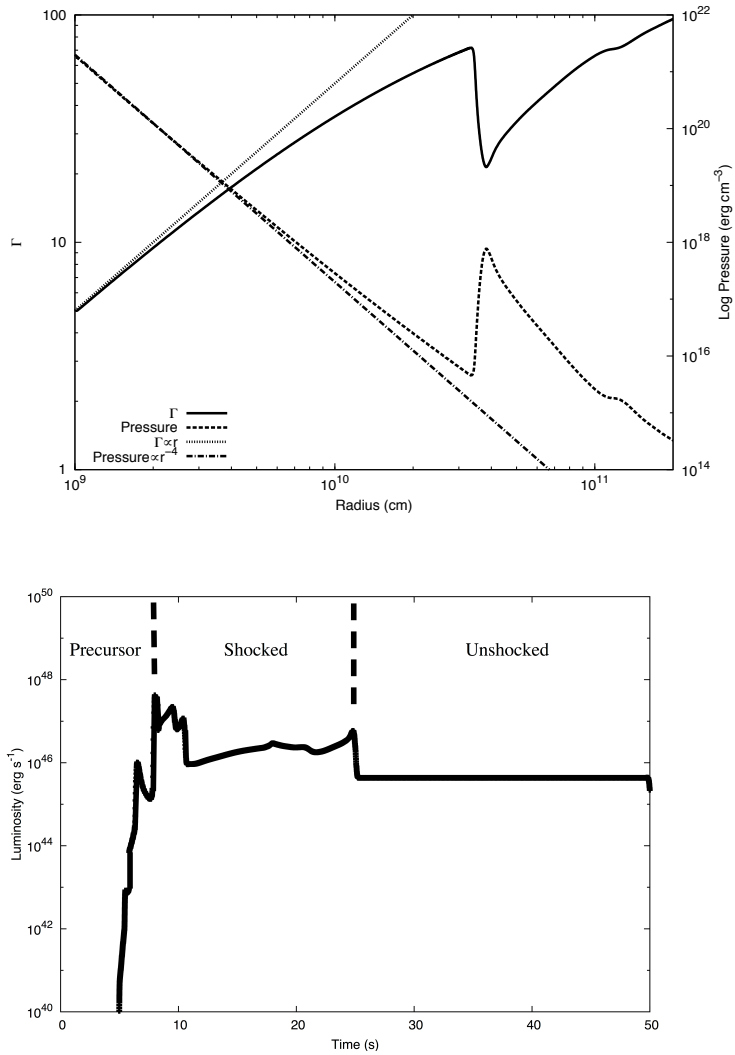
Figure 10.3: On the top panel, Lorentz factor (left y-axis), and Pressure (right y-axis) as a function of the radius, in solid line, and dashed line, respectively. Both quantities are computed at the jet-axis region, the innermost angular grid. The dotted line, and dotted dashed line, shows the theoretical prediction considering a free-streaming jet pressure-dominated jet, for Lorentz factor and the pressure, respectively. This approximation holds very well as long as the jet outflow is not at highly relativistic speeds ($\Gamma \ll 100$). On the bottom panel, the energy flux over time, along the jet on-axis. The energy was calculated at 1.2×10^{11} cm, as in ML07. Dashed lines show the transition times between the three phases of the jet: precursor to shocked, and shocked to unshocked.
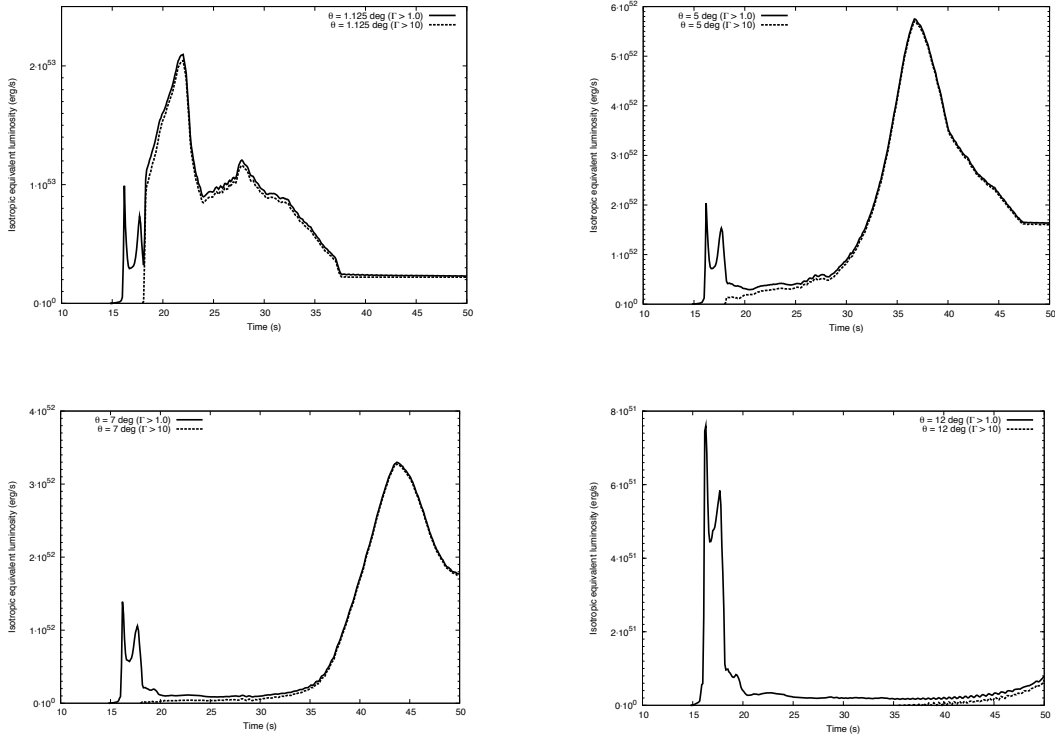
Figure 10.4: Light curves for a similar engine to that of 16TIg5 and t10g5 in ML07. As in ML07's figure 12, energy flux over time is shown for four different viewing angles. Solid and dashed lines are for material with a minimum Lorentz factor of 1.0 and 10, respectively. The four light curves are plotted at angles: 1.125º (top left), 5º (top right), 7º (bottom left), and 12º (bottom right). These light curves were estimated as explained in § 4.4.4, and as in ML07.

Hamid Hamidani - February 2016